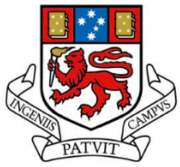

UNIVERSITY
OF TASMANIA

New and improved techniques for assessing drought tolerance in plants

Christopher James Lucani
BSc (Hons)

Submitted in fulfilment of the requirements for the
Degree of Doctor of Philosophy

University of Tasmania
July 2018

Declaration of Originality

This thesis contains no material which has been accepted for a degree or diploma by the University of Tasmania or any other institution, and to the best of my knowledge and belief, this thesis contains no material previously published or written by another person, except where due acknowledgement is made in the text of this thesis.

Signed: ..... Date: 30/7/2018

Christopher James Lucani

Statement of co-authorship

The following people and institutions contributed to the publication of work undertaken as part of this thesis:

Candidate. Christopher J. Lucani
School of Natural Sciences, University of Tasmania, Hobart, Australia

Author 2. Timothy J. Brodribb
School of Natural Sciences, University of Tasmania, Hobart, Australia

Author 3. Gregory J. Jordan
School of Natural Sciences, University of Tasmania, Hobart, Australia

Author 4. Patrick J. Mitchell
CSIRO Land and Water, 15 College Rd, Sandy Bay, TAS 7005, Australia

Chapter 2 has been submitted to Functional Plant Biology and is currently under review. Candidate was the primary author (75%), author 2 assisted with designing the research and writing the manuscript (15%), author 3 assisted with data analysis and writing the manuscript (6%), author 4 assisted with data analysis (4%).

We the undersigned agree with the above stated "proportion of work undertaken" for the above submitted manuscript contributing to this thesis:

Signed: .... Date: 30/7/2018

Professor Timothy Brodribb, Primary Supervisor, School of Natural Sciences, University of Tasmania

Signed: . . Date: 30/7/18

Head of School, School of Natural Sciences, University of Tasmania

Authority of Access

This thesis may be made available for loan and limited copying and communication in accordance with the Copyright Act 1968.

Acknowledgments

My deepest thanks to Tim Brodribb and Greg Jordan, whose guidance, knowledge and support has never failed to steer me safely through the challenges of the PhD journey. It has been a pleasure and an honor.

To my fellow post-grads, some now post-docs and beyond – Maddy, Celia, Freya, Scott, Sam, Louise and many others, thanks for the support, the comradery, the distraction, and the fun.

I thank Patrick Mitchell for all the useful discussions, help, support, and for access to the facilities at the CSIRO.

I am deeply grateful to the school administration staff, especially Jodi Noble, Clancy Carver, and Morgan Green who have deftly dealt with an endless list of administrative queries and issues, especially in regard to the CaviCam.

Most of all I thank my wife, Cynthia, and my two children Freya and Neiva, who have for too long endured an absent husband and distracted father.

Lastly I thank my Mum for her unwavering believe and support.

For Cynthia, Freya and Neiva

I like to think (and
the sooner the better!)
of a cybernetic meadow
where mammals and computers
live together in mutually
programming harmony
like pure water
touching clear sky.

I like to think
(right now, please!)
of a cybernetic forest
filled with pines and electronics
where deer stroll peacefully
past computers
as if they were flowers
with spinning blossoms.

I like to think
(it has to be!)
of a cybernetic ecology
where we are free of our labors
and joined back to nature,
returned to our mammal
brothers and sisters,
and all watched over
by machines of loving grace.

All Watched Over by Machines of Loving Grace
Richard Brautigan, 1967

Abstract

Evaluating how plants respond to dry conditions is critical to managing and predicting the effects of climate change on vegetation. Water in the soil and plant are connected via the xylem, a network of dead and elongated hollow cells that provide conduits through which water flows during transpiration. Water movement is a tug of war between the competing water status of the plant and the soil; when conditions are favourable, water is pulled from the soil under a 'metastable' state of tension established via transpiration and capillary action in the leaf. As soil moisture declines during drought, capillary action in the soil microstructure resists the movement of water into the plant causing tension in the xylem to rise.

Under tension the xylem is highly vulnerable to bubble nucleation, which results in rapid embolism of xylem conduits, reducing xylem hydraulic conductance. This limits the supply of water for transpiration and photosynthesis. Excessive drought conditions cause catastrophic damage as embolism propagates through the xylem leading to plant dieback and death. The tension at which this occurs defines the absolute threshold of drought tolerance, and across species there are a range of thresholds reflecting the diversity in adaptation to different levels of water availability. Traits incorporating these thresholds can be used as powerful predictors of drought survival under extreme climate conditions, however the limited number of accurate and reliable measurements currently available significantly underrepresents the diversity of vegetation.

Although there are a number of techniques for assessing xylem vulnerability, most are only suitable for in-depth study of xylem anatomy and physiology, and the few that have the capacity for broad-scale measurements are limited in access, restricted to short-vesseled species and can be susceptible to artefacts under some conditions. The aim of this thesis was to find a technique that could be used for accurately measuring the vulnerability of xylem to embolism in large numbers of species or individuals.

In the first chapter I provide a brief introduction to the evolutionary history of the xylem, and the development of our understanding of xylem physiology. In detail I describe the mechanisms of xylem water transport, and discuss the limitations in the

context of climate change. Finally, current methodologies for assessing xylem vulnerability are reviewed.

In the second chapter I explore a novel approach for reducing the number of measurements required to assess intraspecific variation, and use the approach to demonstrate significant variation in drought tolerance between two populations of *Eucalyptus globulus*.

In the third chapter I develop procedures to expediate the process of assessing xylem vulnerability using a desktop scanner, and use the procedure to find significant differences in vulnerability between juvenile and adult *Eucalyptus globulus*.

In the fourth chapter I develop a novel system based on the latest optical method of vulnerability assessment. Combining modern electronics, 3D printing technology and collaborative platforms, I develop a cheap, accurate, reliable, widely accessible and Open Source device for assessing drought tolerance, with a broad appeal to plant physiologists, ecologists, forestry managers and educators. This system provides the only current mechanism by which a large and diverse number of species can be measured without significant investment in facilities and training.

In the final chapter I evaluate the approaches presented in the thesis and discuss future applications.

Table of Contents

Chapter 1 - Introduction

The evolution of a homoiohydric system that enabled plants to maintain hydration with a limited supply of water was essential to the ecological success of plants in the terrestrial environment (Raven, 1977). Bathed in the necessary water and resources to survive and procreate, the algal progenitors of land plants had little concern of desiccation and nutrient acquisition, but on land these resources were harder to acquire, not least because they were spatially separated – CO_2 (and light) in the aerial environment, and water and nutrients in the ground below (Raven, 1977; Kenrick and Strullu-Derrien, 2014). In response, plants themselves became spatially segmented, evolving photosynthetic aerial parts protected from desiccation by a waterproof waxy outer layer, the cuticle, and rooting structures to extract water and to mine nutrients from the soil (Kenrick and Crane, 1997). Adjustable pores in the cuticle - the stomata - combined with extensive intracellular spaces, were early innovations that helped maximise CO_2 exposure to the photosynthesising cells (Raven, 1977; Kenrick and Crane, 1997).

An unavoidable consequence of exposing internal surfaces to air is that water vapour can be lost via the same pathway - in the words of the eminent botanist John Raven, "neither man nor nature has been able to produce a material which has a high permeability to CO_2, but a low permeability to H_2O" (Raven, 1977). To avoid the deleterious effects of desiccation, close coordination is required between stomatal conductance to water vapour and plant water status (McAdam and Brodribb 2012; Brodribb et al. 2017), and water must also be replenished at a rate equivalent to loss, thus there must be provision of a low-resistance pathway through which water can be efficiently supplied from the soil (Edwards, 2003). The evolution of the xylem, a network of hollow cells that facilitate the bulk flow of water from the soil to the shoots, enabled plants to maximise CO_2 uptake for photosynthesis (Edwards, 2003), while a diversity of adaptations in stomatal density, size, shape, and in the control of stomatal aperture, allowed plants to finely tune the permeability of the cuticle to optimise CO_2 uptake for water loss under different levels of water availability (Edwards, Kerp and Hass, 1998; Raven, 2002).

The xylem is composed of two types of cells for conducting water: tracheids, long single-celled conduits, and vessels, composed of series of smaller single-celled conduits called vessel elements (Tyree and Zimmermann, 2002). Tracheids were the only form of water-conducting cell in plants for the first 300 million years or so but are still present in most vascular plant groups today. Vessels, which almost certainly evolved from tracheids, are found almost exclusively in angiosperms (Tyree, Davis and Cochard, 1994). Both types of cell are lignified and dead with the apoplast removed at maturity.

The xylem represents one part of the plant vascular system, along with the phloem, and this system allows efficient transport of water and nutrients from the roots to the sites of photosynthesis, and from the sites of photosynthetic activity to the rest of the plant (via the phloem). Together with processes for optimising CO_2 uptake for water loss and protection of reproductive structures, the vascular system enabled vascular plants (the tracheophytes) to extend the range of habitats in which they lived and colonise the land to the extent we see today (Brodribb et al., 2009; Haworth, Elliott-Kingston and McElwain, 2011; McAdam and Brodribb, 2012).

The relationship between plant water status, water uptake, and stomatal conductance defines the evolutionary development and ecological diversity of plants in the terrestrial environment (Brodribb et al. 2017). Understanding how this relationship was resolved in the physiology of plant water relations is now of critical concern as plants face rising temperatures and increases in the occurrence, duration, and severity of droughts due to climate change (Allen et al., 2010; Parmesan and Hanley, 2015). For example, stem and leaf xylem differ significantly in structure and function as the xylem shifts in role from structural support and long-distance transport in the stem, to irrigation of the leaf lamina where the xylem branches into reticulated or longitudinal vein networks so that water can be efficiently delivered to the evaporating surfaces of the leaf mesophyll (Brodribb, Feild and Sack, 2010). We are now beginning to realise that the classical theory of hydraulic segmentation (Zimmermann, 1978), where peripheral and expendable organs are preferentially sacrificed during periods of stress to save more costly tissues, is not consistent among species (Skelton, Brodribb and Choat, 2017). This has important implications,

for example, in accurately representing species vulnerability to drought in climate vegetation models (Anderegg, 2014).

Methods of evaluating xylem traits are essential to understanding the physiology of water stress and the capacity of plants to tolerate drought and our ability to predict and model the effect of climate change on vegetation. This forms the overarching theme of this thesis, but before presenting the thesis aims and overview of chapters, and indeed the chapters themselves, it is useful to first provide some historical context to our understanding of plant water relations, the physiology of water transport and the causes of failure under drought conditions and implications in the context of climate change, and a review of the current methods of evaluating xylem traits relevant to drought survival.

1.1 Historical context

The first empirical understanding of water transport in plants can be traced back to the 18th century and the work of Stephen Hales. Hales pioneered the measurement of blood pressure in animals and was compelled to understand the equivalent mechanism in plants having noticed sap being driven from the cut end of a vine (Hales, 1727).

Before Hales there had been speculation as to the mechanism of water uptake in plants, most notably from Andrea Cesalpino, the Italian physician and botanist, who in 1583 correctly linked the uptake of water by roots with the way water is absorbed by cloth (Kramer and Boyer, 1995), but Hales was the first to seek a quantitative understanding through a series of cutting-edge experiments published in *Vegetable Staticks* in 1727, that measured rates of transpiration and absorption for different species and organs under a range of environmental conditions (Hales, 1727). His experiments demonstrated that rates of transpiration and absorption varied between species, were influenced by light and temperature, and that the source of pressure driving water transport in plants was not the same as in the vascular system of animals - there was, for example, no apparent pumping mechanism. He demonstrated a clear relationship between the absorption of water in the roots and the transpiration of water from the leaves, and linked the movement of water with capillary action and

root pressure (Hales, 1727). Indeed, it is quite remarkable given how close the description to the accepted cohesion-tension theory of water transport, that it was over a century before any more significant progress was made. Nonetheless, in the 19th century several key processes involved in vascular transport became understood, including diffusion, osmosis, permeable and selective membranes, and turgor. In addition to a more detailed understanding of the link between water absorption and transpiration (Kramer and Boyer, 1995) these developments culminated in the publication of Henry Dixon and John Joly's seminal paper of 1895 describing the cohesion-tension theory of sap ascent in plants (Dixon and Joly, 1895).

1.2 Water transport and the cohesion-tension theory

1.2.1 Water transport

There are two processes by which water uptake and transport occurs in plants: diffusion and pressure-driven bulk flow (Taiz and Zeiger, 2006).

Diffusion occurs because of the random movement of molecules colliding in a solution, and assuming all else is equal, probability dictates that molecules will move from a region of high to low concentration as they mix and assume a random distribution (Taiz and Zeiger, 2006). The rate of movement, C_R, can be described using Fick's first law (Fick, 1855):

$$C_R = -D_S \frac{C_S}{L}$$

where D_S is the diffusion coefficient of the substance, C_S is the concentration gradient, and L is the distance. From this we can derive the time, T, it takes for diffusion to occur over a distance, L:

$$T = \frac{L^2}{D_S}$$

This relationship indicates that the speed of diffusion decreases dramatically with increasing distance, and that water transport over a long distance must occur by a process other than diffusion. Over shorter distances diffusion is useful, and in combination with pressure-driven flow caused by cell turgor, provides the process of

osmosis by which water and solutes enter into cells and are transported from cell to cell (Taiz and Zeiger, 2006).

Understanding long distance transport, and the mechanism by which the vast majority of water is moved in plants, brings us to the cohesion-tension theory. First the concept of water potential must be introduced, and this helps us describe water status and the forces acting on, and the direction of water movement in plants and soils (Taiz and Zeiger, 2006).

1.2.2 Water potential

Water potential (Ψ) represents the free energy of water per unit volume (Joules m^{-3}), and is therefore equivalent to a pressure. Ψ is typically reported in pascals (P; 1 newton per square meter) and usually in the range of megapascals (MPa; 1MPa = 10^6 Pascals). In its simplest form, Ψ integrates four components: the effect of dissolved solutes on a liquid (solute potential, Ψ_s), pressure (pressure potential, Ψ_p), gravity (Ψ_g), and the adsorption of water on a surface (matric potential, Ψ_m):

$$\Psi = \Psi_s + \Psi_p + \Psi_g + \Psi_m$$

Dissolved solutes reduce the free energy of water and thus Ψ_s is always negative, and reduces Ψ. Ψ_p describes the hydrostatic pressure of a liquid; if a liquid is compressed, Ψ_p increases, if a liquid is stretched, a tension is generated and Ψ_p becomes negative. Ψ_g describes the influence of gravity, which exerts a downward force on the liquid as it increases with height. Ψ_m is associated with the electrostatic attraction of water to a surface, and is typically excluded from studies of water potential, as we shall do here, because it bears little influence on water potential until water is a very thin film. In thin films of water the effect becomes substantial, but is then more usefully represented in changes in Ψ_p and Ψ_s, especially in the context of capillarity, as we shall see below.

Water moves from high to low total Ψ. Applying this to diffusion, for example, we can see that a solution of water with a higher concentration of dissolved solutes has a more negative Ψ_s, and thus a lower Ψ, and therefore water will move to this solution

from one with a lower concentration as the solutes diffuse the down the concentration gradient in accordance with Fick's first law.

1.2.3 The cohesion-tension theory

The cohesion-tension theory describes the extraction of water from the soil and subsequent flow through the plant via a gradient of Ψ established in the leaves by a process of evaporation and capillary action (Dixon and Joly, 1895).

Capillary action is the spontaneous movement of water in a capillary – a space such as a pore or tube. The movement is caused by the electrostatic attraction and adsorption of water to the walls of the surrounding container which causes the air-water interface to curve (the meniscus) and exert a pull on the surface layer (Taiz and Zeiger, 2006). The interaction of water molecules at the air-water interface results in a strong surface tension that resists and transfers the pull back through the water column causing water to be drawn further into the capillary (Zimmermann, 1983). The hydrostatic tension ($-\Psi_p$) generated by capillarity is related to the surface tension of water (T; 7.28 x 10^{-8} MPa m), the radius of the capillary (r) and the contact angle between the meniscus and container wall (α; Tyree and Sperry, 1989):

$$\Psi_p = \frac{-2T\cos\alpha}{r}$$

Thus the narrower the capillary the greater the pulling force.

During transpiration, water evaporates from the cell walls of the leaf mesophyll into the intracellular spaces, then out through the stomata on the leaf surface (Zimmermann, 1983). Cell walls are made of an intricate matrix of cellulose microfibrils that represent a vast network of nano-scaled capillary pores that generate a substantial $-\Psi_p$ and low Ψ (Zimmermann, 1983). Indeed, given a pore 20nm in diameter the theoretical pull is 14MPa (Hacke and Sperry, 2001).

Soil and leaf water are connected via a continuous column in the xylem, and as water evaporates from the cell walls of the leaf mesophyll into the intracellular spaces of the leaf lamina, capillary action in the cell walls resists the receding meniscus and

tension is transferred down the water column through the xylem conduits, and more water is drawn from the soil (Zimmermann, 1983; Hacke and Sperry, 2001).

It is important to realise the distinction between, for example, water sucked through a straw in a glass, and water drawn from the soil via the leaves. In the first instance, there is practically no tension within the water itself as it is drawn up through the straw - the electrostatic forces of attraction between water molecules are immense, well in excess of 100MPa (Pickard, 1982), and the resistance of the straw is negligible, and thus the water moves through the straw as one.

Conversely, water flow in plants encounters substantial resistance in the soil to leaf pathway (Sack and Holbrook, 2006). The soil itself, like the walls of the mesophyll, represents a vast microstructure of pores and crevices that contribute a substantial source of capillary resistance to water flow into the plant, especially under drought conditions, as we shall see below. Water also encounters hydraulic resistance as it flows along the multitude of narrow xylem conduits, in accordance with Hagen-Poiseuille's law of laminar flow:

$$R_{\mathrm{L}} = \frac{128\,\eta}{\pi {D_{\mathrm{L}}}^4}$$

where η is the viscosity index of water (1.002×10^{-9} MPa s at 20°C) and D_{L} is the conduit diameter. Water also encounters resistance as it flows between conduits (Pickard, 1982) and Ψ_g (the influence of gravity) adds a resistance equivalent to 0.01 MPa per metre of height (Ryan and Yoder, 1997), dependent on water density.

The net effect of these resistances is that the water column - the water bonds themselves - become stretched, placing xylem water in a volatile 'metastable' state that renders the xylem highly susceptible to the explosive growth of bubbles in the presence of nucleation bodies (Sperry and Tyree, 1988).

1.3 Drought and water transport failure

1.3.1 The risks of metastable water

Metastable water in the xylem should boil (Zimmermann, 1983). That is, tiny bubbles trapped in the microscopic crevices of the xylem should rapidly expand as their internal vapour pressure becomes greater than their surface tension and the declining (and ultimately negative) pressure outside (Pickard, 1982). Xylem water does not boil, however, because xylem development excludes air, and air bubbles in the soil water are filtered at the roots, although dissolved air remains (Zimmermann, 1983). Vapour bubbles can form de novo in a metastable water column, a process known as cavitation, but this requires a tension in excess of 20 MPa (Caupin and Herbert, 2006), substantially more tension than is typically experienced by plants (Sperry and Tyree, 1988). Nonetheless, this illustrates the precarious nature of a system operating at a tension below atmospheric pressure and the risk of exposure to external air.

A system operating at a tension below atmospheric pressure that is at risk of exposure to external air is precarious because air can easily enter the xylem due to damage (herbivory, weather, etc.), or forced out of solution in cold environments where xylem water freezes and then thaws (Sperry, 1993). Once a conduit has been exposed to air it rapidly transitions and becomes embolised, a term often, and confusingly used interchangeably with cavitation, and without a system in place to stop embolism from spreading to neighbouring conduits, any slight damage to the xylem would risk the integrity of the entire network (Sperry and Tyree, 1988).

1.3.2 Protection from hydraulic failure

Protection from hydraulic failure is given by bordered pits - porous structures in the xylem cell wall that facilitate water flow between adjoining conduits (Sperry and Tyree, 1988). Pits are regions where modified primary cell wall is exposed through an opening in the secondary cell wall, which is thickened and overarches to create a pit chamber (Choat, Cobb and Jansen, 2008). In angiosperms and some conifers, water flows through the pores of the primary wall and middle lamella, while in the most conifers the primary cell wall and middle lamella differentiates into a centrally

thickened, non-porous region, the torus, suspended by a ring of highly porous fibres called the margo (Choat, Cobb and Jansen, 2008).

The remarkable mechanisms by which pits prevent the spread of embolism is different for torus-margo pits vs pits with a homogenous membrane. For torus-margo pits, the sudden pressure differential between an embolised and non-embolised conduit causes the margo to deflect against the pit border opening, causing it to shut like a valve and preventing the passage of air (Tyree and Zimmermann, 2002; Cochard et al., 2009; Delzon et al., 2010). In pits with a homogenous membrane, as the embolising conduit fills with air and water is drawn into surrounding conduits, the receding air-water interface reaches the pit membrane and breaks into small menisci at the opening of each pore and is drawn in (Tyree and Zimmermann, 2002; Choat and Pittermann, 2009). Pore capillarity arrests the receding meniscus as the surface tension balances the pressure difference across the pore (Sperry and Tyree, 1988). The resulting barrier is only broken when the pressure difference exceeds safety thresholds.

1.3.3 Exceeding safety thresholds

The biophysical properties of the pits can only be effective when co-ordinated with the tensions experienced by the xylem; as with any safety valve, the operating range should be appropriate to the system being protected. If the pit pores are too large then the capillary force will be too weak to prevent the propagation of air through the pit membrane, and if the torus-margo pit is not sufficiently robust to withstand the pressure differential, then it could deform, rip or dislodge and allow air to pass through the margo (Sperry and Tyree, 1988).

Critically in the context of drought, pits will also fail if the xylem tension exceeds their capacity. Xylem tension is predominantly influenced by two sources – vapour pressure deficit (VPD) and soil water (Taiz and Zeiger, 2006). VPD represents the difference in vapour pressure between the intracellular spaces of the leaf and the atmosphere. Increases in VPD due to changes in temperature and humidity will cause a higher rate of evaporation from the leaf mesophyll and reduce leaf Ψ. As soil moisture declines, solutes in plant cells become concentrated and Ψ_s becomes more negative, as does Ψ_p due to capillarity as water recedes deeper into the geometry of

the soil microstructure. Soil and xylem water potential are part of the same continuum, and so as soil Ψ declines so does xylem Ψ.

Both of these processes risk driving xylem Ψ to critical thresholds of membrane pore failure. In response to increasing VPD, plants can reduce stomatal aperture, or close the stomata entirely, thereby increasing stomatal resistance to diffusion and reducing transpirational flux (Jones and Sutherland, 1991; Cochard et al., 2002; Brodribb and Holbrook, 2003). This can also buffer moderate declines in soil Ψ, but under excessive conditions when the stomata have already closed, and soil Ψ continues to decline, there is little the plant can do to stop xylem Ψ reaching critical pore thresholds, other than physically disconnecting the roots from the soil (North and Nobel, 1997, 1998).

Once pit safety thresholds have been exceeded, embolism propagates through the xylem, uncoupling conduits from the water column and reducing xylem hydraulic conductance (Sperry and Tyree, 1988). Loss of conductance caps rates of transpiration and photosynthesis (Brodribb and Feild, 2000), thus recovery is slowed, growth rate is diminished, susceptibility to pests and pathogens increases, and die-back ensues (McDowell et al. 2008; Anderegg et al. 2015). 50-90% losses of conductivity are fatal (Blackman, Brodribb and Jordan, 2009; Brodribb and Cochard, 2009; Urli et al., 2013).

1.4 Xylem vulnerability and climate change

Xylem vulnerability is commonly assessed as the Ψ resulting in a 50% loss of xylem conductivity (P_{50}; Sperry & Tyree, 1988). Across species, this P_{50} ranges from ~-1 MPa to -18 MPa (Choat et al., 2012; Larter et al., 2017) - an incredible tension close to theoretical thresholds of cavitation (Larter et al., 2017) - reflecting a diversity of adaptations to different levels of water availability. In general, gymnosperms can tolerate higher tensions than angiosperms, and species from xeric environments tend to have a lower (more negative) P_{50} than those from more mesic environments, a pattern that can be reflected across species distributions as well (Maherali, Pockman and Jackson, 2004; Choat et al., 2012; Brodribb et al., 2014; Larter et al., 2017).

The hydraulic safety margin (HSM) is the difference between the P_{50} and the minimum Ψ typically experienced in the field and represents the degree to which plants normally operate near dangerous levels of hydraulic failure (Choat et al., 2012). Broad-scale analysis of HSMs across species indicate that plants operate within remarkably narrow safety margins (Choat et al., 2012). This may be surprising, but also a logical corollary of evolutionary optimisation - if safety comes with a cost, as suggested by Choat et al. (2012), then maintaining a system far in excess of the xylem tensions typically experienced would reduce fitness as more energy is invested in embolism resistance/recovery than growth and reproduction.

Under climate change, where new conditions of drought and heat can push plants beyond their normal range of operation, narrow safety margins are a considerable cause for concern (Choat et al. 2012). And indeed, widespread drought-induced forest decline due to climate change is already a global phenomenon (Allen et al., 2010; Allen, Breshears and McDowell, 2015).

The HSM is currently the best predictor of drought-induced mortality (Anderegg et al., 2016), and the inclusion of species HSMs is seen as a vital component in the next generation of trait-based models predicting the effect of climate change on plants (Anderegg et al. 2016; Anderegg et al. 2015; Soudzilovskaia et al. 2013; Skelton et al. 2015). Accurately representing the vulnerability of plants using the HSM depends on the number of accurate and reliable P_{50} values and the spatial and temporal variability of P_{50} due to genetic and phenotypic variation, ontogeny, season and plant development (Anderegg, 2014). These axes of variation have been explored in remarkably few studies, yet the evidence indicates there is a range of variation with some species showing significant variation across their distribution (Schuldt et al., 2016) while others appear to be remarkably consistent across broad distributions and environmental clines (Lamy et al., 2014).

Assessing within-species variance in xylem vulnerability is also critical for identifying drought-tolerant genotypes that can be used for agriculture (Tester and Langridge, 2010) and in assisted migration (Aitken and Whitlock, 2013), which is increasingly being seen as one of the only viable methods of protecting key species under climate change (Aitken and Bemmels, 2016).

Thus a significant number of xylem vulnerability measurements are required, yet to date the most comprehensive dataset of measurements contains values for only 384 angiosperms and 96 gymnosperms (Choat et al., 2012). For context, in Australia, a continent likely to be one of the most adversely affected by higher temperatures and drought under climate change (Butt, Pollock and Mcalpine, 2013; Booth et al., 2015), less than 15 of the 900 species of eucalypts that dominate the vegetation have been assessed for xylem vulnerability (Choat et al., 2012; Blackman et al., 2017).

Methods of assessing xylem vulnerability are critical to increasing the number measurements. These will now be reviewed.

1.5 Measuring xylem vulnerability

Assessing xylem vulnerability can be divided into two parts: inducing embolism and measuring embolism (Cochard et al., 2013).

1.5.1 Inducing embolism

Currently there are three methods of inducing embolism in the xylem: dehydration, air-injection and centrifugation (Cochard et al., 2013).

Dehydration is the most widely used method of inducing embolism (Cochard et al., 2013). It is simple and easy to implement, does not require additional equipment, and most closely matches the natural process of drought-induced decline in plant Ψ. For *in-situ* (Breda et al., 1993) or potted plants (Tyree and Yang, 1992) water can be withheld, and excised segments can be air-dried naturally (Sperry, 1986) or under controlled environmental conditions (Kikuta, Hietz and Richter, 2003).

The main limitation of the approach is the inability to control the sample water potential, which is primarily driven by the rate of dehydration, but also osmotic and physical changes in the cells caused by decline in turgor (Taiz and Zeiger, 2006). This has two implications. The first is that the speed of a vulnerability assessment is limited by the rate of water loss, and for some species it can take many days to complete a cycle of dehydration. Secondly, if using a Scholander pressure chamber to destructively measure water potential (Scholander, 1964), then multiple sample

sections must be sacrificed to track the water status of the sample. This is necessary to target a range of Ψ sufficient to produce a valid vulnerability curve (Sperry, Donnelly and Tyree, 1988). Thus the approach can be both labour and sample intensive. Alternative psychrometric methods of assessing Ψ can provide regular and automated measurements within a single sample (Rodriguez-Dominguez et al., 2018), and can therefore reduce the overall number of measurements. However, the cost of a commercial psychrometer, which can be in the region of several thousand dollars, can be prohibitive.

In centrifuge and air-injection approaches the pressures necessary to induce embolism can be precisely controlled and generated in the sample (Crombie, Hipkins and Milburn, 1985; Sperry and Tyree, 1990; Holbrook, Burns and Field, 1995). Air-injection works on the principle that the force acting on the menisci of the air-water interface at the pit membrane is equivalent whether derived from tension in the water column drawing the meniscus in, or from positive pressure in the adjoining air space pushing the meniscus in (Tyree and Sperry, 1989). Thus by applying positive air pressure embolism can be induced in the sample. Initially this was achieved by inserting one end of the sample in a pressure chamber and applying pressure (Crombie, 1983; Sperry and Tyree, 1990), but was later improved by the provision of a double-ended pressure chamber (the 'pressure-sleeve' method; Cochard et al., 1992; Salleo et al., 1992), in which a stem segment can be fitted such that the ends protrude from either side. This means the sample can be connected in line with apparatus to measure conductance while precise increments of pressure are simultaneously applied using a gas regulator to induce embolism (Cochard, Cruiziat and Tyree, 1992; Salleo et al., 1992).

Air-injection is a popular method that is still widely used (Cochard et al., 2013), and has also been adapted to measure embolism thresholds in individual vessels by using a microcapillary to precisely apply the necessary pressure (Melcher, Zwieniecki and Michele Holbrook, 2003; Choat et al., 2005).

Centrifuge techniques, as the name suggests, use centrifugal force to generate tension in the xylem by spinning the sample to precise velocities in a rotor (William et al., 1995). Early centrifuge designs were only used to generate the tension (Alder, 1997), after which the sample was removed so that the presence of embolism could be

assessed by other means. In later designs (Cochard et al., 2005; Li et al., 2008), and in particular in the 'Cavitron' implementation (Cochard et al., 2005), the system was adapted so that the conductance of stem segments could be simultaneously measured by maintaining both ends of the cut segment under water, and then inducing flow by increasing the volume of water at one end and creating a pressure differential (Cochard et al., 2005).

The most significant limitation of centrifuge and air-injection methods is the susceptibility to an 'open-vessel' artefact caused by the presence of vessels open at one or both ends of the pressurised segment (Torres-Ruiz et al., 2014). This is most likely due to the introduction of nucleation bodies into open vessels that extend close to the centre of rotation and can result in a significant loss of conductance at higher water potentials leading to an overestimate of vulnerability (Cochard et al., 2013). In centrifuge systems that combine measurements of conductance, the open-vessel artefact places a limit on the maximum length of vessel that can be measured, which must be less than the diameter of the rotor (Cochard et al., 2013).

Centrifuge and air-injection techniques are faster, use significantly less sample, and are less labour intensive than the other approaches mentioned. However, they require specialised equipment, and in the case of centrifuge-based systems, are limited to a few specialised facilities because the equipment is costly to build and setup, and training is required to ensure safety during measurement because of the inherent dangers of high-velocity rotors. Indeed, one solution to the open-vessel artefact is simply to build larger diameter centrifuges, but a significant investment in engineering and cost is required to ensure their stability and safety, and currently there is only one centrifuge capable of accommodating stems 1m in length (Charrier et al., 2018).

1.5.2 Measuring embolism

The simplest method of evaluating the presence of embolism is by observing axial sections of xylem through a microscope (Sperry, 1985), and indeed this method was used by early researchers to confirm the presence of air in the xylem (Haines 1935). Although the method is simple, it is also highly susceptible to artefacts because it is difficult to prepare sections without embolising functional conduits (Cochard et al.,

2013), or dissolving embolisms and filling unfunctional conduits (Lewis, Harnden and Tyree, 1994). It is also labour and thus time intensive and the end result is a limited field of view. For all these reasons other less challenging methods with better resolution are favoured.

Adding dyes such as crystal violet, safranin, and copper sulphate to the transpiration stream and taken up through functional conduits during active transpiration, or by applying moderate pressure (Newbanks, Bosch and Zimmermann, 1983; Sperry, 1986; Jacobsen et al., 2007), can very simply and effectively differentiate between functional and non-functional conduits (Hietz et al., 2008), and indeed can provide quite detailed spatial resolution considering the simplicity of the method. Although xylem staining is still in use today, the procedure is labour intensive, has low temporal resolution, and is susceptible to artefacts because the stain can spread to non-functional conduits (Newbanks, Bosch and Zimmermann, 1983).

Scanning electron microscopy (SEM), and in particular low-temperature SEM (CryoSEM), uses a focused beam of electrons to scan the surface of small sections of xylem tissue and provide unparalleled definition and spatial resolution of embolised conduits and structure of bordered pits (Zimmermann, 1983; Canny, 1997; Choat, Cobb and Jansen, 2008). The main limitation of SEM is the difficulty in preparing samples without influencing the xylem microstructure and inducing embolism (Cochard et al., 2015), the limited field of view, plus the cost and access to equipment, and the inability to capture dynamic processes (Choat, Cobb and Jansen, 2008). For these reasons SEM is impractical for routine study, but excellent for in-depth studies of xylem anatomy and physiology (for example see Li et al., (2016)).

Magnetic resource imaging (MRI) was the first technique to provide non-invasive three-dimensional visualisation of embolism in the xylem (Holbrook et al., 2001). MRI works by manipulating strong magnetic fields to align water molecules (or indeed any other polar molecule) such that they share a combined magnetic field (Kathiravan, 2013). Radio waves are applied to the magnetic field causing the molecules to deflect and resonate, and when the radio emission is removed the molecules are released to their previous orientation and energy is liberated as radio waves (Kathiravan, 2013). The radio emissions are captured by receiver coils, and an image is constructed using the signal intensity (Kathiravan, 2013). Samples are

scanned in slices resulting in 2D image stacks that can be combined to produce a final tomographic 3D image (Kathiravan, 2013).

The spatial resolution of MRI (~20μm) is only sufficient for imaging larger conduits, and scan times per slice are typically too large (>15 mins) to capture dynamic processes in detail (Tötzke et al., 2013). Additionally, working with strong magnetic fields adds practical limitations, for example electronic and metal devices cannot be near or attached to the sample during scans, and sample preparation can be difficult and laborious because samples must be fitted into the bore of the MRI magnet (Tötzke et al., 2013). MRI is costly and access to equipment is limited, and for xylem studies MRI is generally now deprecated in favour of other methods such as high-resolution x-ray computed microtomography (MicroCT) that offer higher resolution and faster scan times.

MicroCT functions much like standard x-ray imaging except that multiple beams are fired through the sample from different angles and combined to generate a more detailed image of the internal structure (Choat et al., 2016). MicroCT produces 3D tomographic images constructed from multiple image slices. The resolution of MicroCT (< 2μm) is much higher than MRI, and the scan times can be significantly faster which enables high resolution capture of dynamic processes.

MicroCT is currently seen as the 'gold standard' for *in-vivo* xylem visualisation (Venturas, Sperry and Hacke, 2017), and has generated some of the most remarkable and highly resolved images of the xylem and sequences of xylem physiology in action (Brodersen et al., 2013). The main limitations of MicroCT are the narrow field of view, typically just a few millimetres, and the cost and access to equipment (Cochard et al., 2013; Venturas, Sperry and Hacke, 2017). It is also difficult to distinguish between non-embolised active conduits, and functional but non-conductive immature conduits, thus the percentage of functional xylem lost to embolism can be underestimated (Perez-Donoso et al., 2006; Jacobsen and Pratt, 2012; Jacobsen et al., 2015).

X-ray beams from synchrotron facilities harvested as a by-product of particle acceleration using in MicroCT provide the fastest scan times and highest resolved low-noise images, however access to these facilities is costly, competitive and thus

very limited (Nolf et al., 2017). Smaller laboratory-based MicroCT solutions are rapidly improving in quality and affordability, but are still currently too prohibitively expensive for most labs, plus there is a trade-off in scan times and resolution (Nolf et al., 2017).

Neutron radiography (NR) is a non-destructive imaging technique based on neutron absorption. Neutrons have a weak affinity for most materials but a strong affinity for hydrogen-containing compounds, and are therefore particularly sensitive to water and organic matter (Nakanishi and Matsubayashi, 1997). NR has been used to measure sap flow and root uptake from soils in plants (Oswald et al., 2008; Matsushima et al., 2009), but currently has only been used in one study to image xylem embolism (Tötzke et al., 2013). The resolution of NR is comparable to MRI and thus only capable of imaging larger conduits, however it can provide sufficient temporal resolution to image dynamic processes in 2D, and there is increasing capacity for 3D tomographic visualisation at a useful temporal resolution (Tötzke et al., 2017), although this has yet to be applied to the study of xylem vulnerability. For assessing xylem vulnerability MicroCT provides higher resolution than NR for the same cost and effort, but for some experimental setups, and especially for the study of plant and soil interactions and water uptake (Oswald et al., 2008; Tötzke et al., 2017), the unique properties of neutron absorption are useful.

Acoustic emissions (AEs) underpinned much of the early work investigating water stress in plants (Milburn and Johnson, 1966; Milburn, 1973; West and Gaff, 1976). As a conduit embolises the rapid transition causes vibration and acoustic emission in the audible to ultrasonic range which can then be recorded and analysed (Ritman and Milburn, 1988). AEs offer a number of benefits over other techniques; the assessment is non-invasive, provides high temporal resolution, and acoustic detectors are relatively inexpensive and can be attached to a plant *in-situ* to allow for active monitoring of drought stress. However, the significant limitation of the approach is that although the number and frequency of AEs correlates well with drought stress (Nolf et al., 2015), not all AEs emanate from embolising conduits, for example they can be the result of secondary processes related to drying, such as cell wall shrinkage, or embolism occurring in cells other than the xylem, such as parenchyma and fibres (Ritman and Milburn, 1988; Cochard and Tyree, 1990; Nolf et al., 2015).

Other methods are typically used in favour of AE analysis because of the ambiguity in emission source, however, recent studies have demonstrated that advanced analysis and filtering of acoustic signals can distinguish between embolism and non-embolism events with a relatively high degree of accuracy (Wolkerstorfer, Rosner and Hietz, 2012; Nolf et al., 2015).

One of the most promising techniques for assessing xylem vulnerability is the recently developed 'optical method' (Brodribb et al. 2016), which is based on evaluating visible-spectrum light transmission through the xylem. Embolised conduits reflect more light than water-filled conduits because of the additional air-water interfaces and with sufficiently bright light transmission or reflection the subtle changes in light intensity that accompanies the transition to embolism can be detected using a standard light sensor (Brodribb et al. 2016). Working in the visible spectrum offers a significant reduction in the complexity and cost of equipment necessary to detect embolism formation *in-vivo*, offering a cost effective, non-invasive and potentially more accurate and reliable alternative to existing methods. The approach is still in its infancy and only a handful of studies have applied the technique (Brodribb et al. 2017; Brodribb et al. 2016; Brodribb et al. 2016; Skelton et al. 2017; Hochberg et al. 2017; Johnson et al. 2018), however comparisons with bench-mark methods indicate it is both reliable and accurate for assessing both stem (Brodribb et al. 2017) and leaf (Brodribb et al. 2016) xylem.

Finally, approaches that measure the loss of conductance (K) associated with embolism formation are the most widely used (Cochard et al., 2013), most cost effective and accessible methods of assessing species vulnerability using stem, leaf, and root xylem. In stem or root segments K can be determined by inducing water flow from a connected water reservoir and measuring the flow rate (mmol of water s^{-1}) for a given head of pressure (MPa) (Sperry, Donnelly and Tyree, 1988). This is normalised by segment length to give specific hydraulic conductivity (k; mmol s^{-1} MPa^{-1} m^{-1}). For segments with low resistance, flow can be induced by simply raising the reservoir above the stem segment to create a pressure differential, while for segments with higher resistance positive pressures (Tyree et al., 1995) or a vacuum (Kolb, Sperry and Lamont, 1996) can be used to induce flow.

In detached leaves or shoots, water flow from a connected reservoir can be induced via rehydration when the stomata are closed (the 'rehydration method') (Brodribb and Cochard, 2009), or via transpiration when the stomata are open (the 'evaporative flux method') (Yang and Tyree, 1993; Sack and Scoffoni, 2012). Leaf Ψ provides the driving force, and the flow rate is determined by measuring the amount of water taken up divided by the duration of uptake. An alternative method of determining the flow rate is to route the water through a tube of known conductance, which can then be used to calculate the flow rate using the pressure drop across the tube measured via an in-line pressure transducer (Brodribb and Cochard, 2009). Leaf K (K_{leaf}) is normalised by leaf area (mmol s^{-1} MPa^{-1} m^{-2}). Whole-plant K can be determined using sap-flow measurements divided by the difference in leaf and soil water potential, and root K can be measured using similar methods for detached shoots but with vacuum or positive pressure as the driving force (Marshall, 1958; Granier, 1985; Steinberg, van Bavel and McFarland, 1989).

A variant of the hydraulic conductance approach is to measure volume of air in the stem or leaf (the 'pneumatic method'; Pereira et al. 2016; Ennajeh et al. 2011), which increases proportionally with the decline in K due to embolism.

It should be noted that all invasive methods that involve cutting the xylem can be susceptible to an artefact relating to xylem exposure (Wheeler et al., 2013). Although segments are cut under water to ensure that exposed conduits are not immediately embolised on contact with air, the presence of air on the cutting blade or in exposed air spaces surrounding the cut can also seed embolism in exposed conduits under some conditions. Although precautionary steps can be taken to eliminate or mitigate the issue (Wheeler et al., 2013), it highlights the risk of using invasive techniques to measure a system inherently sensitive to exposure.

To summarise:

- Xylem sections and xylem staining are simple approaches for identifying embolism, but are labour intensive, susceptible to artefacts and provide only low temporal and spatial resolution.
- SEM, MRI, MicroCT and NR are advanced techniques that can deliver exceptional spatial and temporal resolution, but are only suitable for in-depth

study of xylem anatomy and physiology because of equipment and facility costs, limited access to equipment, and the time and difficulty in preparing and measuring samples.

- Centrifuge and air-injection methods can precisely the generate tensions needed to induce embolism and are thus much faster and less sample intensive than techniques that used dehydration. Systems that allow for conductance to be simultaneously measured while tensions are applied can provide the only viable high-throughput assessments of xylem vulnerability, but come at the cost of only being able to measure stem segments of short-vesseled species because of physical limitations and the risk of artefacts.

- Measurements of conductance used in combination with sample dehydration can provide reliable, accurate and cost-effective evaluations of xylem vulnerability, but can be sample intensive if using a Scholander pressure chamber to measure water potential, or less sample intensive, but expensive, if using a commercial psychrometer.

- The optical method is non-invasive and can be used to measure both stem and leaf xylem, is not susceptible to any 'open-vessel' artefacts and therefore applicable to both short and long-vesseled species, and can provide a high degree of spatial and temporal resolution. However, the approach is still only recently developed.

1.6 Thesis aim and chapters

As we have seen, the biophysical properties of the xylem set ultimate thresholds of drought tolerance (Zimmermann, 1983), and the HSM, which incorporates the P_{50}, a standard metric used to evaluate xylem vulnerability to hydraulic failure (Choat et al., 2012), is the best predictor of survival (Anderegg et al., 2016), and therefore vital for predicting drought-induced mortality due to climate change. However, the current number of vulnerability assessments is woefully inadequate to accurately represent vegetation in the next generation of climate change models (Anderegg et al. 2016; Anderegg et al. 2015; Soudzilovskaia et al. 2013; Skelton et al. 2015), both in breadth and sufficient resolution to capture the variation in vulnerability that may be

present among species populations and across distributions, or as a result of plant age and development (Anderegg, 2014).

As discussed, few of the current methods available are capable of high-throughput assessments, and of these there are limitations in equipment availability, accessibility and affordability and, most crucially, in the type of plants that can be evaluated, which are limited to stem sections of short-vesseled species. Thus there is a significant gap in capacity for measuring herbaceous species, including grasses and most crop plants, and of the majority of angiosperms.

Conductance-based techniques provide the right combination of broad accessibility, affordability, robust measurements, and capacity to measure short- and long-vesseled species using stem, leaf or root xylem, but the procedure can be time-consuming and sample intensive.

Thus the research aim of the thesis was to determine: *Is it possible to find a technique can be used for accurately measuring the vulnerability of xylem to embolism in large numbers of species or individuals.*

This question has been addressed in the following chapters:

Chapter 2 – ***Using a new 'single-point' approach to assess relative differences in vulnerability***

In this chapter I explore the application of a novel 'single-point' approach for assessing intraspecific variation in xylem vulnerability that can significantly reduce the number of measurements required for a conductance-based assessment.

Chapter 3 - ***CaviScan: automated embolism imaging using a desktop scanner***

In chapter 3 I develop protocols to expediate the process of assessing xylem vulnerability with the optical method and a desktop scanner, and use the procedure to investigate variation in vulnerability associated with ontogeny and plant development.

Chapter 4 - ***CaviCam and OpenSourceOV.org: a new device and online resource for assessing drought tolerance in plants***

In chapter 4 I present a new platform for assessing the drought tolerance of plants with a capacity to significantly increase the number of vulnerability assessments via affordability, broad accessibility, and the capacity to measure both stem and leaf xylem in short- and long-vesseled species.

Chapter 5 - ***Conclusion***

In the final chapter I evaluate the approaches presented in the context of the research aims and discuss future applications.

A note on chapter format

Chapter 2 has been published but has been modified here to include additional detail in the methods and a new introduction that better fits the narrative of the thesis.

Chapter 2 – Using a new 'single-point' approach to assess relative differences in vulnerability

A version of this chapter has been published in *Functional Plant Biology*:

Lucani CJ, Brodribb TJ, Jordan G, Mitchell PJ (2018) Intraspecific variation in drought susceptibility in *Eucalyptus globulus* is linked to differences in leaf vulnerability.

2.1 Introduction

Predicting how vegetation responds to increasing water stress is a critical factor in addressing the challenges of a rapidly changing climate (Allen, Breshears and McDowell, 2015). Incorporating key functional traits in the next generation of dynamic global vegetation models is seen as a vital step in improving forecast accuracy, especially those that underpin plant productivity and response to drought (Soudzilovskaia et al., 2013; Yang et al., 2015). Xylem traits are relevant to both of these aspects of plant function (Brodribb, 2009), setting physical limits to photosynthetic capacity (Nardini and Salleo, 2000; Aasamaa, Sõber and Rahi, 2001), as well as vulnerability to hydraulic failure (Sperry and Tyree, 1988; Tyree and Zimmermann, 2002) - a key determinant of drought-induced mortality (McDowell et al., 2011).

Catastrophic hydraulic failure occurs because once the stomata are closed, declining moisture within the soil continues to influence the pressure gradient in the xylem (Sperry and Tyree, 1988; Tyree and Zimmermann, 2002). The resulting increase in water column tension eventually causes gas emboli to form and propagate (Sperry and Tyree, 1988; Tyree and Zimmermann, 2002), reducing capacity to transport water, leading to acute water stress and eventual death by catastrophic desiccation (Tyree and Zimmermann, 2002). The tension at which this occurs is species dependent and highly variable between taxa and across environments (Brodribb and Hill, 1999; Maherali, Pockman and Jackson, 2004; Nardini and Luglio, 2014). Plants appear to function close to hydraulic failure thresholds (Choat et al., 2012),

highlighting the importance of this trait in predicting the effects of climate change on woody plants (Delzon and Cochard, 2014; Anderegg et al., 2016).

Xylem vulnerability is typically reported as the tension (P; negative pressure, -MPa) associated with a 50% loss in conductivity (P_{50}), and there are an increasing number of P_{50} values in the literature (Cochard and Delzon, 2013) and plant trait databases (Kattge et al., 2011) that can feed into dynamic global vegetation models. Understanding within-species variance is critical to improving the accuracy of vegetation models (Thuiller et al., 2008), yet few studies quantify intraspecific variation in xylem traits (Maherali & DeLucia, 2000; Martínez-Vilalta et al., 2009; López et al., 2013) and evidence suggests this variation could be substantial (Anderegg, 2014). Furthermore, most evaluations of vulnerability are limited to stem xylem, with few exploring vulnerability in the leaves, and fewer still assessing intraspecific variation in this trait (Blackman et al., 2017). Leaf xylem is functionally diverse (Blackman, Brodribb and Jordan, 2012; Brodribb et al., 2014), may be more vulnerable than stem xylem and has an integral role in plant productivity, contributing a substantial resistance in the hydraulic pathway (Sack and Holbrook, 2006) that sets upper limits on stomatal conductance and photosynthetic capacity (Brodribb and Holbrook, 2005).

Traditional methods of assessing leaf vulnerability are labour intensive because analysis of the non-linear relationship between leaf hydraulic conductivity (K_{leaf}, mmol m^{-2} s^{-1} MPa^{-1}) and leaf water potential (LWP) requires multiple measurements of K_{leaf} throughout the full range of LWP. This typically precludes the larger sample sizes required for a genetically robust assessment of variation within species. We hypothesised however, that if K_{leaf} in unstressed plants and the slope of the logistic response of K_{leaf} to LWP found most evergreen species (Blackman, Brodribb and Jordan, 2012; Brodribb et al., 2014) was consistent, it might be possible identify relative differences in vulnerability by comparing hydraulic conductance at a common water potential close to the inflection point where the response is most sensitive (Fig. 2.1). This would significantly reduce the number of measurements per individual and allow for a much broader assessment of variation.

Eucalyptus globulus Labill. is an ecologically and economically important forest tree species with high genetic variation (Dutkowski and Potts, 1999; Freeman et al.,

2001) that exhibits significant intraspecific variability in a number of traits, including drought susceptibility (Dutkowski and Potts, 2012). Using this novel single-point approach we compare intraspecific variation in leaf vulnerability between two populations of *E. globulus* with contrasting drought tolerance *in situ* and in a common garden.

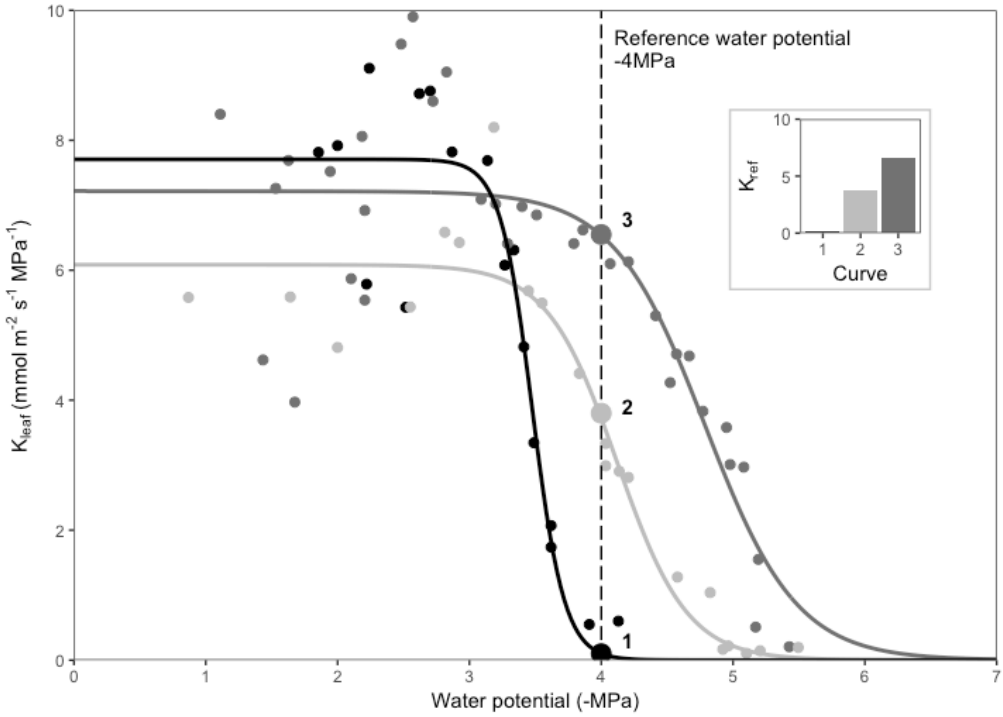

Figure 2.1 Three examples representing the range of vulnerability curves (sample points plus fitted 3-parameter sigmoid) from a reference dataset of 21 vulnerability curves (Table 2.2). Inset bar chart shows differences in K_{leaf} at a reference water potential of -4MPa (vertical dashed line; K_{ref}).

2.2 Materials and Methods

2.2.1 Study sites

Dutkowski & Potts (2012) identified significant differences in drought susceptibility between genetically and geographically distinct subraces of *E. globulus* Labill. on the basis of the percentage leaf loss that occurred in field trials in Western Australia after a severe summer drought. On the basis of this analysis we selected two localities from provenances in the trial that were at the extremes of drought tolerance: Blue Gum Hill (43.047°S, 146.871°E) in Southern Tasmania (drought-sensitive); and Jeeralang North (38.345°S, 146.509°E) in the Strzelecki Ranges in Victoria (drought-tolerant; Table 2.1).

Foliage samples of *Eucalyptus globulus* ssp. *globulus* were taken for analysis from populations *in-situ* and progeny of the same populations grown in a common garden field trial operated by Sustainable Timber Tasmania at Oigles Road (43.161°S, 146.859°E) near the Blue Gum Hill area in Southern Tasmania (Table 2.1).

2.2.2 Sampling

From the common garden in Southern Tasmania, a single tree from each of 9 families (progeny from the same parent tree in the native stand) from Jeeralang North and 10 families from Blue Gum Hill were sampled. From *in-situ* stands at Jeeralang North in the Strzelecki Ranges and Blue Gum Hill in Southern Tasmania, 8 mature trees, at least 80-100 metres apart, were randomly sampled thus limiting confounding genetic and environmental differences. For all sites 3-4 sun-exposed branches ~2-3m in length were cut from a canopy height of 3-6 metres. Only branches that did not show significant stem or leaf damage were sampled. Cut branches were immediately bagged and sealed in thick clear plastic bags with damp tissue paper to reduce transpirational water loss and maintain photosynthetic function. From each branch a minimum of 3 fully expanded leaves from separate branchlets were used for measurement of hydraulic conductance. Sampling took place during the wetter months June-August 2014 and April 2015 to minimise risk of native embolism.

Table 2.1 Sampling sites and associated bioclimatic parameters (Fick and Hijmans, 2017). In Tasmania: Oigles Road (the common garden), Blue Gum Hill, Tolmans Hill and Pepper Hill. In Victoria: Jeeralang North in the Strzelecki Ranges.

Locality	Oigles Road *Common Garden*	Blue Gum Hill	Tolmans Hill	Pepper Hill	Jeeralang North
Region	Southern Tasmania	Southern Tasmania	Southern Tasmania	North-East Tasmania	Strzelecki Ranges, Victoria
Latitude	43.1611°S	43.0469°S	42.9102°S	41.6322°S	38.3448°S
Longitude	146.859°E	146.8714°E	147.3205°E	147.8313°E	146.5085°E
Annual Mean Temperature	10.39	10.36	11.11	9.89	12.53
Mean Diurnal Range (°C) *Mean of monthly (max temp - min temp)*	7.63	7.98	6.89	8.97	9.33
Isothermality (°C)	49.25	49.28	46.88	46.70	46.90
Temperature Seasonality standard deviation *100	275.79	287.06	281.02	362.23	369.73
Max Temperature of Warmest Month (°C)	17.70	18.00	18.00	18.60	22
Min Temperature of Coldest Month (°C)	2.20	1.80	3.30	-0.60	2.10
Temperature Annual Range (°C)	15.50	16.20	14.70	19.20	19.9
Mean Temperature of Wettest Quarter (°C)	7.47	7.32	8.03	5.92	10.1
Mean Temperature of Driest Quarter (°C)	13.73	13.83	13.60	14.35	17.1
Mean Temperature of Warmest Quarter (°C)	13.73	13.83	14.63	14.35	17.1

Table 2.1 continued

Locality	Oigles Road *Common Garden*	Blue Gum Hill	Tolmans Hill	Pepper Hill	Jeeralang North
Mean Temperature of Coldest Quarter (°C)	6.87	6.70	7.72	5.47	7.9
Annual Precipitation (mm)	1307	1255	885	927	993
Precipitation of Wettest Month (mm)	146	139	93	104	107
Precipitation of Driest Month (mm)	68	64	55	42	45
Precipitation Seasonality (%mm) Coefficient of Variation	22.07	22.28	16.64	20.94	21.57
Precipitation of Wettest Quarter (mm)	413	396	256	287	302
Precipitation of Driest Quarter (mm)	229	217	182	175	177
Precipitation of Warmest Quarter (mm)	229	217	184	175	177
Precipitation of Coldest Quarter (mm)	390	374	241	285	289

2.2.3 Determining a reference water potential

In order to establish a reference water potential that could be used to compare vulnerability among the sampled populations, we calculated the median P_{50} from a pre-existing dataset of complete vulnerability curves for 21 individuals (Table 2.2), spanning a range of the species distribution in Tasmania (Table 2.1). Sampling was as above, but with ~30 leaves measured per branch, or across multiple branches. This pooled dataset, although substantial, was not in itself appropriate to assess intraspecific variance, but was suitable for indicating a general range in vulnerability for the species. Vulnerability curves were constructed using measurements of K_{leaf} determined using the rehydration method (Brodribb & Cochard, 2009; and described below). The median inflection point for this dataset was 4.121±0.074 MPa and on this basis we concluded that -4 MPa provided an appropriate reference water potential to distinguish relative variation in vulnerability in the species.

2.2.4 K_{leaf} at the reference water potential (K_{ref})

Branches were dried on a bench until the reference water potential (–4 MPa) had been reached. To aid the process of drying the sample to the target water potential, a computer program was written in PHP (PHP Group, http://php.net, accessed 27 July 2016) and JavaScript that estimated drying times using inputted values of time and measured water potential. Each branch was placed in a separate bag and the bag was given a unique ID and entered into the program. Periods of sample drying (per bag) were precisely managed by the program which provided sound alerts when a configurable duration of bench drying had elapsed. The sample was then returned to the bag and the bag sealed so the water potential could equilibrate. An equilibration timer was set to 15 min and once equilibration was complete the program emitted another alert and a leaf was extracted from the sample and wrapped in damp tissue and transferred to a pressure chamber to determine the water potential. The water potential was then entered into the program. If the water potential had yet to reach the reference water potential then another drying timer was set and the procedure was repeated until the reference water potential had been reached. Samples that had reached the reference water potential were left sealed in their bags until they could be measured.

To estimate drying times, once the program had a minimum of two values of water potential and drying time it was able to fit a linear regression and then use the terms of the regression to calculate the estimated water potential for the next configured drying time. Different phases of drying (e.g. pre- and post-turgor loss) were identified by sequentially applying a linear regression to each point and evaluating changes in the standard error of the regression. Where the standard error of the regression exceeded a configurable threshold value (typically 10%) then a new phase was assumed and a new regression was fitted to the current phase. Only the terms of the most recent regression were used to predict the water potential at drying time.

Although changes in temperature and humidity would have affected estimates of water potential, we found that the conditions of the laboratory were stable enough for this not to substantially affect drying rates for most of the samples and they were not incorporated into the program to keep the software and tracking procedure as simple as possible.

Overall the software worked well in estimating water potential from drying rates and less than 5% of samples were excluded because they exceeded the target water potential (by more than 10%). The software source code and instructions for use (including screenshots) and installation have been made available online at https://github.com/clucani/DYB.

K_{leaf} was determined using the rehydration method (Brodribb and Cochard 2009). Briefly, a leaf was excised under water and immediately connected to a flow meter for ~30s to continually monitor the rate of water uptake (mmol s^{-1}) as the leaf rehydrates. The driving force for uptake, and consequently K_{leaf}, can be measured at two points during rehydration: once at the initial point of rehydration (when the sample is first connected to the flow meter) by using the LWP of a neighbouring leaf, which is expected to be in equilibrium until the point the measured leaf was excised, and a second time when the leaf is disconnected from the flowmeter by measuring the LWP of the leaf itself. The driving force is often confused to be the difference between the initial and final LWP, but in fact the two values of K_{leaf} are the product of instantaneous measurements of flow rate and driving force at separate points in the rehydration. In theory K_{leaf} should be constant throughout rehydration and therefore the initial and final K_{leaf} values should be similar, thus they provide a

measure of internal verification and if the values substantially differ then this might suggest an incorrect water potential measurement or a blockage in the xylem or flow meter apparatus. In this study where the initial and final values differed by >30% they were discarded (~1% of cases). A mean of initial and final K_{leaf} (which differed overall by a mean of 6.4%) was used in the analysis. More information about the technique can be found on PrometheusWiki at http://prometheuswiki.org/tiki-index.php?page = Non-steady+state+rehydration+to+determine+leaf+hydraulic+conductance%2C+vulnerability+and+capacitance (accessed 30 May 2017).

2.2.5 K_{max}

To test for a systematic difference in the slope of the relationship between K_{leaf} and LWP between the sites, maximum values of leaf hydraulic conductance (K_{max}) were determined using the mean of three replicate leaves per sample for three sampled trees at each locality. K_{max} were determined from measurements of K_{leaf} at a LWP > -3MPa, the water potential range preceding incipient K_{leaf} decline within the reference dataset (Fig. 2.1).

2.2.6 Statistical analysis

Differences in K_{ref} and K_{max} between localities were analysed using one-way ANOVA. The untransformed data satisfied assumptions of normality (Shapiro-Wilk test) and homogeneity of variance (Bartlett test). K_{ref} data was rank-transformed to achieve normality, and *t*-tests were used to identify significant comparisons. Differences in variance were tested using a pair-wise Bartlett test on untransformed data and correlations were tested using Pearson's test on untransformed data. Analysis was performed with and without a Southern Tasmania outlier identified in the common garden. All analysis was performed using R version 3.2.4 (R Development Core Team, 2011).

Table 2.2 P_{50} (MPa) values for 21 vulnerability curves of *Eucalyptus globulus* sampled from Oigles Road, Blue Gum Hill, and Tolmans Hill in Southern Tasmania, and Pepper Hill in North Eastern Tasmania (Table 2.1). Mean P_{50} for the sample dataset is 4.12±0.34 MPa with a median value of 4.121±0.074 MPa.

Number	Site	P_{50}
1	Oigles Road	3.491
2	Blue Gum Hill	3.587
3	Oigles Road	3.635
4	Oigles Road	3.896
5	Blue Gum Hill	3.952
6	Blue Gum Hill	3.966
7	Oigles Road	3.971
8	Pepper Hill	4.011
9	Oigles Road	4.018
10	Oigles Road	4.094
11	Oigles Road	4.121
12	Tolmans Hill	4.125
13	Oigles Road	4.136
14	Oigles Road	4.146
15	Blue Gum Hill	4.163
16	Oigles Road	4.231
17	Tolmans Hill	4.435
18	Tolmans Hill	4.541
19	Oigles Road	4.543
20	Tolmans Hill	4.600
21	Tolmans Hill	4.859

2.3 Results

At the reference water potential of 4 MPa K_{ref} differed significantly among provenances ($F_{3,31}$ = 7.3, P = 0.011), but only when sampled *in situ* and not in the common garden (Table 2.3; Fig. 2.2).

In the wild, Strzelecki trees had a higher K_{ref} (4.250±0.411 mmol m^{-2} s^{-1} MPa^{-1}) than trees in Southern Tasmania (3.094±0.736 mmol m^{-2} s^{-1} MPa^{-1}; P<0.01), and although the trend was similar in the common garden, there was no evidence to suggest the differences were genetic, either with (P=0.764) or without outliers (P=0.765) included in the analysis. K_{ref} was lower for Strzelecki trees in the common garden (3.432±0.449 mmol m^{-2} s^{-1} MPa^{-1}), providing marginal evidence (P=0.08) that differences were due to plasticity. Removing the Southern Tasmania outlier from the common garden this effect became highly significant (P=0.011).

Table 2.3 Number of trees (families) sampled, mean K_{ref} (mmol m^{-2} s^{-1} MPa^{-1}), and LWP (MPa) for Jeeralang North and Blue Gum Hill provenances *in-situ* and in the common garden. Values are means ± SD.

Provenance	Jeeralang North		Blue Gum Hill	
	In-situ	Common Garden	*In-situ*	Common Garden
No. trees	8	9	8	10
K_{ref}	4.250 (±0.083)	3.432 (±0.060)	3.094 (±0.124)	3.402 (±0.137)
LWP	4.018 (±0.004)	4.060 (±0.010)	4.034 (±0.031)	4.056 (±0.008)
K_{max}	5.884 (±0.645)	5.265 (±0.359)	6.113 (±0.728)	5.266 (±0.468)

There was no evidence that the differences observed were the result of differences in the target water potential, which was consistent between provenances at all sites ($F_{3,31}$=0.8, P=0.48). Although K_{ref} was weakly correlated with water potential (0.30; P=0.07), analysis of covariance indicated the provenance x site interaction was still significant, even allowing for the covariation with water potential, and this did not affect the significance of differences observed. Additionally, there were no differences in K_{max} between any of the provenances at any of the sites ($F_{3,8}$=0.9,

P=0.48) providing no evidence of intrinsic differences in conductance between localities.

Within-provenance variation in K_{ref} was consistent between *in-situ* and common garden plants. Comparing provenances, Southern Tasmania had a significantly larger variance (1.03; *P*<0.05) than Strzelecki both *in-situ* (0.17) and in the common garden (0.2).

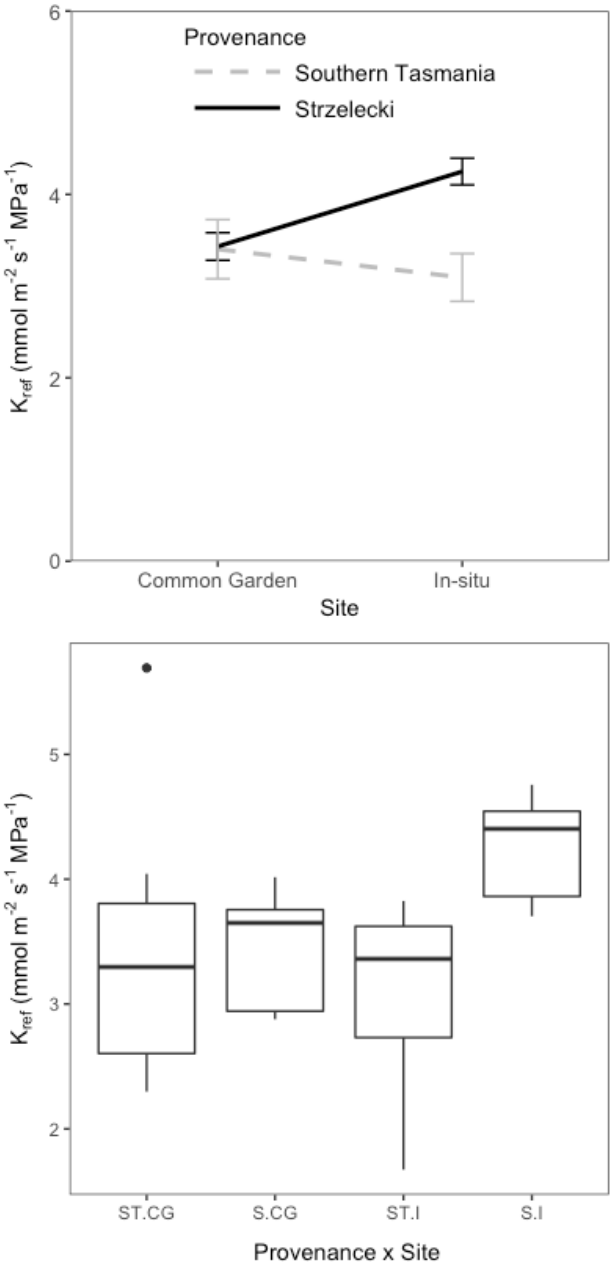

Figure 2.2 *Top panel* Provenance by site plot showing mean K_{ref} (K_{leaf} at a 4MPa) ± SE for two provenances of *Eucalyptus globulus*: the Strzelecki Ranges in Victoria (solid dark line) and Blue Gum Hill in Southern Tasmania (dashed grey line), in a common garden and in the native stand. *Bottom panel* Box and whiskers plot of the same data (ST=Southern Tasmania, S=Strezlecki, CG=common garden, I=*in-situ)* with outliers identified. Mean K_{ref} was significantly higher than Southern Tasmania *in-situ* (*P*<0.01) and marginally higher than Strzelecki in the common garden (*P*=0.08). No difference between provenances in the common garden.

2.4 Discussion

Using a novel single-point approach we assessed intraspecific variation in leaf vulnerability between two provenances of *E. globulus* with contrasting drought tolerance (Toro et al., 1998; Dutkowski and Potts, 1999). By comparing K_{leaf} at a critical point in the vulnerability curve (K_{ref}) we were able to detect significant phenotypic differences between trees in the wild, and provide marginal evidence of plasticity in trees from the Strzelecki Ranges in Victoria. Analysis of K_{max} provided no evidence to suggest that differences in K_{ref} were the result of systematic differences in traits that might affect water flow at any LWP, such as native embolism, vessel density, size and distribution, or pit frequency and porosity (Tyree, Davis and Cochard, 1994). Differences in the vulnerability of the extra-xylary pathway (Scoffoni et al., 2017) are unlikely in this case, given the strong relationship between embolism formation and K_{leaf} decline previously observed in the species (Brodribb et al. 2016).

In line with trends in drought susceptibility among provenances in *Eucalyptus globulus* trials in Western Australia (Dutkowski and Potts, 1999) and Spain (Toro et al., 1998), our results indicate that trees from the Strezlecki Ranges in the Victoria are less sensitive to water stress than trees from Blue Gum Hill in Southern Tasmania. A physiological cause for the observed drought damage in the trials in Western Australia and Spain was not determined; our results suggest that underlying differences in xylem vulnerability are likely to be the cause. Indeed there is mounting evidence that hydraulic traits are tightly linked with survival and species distribution in *Eucalyptus* and closely related genera. Surveys of hydraulic traits in eucalypt species growing along clines of water availability have found strong relationships in hydraulic architecture and efficiency (Pfautsch et al., 2016), water use efficiency (Givnish et al., 2014), Huber value (Carter and White, 2009), and stem xylem vulnerability (Zolfaghar et al., 2015).

In contrast to studies by Dutkowski and Potts (1999) and Toro et al. (1998) we found no evidence of a genetic effect; however, given the relatively low sample size, and that our data looks to be trending in the same direction, a larger sample size may help to reveal an underlying genetic signal. Evidence for plasticity was stronger, and

indeed genetic differences in phenotypic plasticity have been identified in other eucalypt species (McLean et al., 2014).

In *Corymbia*, a closely related genus, Blackman et al. (2017) recently found evidence of plasticity in leaf vulnerability in response to temperature, with cooler-climate populations more vulnerable than those from warmer climates. Dutkowski & Potts (1999) also found that drought tolerance was most closely associated with temperature, and that the Strzelecki Ranges, the most drought tolerant of the subraces, had the highest seasonal variation in temperature, in addition to the least rainfall in winter, compared with Southern Tasmania, which had some of the lowest seasonal temperature variation. Temperature is undoubtedly a strong candidate as a driver of selection, and the increased evaporative demand associated with higher temperatures is a well-known driver of drought induced mortality (Adams et al., 2009; Matusick, 2012; Will et al., 2013; Mitchell et al., 2014), and a key component in the most severe of recent drought events (Breshears et al., 2005).

An interesting result was the difference in K_{ref} variation between the two localities. Blue Gum Hill had especially broad ranges in K_{ref} values in both the common garden and in the natural stand, including many values higher than those found in Strzelecki. Although this is based on a small sample size this suggests the presence of some remarkably drought tolerant individuals in the relatively mesic environment of Southern Tasmania. One possible explanation for this is the complex environmental and genetic history of the species, heavily influenced by cycles of glaciation in south eastern Australia during the Quaternary, which included periods of aridity and temperature depression (McKinnon et al., 2004). If past cycles of aridity selected for tougher xylem, then it is possible that some of these drought-tolerant genotypes could remain today under an environment where selection against drought tolerance is weak, which may be likely in the relative cool and wet of Southern Tasmania, if any trade-offs in productivity (and influence on fitness) are minimal (Gleason et al. 2016). Conversely in Victoria, where selection for hydraulic traits appears to be strong, we may be seeing a more constrained expression of diversity in vulnerability. A broader survey of individuals and larger sample size would be necessary to confirm the hypothesis.

Although the approach demonstrated a capacity to identify variation in vulnerability, there are limitations. Drying down multiple samples to a common water potential is challenging without software to keep track of the various drying rates, and determining an appropriate reference water potential is best derived from a sample set of full curves representing the range in variation for the sample group. Additionally, it is critical that K_{max} is consistent between populations to ensure that any differences in K_{leaf} at the reference water potential are not the result of pre-existing embolism or systematic differences in K among populations. For these reasons the approach is better suited for large-scale studies of variation in vulnerability.

Genetic variation in hydraulic traits in *Eucalyptus* have been explored in remarkably few studies (McLean et al., 2014; Pfautsch et al., 2016; Blackman et al., 2017) yet this is critical for understanding and predicting the effects of climate change on vegetation in Australia, which is particularly susceptible to extreme drought and heat under current and future climate scenarios (Butt, Pollock and Mcalpine, 2013; Mitchell et al., 2014). Eucalypts have poor seed dispersal and long generation times, and therefore have limited capacity to migrate or evolve to rapid climate change (Booth et al., 2015). Under these conditions phenotypic plasticity becomes a critical factor (Nicotra et al., 2010), highlighting the urgent need (Allen, Breshears and McDowell, 2015) for rapid phenotyping techniques and technologies.

Chapter 3 – CaviScan: automated embolism imaging using a desktop scanner

3.1 Introduction

Although the single-point approach presented in Chapter 2 may have benefits at scale it is less suitable, even counter-productive, for measuring smaller sample sizes and individuals. As an alternative to a conductance-based approach, the recently developed 'optical method' offers an exciting new approach for *in-vivo* imaging of embolism in the xylem (Brodribb et al. 2016), and its application as a high-throughput technique for assessing xylem vulnerability has yet to be explored.

The technique works by capturing images of the xylem at regular intervals over a period of time using transmitted or reflected light and analysing the subtle differences in light intensity that occur when conduits in the xylem embolise (Brodribb et al. 2016). Images of the xylem can be captured using a digital camera or a document scanner. The advantage of a document scanner is that it has a significantly larger field of view than a camera, and thus provides a means of imaging larger leaves and multiple samples.

The current limitations to imaging multiple samples in a scanner is that it is difficult to find all the features necessary to optimise the procedure within a single scanning software application, nor are some of the desirable features even available, to my knowledge, in any of the current scanning software applications. Desirable features include: 1) the ability to automate the scanning procedure and configure the interval between scans, 2) to set the duration or limit the number of scans, 3) to scan sub-regions (i.e. regions of interest; ROI) of the total scannable area, 4) to configure different settings (e.g. resolution, image type, etc) for each ROI, and 5) to configure the organisation of output folders and files.

In particular, the ability to use and configure different ROIs would be particularly useful. Although multiple ROI capability is available in some of the scanning software I tried it was either difficult configure (and in some cases quite bizarre in the manner of configuration), or incompatible or awkward to configure with the automation of scanning.

Of the software that did provide multiple-ROI capability, none allowed for the configuration of different scan settings per ROI. This would be useful, and indeed necessary if only one scanner was available, for scanning both leaves and stems on the same scanner. This is because leaves and stems are scanned using different light sources - leaves work best with light transmission, while stems work best with reflected light. It is worth noting that the capability for light transmission is only available on some scanners, typically provided as a feature for scanning transparencies (e.g. slides).

Scanning the entire scannable area at high resolution can take minutes, thus a significant benefit of multiple ROIs is that they can reduce the scan time by scanning only relevant regions. This increases the temporal resolution of embolism events. Without sub-region capability either the temporal resolution of embolism events must be traded for the number of samples imaged, or *vice-versa*, the number of samples imaged per scan must be reduced so that the time between scans is less.

The aim of this chapter was to develop a new process to meet the features outlined above. The process was then used to assess and compare the vulnerability to cavitation in leaves and stems and between juvenile and adult *E. globulus*.

Incorporating trait variability is an important dimension for accurately predicting climate-induced forest tree mortality, range-shifts, rates of adaptation, and changes in community assembly and biodiversity (Anderegg, 2014). In this context, studies are emerging that assess intraspecific variation across environmental gradients and between populations (Choat, Sack and Holbrook, 2007; Martínez-Vilalta et al., 2009; Lamy et al., 2014; Hajek et al., 2016; Blackman et al., 2017). Ontogenetic variation is another important axis of variability that has received little attention (Anderegg, 2014). After all, all individual metamers (individual plant segments) are variable to some degree, representing a continuum of morphological, anatomical and physiological changes, that accompany plant development from embryo to adult vegetative and reproductive phases towards senescence (Jones, 1999). Given the substantial changes in xylem anatomy that occurs during plant maturation it is surprising that few studies have assessed changes in xylem vulnerability associated with life history (Sperry and Saliendra, 1994; Pasquet-Kok, Creese and Sack, 2010).

Some of the most remarkable developmental transitions in plants occur in heteroblastic Eucalypt species. Among these, the Tasmanian Blue Gum (*Eucalyptus globulus* Labill.) presents a dramatic example of distinct juvenile and adult phases that transition at 1-3 years, marked by stark morphological and anatomical differences in the leaves and stems (James and Bell 2001; James and Bell 2000b). Adult leaves are isobilateral, alternate, amphistomatous, petiolated, vertically orientated, oblong, shiny, dark green in colour and grow on cylindrical stems, while juvenile leaves are opposite, dorsiventral, hypostomatous, sessile, horizontally orientated, broad, blue-grey/glaucous in colour, and grow transversely on quadrangular stems (Fig. 3.1). Juvenile and adult leaves also differ in their leaf anatomy (Johnson 1926; James et al. 1999; James and Bell 2001; James and Bell 2000a), gas exchange (James and Bell 2000b), photosynthetic chemistry (Velikova et al., 2008), and susceptibility to pests (Brennan et al., 2001; Rapley, Allen and Potts, 2004) and fungal pathogens (Dungey et al., 1997; Carnegie and Ades, 2005; De Little, Foster and Hingston, 2008). To our knowledge there are no studies comparing traits in juvenile and adult stems.

The timing of phase-change is adaptive (Jordan et al., 2000) and under strong genetic control (Jordan, Potts and Wiltshire, 1999), although across the broad distribution of the species the ecological significance appears to be variable (Jordan et al., 2000). Nonetheless, it seems clear that adult leaves have traits associated with xeromorphy that act to maintain or improve water use efficiency by minimising light interception and high temperature due to their vertical orientation (James and Bell 2000a; James and Bell 2000b; James and Bell 2001; James et al. 1999; Johnson 1926). Conversely, juvenile leaves have traits that are associated with maximising light interception and photosynthesis for growth (James and Bell 2000a; James and Bell 2000b; James and Bell 2001; James et al. 1999; Johnson 1926).

Given the close association between hydraulic traits and plant productivity (Brodribb, Feild and Jordan, 2007) and survival (Blackman, Brodribb and Jordan, 2009; Brodribb and Cochard, 2009; Urli et al., 2013), and evidence to suggest there may be differences in xylem vulnerability between juvenile and adult foliage in at least one other species (Pasquet-Kok, Creese and Sack, 2010), I hypothesised that the phase-change in *E. globulus* could also be associated with changes in xylem

vulnerability, and in particular that adults would be less vulnerable to drought-induced cavitation than juveniles, in keeping with a shift towards xeromorphy.

Figure 3.1 *E. globulus* adult and juvenile leaves and stems. *Left* Adult leaves are isobilateral, amphistomatous, petiolated, vertically orientated, oblong, shiny, dark green in colour and grow on cylindrical stems. *Right* Juvenile leaves are dorsiventral, hypostomatous, sessile, horizontally orientated, broad, blue-grey/glaucous in colour, and grow transversely on quadrangular stems.

3.2 Methods

3.2.3 Plant material and sampling

Three juvenile and three adult *E. globulus* plants were sampled in the wetter Winter months between July and August near the grounds of the University of Tasmania at 42°54'24.8"S 147°19'26.8"E.

From three adult trees 16-20 metres in height, a sun-exposed branch approximately 2-3 metres in length was sampled in the morning from a canopy height of 8-10 metres. For juvenile material, three 1-2 year old neighbouring plants were sampled by cutting whole plants at the base. Canopy cover at the sampling site was <10%, so there was little difference in light climate between juvenile and adult samples. Samples were immediately bagged after cutting and sealed in thick clear plastic bags to reduce transpirational water loss before the short walk back to the laboratory for measurement.

For each sample two leaves from opposite lateral shoots and two stems from a second set of opposite lateral shoots on the same branch/stem were measured. As a result, there were 6 trees, a total of 3 branches and 3 whole plants, 12 leaves and 12 stems.

3.2.4 Optical measurement of xylem vulnerability

Leaves and stems were securely attached to a document scanner (Perfection V800, EPSON) and entire leaves and section of stem ~10mm in length were scanned every 5 minutes at a resolution of 4200 DPI. For each stem section a small section of bark was carefully removed to reveal the intact xylem.

Water potential (WP; MPa) was measured automatically every 15 minutes using a psychrometer (ICT International, Armidale, NSW, Australia) attached to the main stem or branch within 1-2 nodes of the measured lateral shoots. Psychrometer values were confirmed every 4-6 hours with leaf measurements of WP using a Scholander pressure chamber. Given that the sample was disconnected from the soil and the stomata closed during the experiment, the WP of lateral shoots and the main stem were expected to be in equilibrium until catastrophic embolism resulted in compartmentalisation of vascular tissue. At this point conductivity would have been lost almost entirely.

Optical vulnerability was determined as described by Brodribb et al. (2016). Briefly, to quantify embolism, captured images were imported into ImageJ as a sequence (an ImageJ ‘stack’) and each image in the stack converted to an 8-bit grayscale image i.e. each pixel having a value from 0 (black) to 255 (white). Images were subtracted using the Image Calculator function and this produced a new result stack where differences between images are revealed as pixels having a value > 0. Noise was removed using an outlier function (the ‘Remove Outliers’ function in ImageJ) and by manual removal where it was clear that pixels were unrelated to an embolism event e.g. outside the venation, randomly distributed within the venation, or the result of insect movement or scanning artefact. In particular we encountered a pattern of banding caused by inconsistent speed in the movement of the scanner head. This was clearly identifiable and the associated pixels were manually removed. Embolism per image was quantified as the count of non-zero pixels divided by the total count of

non-zero pixels per sequence to represent % of total embolism. WP at the point of image capture was calculated using the terms of an appropriate regression model fitted to psychrometer measurements of WP over time. In all cases, regressions were linear because this fitted the data well. Leaves and branches were scanned until no cavitations were recorded for a period of > 3 hours, at this time it was assumed 100% of vessels were cavitated. The entire scan time was typically 30 hours. Xylem vulnerability was evaluated and compared using the WP resulting in a 12% (P_{12}), 50% (P_{50}) and 88% (P_{88}) increase in embolism area. P_{12} represents the WP that initiates air-seeding and relates to the lower threshold of pit membranes (Choat, Cobb and Jansen, 2008), and P_{88} the critical threshold of plant mortality (Urli et al., 2013). An advantage of the optical method is that these values could be taken directly from the processed data without fitting a regression model because of the short time interval between captures and the resulting large number of points in the curve. The WP range associated with the bulk of embolism events was analysed using the WP range $P_{88} - P_{12}$.

3.2.5 Controlling the scanning procedure using a new program – CaviScan.

The scanning procedure was defined and controlled using AutoIT© automation software (AutoIT, 2010) in combination with VueScan© scanning software.

VueScan is generic scanning software that can be used to control a significant number of common and uncommon scanners. Indeed, the point of difference for the product is that continues to support older models of scanner when they are no longer supported from OEM (operator equipment manufacturer) or operating system software.

AutoIT provides a scripting language that can be used to interface with software that runs on the Windows operating system. Traditionally the only way to programmatically interface with software such as VueScan is for the software developer to provide a programming library that contains the necessary functions. VueScan do not provide such a library. An alternative approach is to use automation software which interacts with software via its user interface. At a basic level this provides a way of accessing software features by directing, for example, a mouse pointer over to a location on the screen and emitting events (e.g. a click or double-

click) to activate a UI component (e.g. a button). At a more advanced level the software allows complex procedures to be defined by interfacing with the user interface on the basis of lower-level component IDs. Thus, for example, a button can be targeted using its component ID instead of by moving the mouse to the relevant position on the screen. One of the most significant benefits is that the computer can still be used for other tasks while the automation script is accessing the software; controlling the software using positioned mouse clicks requires that the software window be in the same position and that the mouse is not used during the procedure.

Using AutoIT a highly configurable and flexible script was developed: *CaviScan.* The script provides a number of configuration options for setting the scan interval, the length of time to repeat scans (the duration) and the output folder and filename format. The script is then divided into two routines: 1) pre-scan, and 2) the scanning procedure.

The pre-scan routine, as the name suggests, is run before the scanning procedure is executed and provides a way of issuing setup commands that will apply to the entire procedure. The scanning procedure routine defines the ROI(s) to be scanned and is repeated until the sequence is complete. The advantage of the two sections can be illustrated with the example of the light source selection (e.g. transmission for leaves and reflection for stems). If all ROIs are to be scanned using the same light source then the command for configuring the light source is better placed in the pre-scan routine rather than in the main scanning procedure where it would unnecessarily increase the scan time by repeating the steps to configure the light source options in the VueScan UI. Conversely if both leaves and stems are scanned in a cycle then the light source command would be required in the scanning procedure routine to alternate the light source.

Several functions are provided for defining the scan settings for each ROI in the scanning procedure, including a sample name, the dimensions of the ROI, the resolution, image type (8-bit grayscale, 16-bit colour, etc.) and file type (e.g. PNG, JPEG, etc.).

To obtain the dimensions of the ROI the user uses the VueScan interface and ROI tool to select the ROI and then copies the ROI dimension settings from the interface into the script.

CaviScan is activated by double-clicking the CaviScan script file. Once activated it runs a series of configuration procedures to setup VueScan to ensure the consistency of scans, for example by turning off features such as 'infrared dust filtering' which can result in subtle differences between scans, then runs the pre-scan routine and then repeats the scanning procedure routine until the designated time and at the interval provided in the configuration.

During the scanning procedure CaviScan configures the output folder and file name settings of VueScan so that files are organised in a useful structure that separates scan resolutions and image types.

To control multiple scanners using a single computer, a routine was added to the script initialisation process to 'attach' the currently active CaviScan script to the currently active and maximised VueScan software instance. Once attached the commands from CaviScan are only directed at the designated instance of VueScan, thus multiple instances, and therefore multiple scanners, can be controlled using multiple CaviScan scripts running on the same computer.

The CaviScan script and detailed operating instructions are provided online at https://github.com/OpenSourceOV/scanner-image-capture-instructions and https://github.com/OpenSourceOV/caviscan.

3.2.6 Statistical Analysis

A student's *t-test* was used to compare differences in P_{50} between juvenile/adult leaf *vs* stem, and between juveniles and adults with stem and leaf data combined. To satisfy assumptions of normality (Shapiro-Wilk) and homogeneity of variance (Bartlett), juvenile and stem P_{50} data was rank-transformed. Stem P_{50} data was not normally distributed owing to the similarity in vulnerability curves and could not be transformed to normality, therefore a non-parametric test (Mann-Whitney) was used to compare the median P_{50} value of adult leaves and stems, juvenile leaves and stems, and adult and juvenile stems.

P_{88} and P_{12} values were compared using one-way ANOVA and post-hoc pairwise t-tests on untransformed (P_{88}) and rank-transformed (P_{12}) data having met assumptions of homogeneity of variance and normality.

Differences in $P_{88} - P_{12}$ were analysed using one-way ANOVA on data untransformed, homoscedastic, and normally distributed.

A student's *t-test* was used to compare differences in leaf and stem coefficients of variation (*CV*) using combined P_{12}, P_{50}, and P_{88} values.

Differences in the slope of the fitted regression was analysed using a one-way ANOVA having satisfied assumptions of normality and homoscedasticity.

All analysis was performed using R version 3.2.4 (R Development Core Team, 2011).

3.3 Results

Juvenile leaves of *E. globulus* were more vulnerable than adult leaves (Fig. 3.2; Table 3.1), with a significantly higher mean P_{50} (-3.32±0.04 MPa; $P<0.05$) and P_{12} (-2.86±0.24 MPa; $P<0.05$) than adults (-4.44±0.06 MPa; $P<0.05$) and P_{12} (-3.99±0.01 MPa; $P<0.05$). There was no significant difference in vulnerability between juvenile and adult stems ($P=0.08$).

Per individual there were no significant difference between stems and leaves in P_{12}, P_{50}, or P_{88} (Table 3.2; Fig. 3.3). Indeed, the values were remarkably similar and across all samples P_{50} stem and leaf varied only by 9±4%, P_{12} by 12±3% and P_{88} by 6±5%.

Replicates per organ were also consistent, particularly for leaves, which had a mean *CV* of 0.04±0.03. Stem replicates were comparatively less consistent, but still had low variance, with a mean *CV* of 0.12±0.03.

When extreme values for embolism events are excluded (i.e. data were restricted to the range $P_{88} - P_{12}$ (Table 3.1) most embolisms occurred within a narrow 1MPa range (0.94±0.87 MPa for adults, 0.87±0.33 MPa for juveniles). Analysis of the

slopes of the fitted regressions (*b*; Table 3.2) indicated the formation and spread of embolism was consistent across all samples ($F_{3,8}$=1.3, *P*=0.33).

Comparing the *WP* resulting in the first embolism (WP_{first}) and last embolism (WP_{final}), in juveniles embolism initiated in the leaves and stems at the same *WP* (-3.80±0.33 MPa; P=0.68; Table 3.1, WP_{first}) and concluded at -4.90±0.17 MPa. In adults embolism initiated first in the stems (-2.25±0.33 MPa) and then in the leaves (-3.75±0.09 MPa; *P*<0.05; Table 3.1) and finished at -5.11±0.26 MPa. There was no significant difference in WP_{final} between leaves and stems for either adults or juveniles.

Comparing the WP_{first} between adults and juveniles, embolism initiated in juvenile leaves at -2.25±0.33 MPa, over 1 MPa earlier than adult leaves (-3.75±0.09 MPa, P<0.05; Table 3.1). There was no significant difference in WP_{final} between juvenile and adult stems, leaves, or stems and leaves combined.

Table 3.1 Leaf, Stem and combined Leaf and Stem P_{12}, P_{50} and P_{88} for juvenile and adult *E. globulus* (values are mean ± SE in brackets). *b* indicates the slope of the % embolism/WP regression. Values followed by the same letter are significantly different (*P*<0.05, * indicates *P*<0.01).

	Leaf, *n=3*	Stem, *n=3*	Combined, *n=6*
Adult			
- P_{12}	3.99 (±0.01) *e*	3.44 (±0.08)	3.72 (±0.13) *c**
- P_{50}	4.44 (±0.06) *b*	4.10 (±0.01)	4.27 (±0.08) *a**
- P_{88}	4.68 (±0.27)	4.64 (±0.27)	4.66 (±0.17) *d*
- WP_{first}	3.75 (±0.09) *f*	2.25 (±0.41)	3.01 (±0.38)
- WP_{last}	5.09 (±0.42)	5.13 (±0.38)	5.11 (±0.26)
- WP_{last} - WP_{first}	1.34 (±0.51)	2.88 (±0.65)	2.11 (±0.51)
- $P_{88} - P_{50}$	0.69 (±0.26)	1.20 (±0.20)	0.94 (±0.19)
- *b*	0.26	0.38	0.34
Juvenile			
- P_{12}	2.86 (±0.24) *e*	2.99 (±0.06)	2.93 (±0.15) *c**
- P_{50}	3.32 (±0.04) *b*	2.97 (±0.11)	3.15 (±0.09) *a**
- P_{88}	3.89 (±0.21)	3.72 (±0.45)	3.80 (±0.23) *d*
- WP_{first}	2.60 (±0.31) *f*	2.43 (±0.21)	2.52 (±0.17)
- WP_{last}	4.69 (±0.32)	5.10 (±0.09)	4.90 (±0.17)

- WP_{last} - WP_{first}	2.10 (±0.50)	2.67 (±0.12)	2.38 (±0.26)
- $P_{88} - P_{50}$	1.03 (±0.11)	0.71 (±0.24)	0.87 (±0.14)
- b	0.24	0.39	0.32

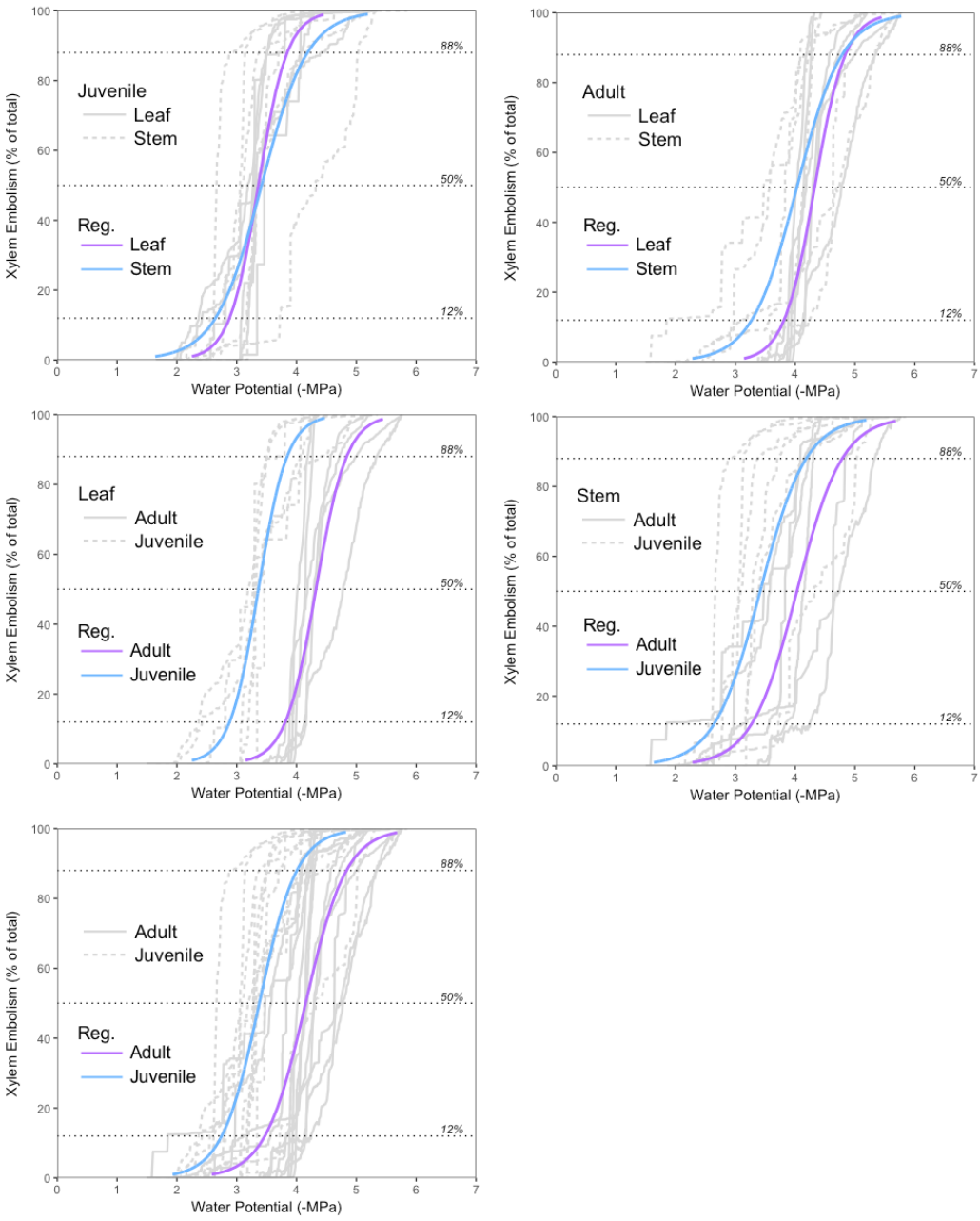

Figure 3.2 Comparison of juvenile and adult *E. globulus* stem and leaf vulnerability curves. Horizontal dotted lines indicate xylem embolism at 12%, 50%, and 88% of total xylem embolism. Solid coloured lines describe a logistic regression fitted to the data. *Top panels* Juvenile *vs* adult leaf (solid grey line) and stem (dashed grey line) reps with fitted leaf (solid purple line) and stem (solid blue line) regressions. *Middle panels* Same data as top panel grouped by organ: adult (solid grey line) *vs* juvenile (dashed grey line) replicates with fitted adult (solid purple line) and juvenile (solid blue line) regressions. *Bottom panel* Adult vs juvenile combining leaf and stem data with fitted adult (solid purple line) and juvenile (solid blue line) regressions.

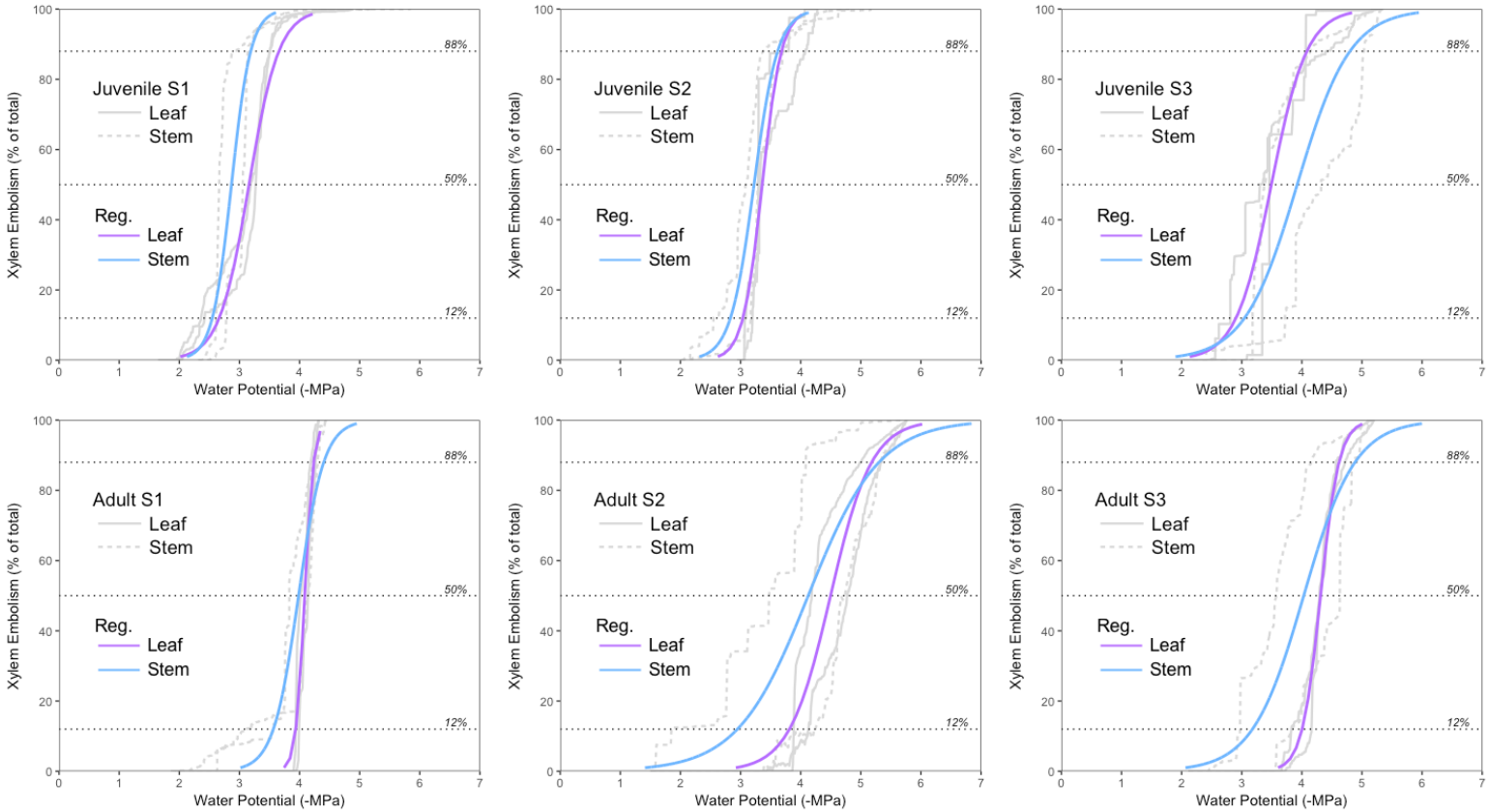

Figure 3.3 Vulnerability curves for three adult and three juvenile *E. globulus* plants. Plots show leaf (solid grey line) and stem (dashed grey line) replicates and fitted leaf (solid purple line) and stem (solid blue line) regressions. Horizontal dotted lines indicate xylem embolism at 12%, 50%, and 88% of total xylem embolism.

Table 3.2 A comparison of juvenile and adult *E. globulus* leaf and stem parameters, including water potential resulting in a 12% (P_{12}), 50% (P_{50}) and 88% (P_{88}) increase in embolism area, water potential at first (WP_{first}) and last (WP_{last}) embolism event, the ranges $WP_{last} - WP_{first}$ and $P_{88} - P_{12}$, and the slope coefficient (b) for the logistic regression model fitted to leaf and stem values (Fig. 3.2). Where applicable, values are shown as mean ± SE.

Adult sample	1		2		3	
	Leaf, *n=2*	Stem, *n=2*	Leaf, *n=2*	Stem, *n=2*	Leaf, *n=2*	Stem, *n=2*
Adult						
- P_{12}	3.97 (±0.03)	3.34 (±0.23)	4.00 (±0.13)	3.60 (±0.66)	4.00 (±0.18)	3.40 (±0.42)
- P_{50}	4.32 (±0.01)	4.12 (±0.77)	4.50 (±0.42)	4.10 (±0.86)	4.49 (±0.42)	4.10 (±0.91)
- P_{88}	4.22 (±0.04)	4.26 (±0.04)	5.17 (±0.18)	5.18 (±0.16)	4.64 (±0.07)	4.50 (±0.34)
- WP_{first}	3.94 (±0.00)	2.19 (±0.27)	3.66 (±0.22)	1.59 (±0.01)	3.67 (±0.07)	3.00 (±0.55)
- WP_{last}	4.31 (±0.01)	4.45 (±0.00)	5.76 (±0.01)	5.78 (±0.01)	5.20 (±0.01)	5.18 (±0.01)
- WP_{last} - WP_{first}	0.37	2.26	2.1	4.19	1.53	2.18
- $P_{88} - P_{50}$	0.25	0.92	1.17	1.58	0.64	1.10
- b	0.07	0.21	0.34	0.59	0.15	0.43
Juvenile sample	1		2		3	
	Leaf, *n=2*	Stem, *n=2*	Leaf, *n=2*	Stem, *n=2*	Leaf, *n=2*	Stem, *n=2*
- P_{12}	2.39 (±0.03)	2.70 (±0.08)	3.13 (±0.06)	2.86 (±0.31)	3.07 (±0.27)	3.44 (±0.27)
- P_{50}	3.39 (±0.12)	2.87 (±0.28)	3.35 (±0.01)	3.20 (±0.14)	3.24 (±0.06)	2.87 (±0.26)
- P_{88}	3.50 (±0.00)	3.03 (±0.11)	3.94 (±0.13)	3.54 (±0.16)	4.23 (±0.18)	4.59 (±0.45)
- WP_{first}	2.01 (±0.04)	2.43 (±0.06)	3.07 (±0.00)	2.07 (±0.02)	2.73 (±0.36)	2.80 (±0.39)
- WP_{last}	4.65 (±0.16)	5.09 (±0.05)	4.18 (±0.11)	4.95 (±0.23)	5.27 (±0.07)	5.26 (±0.09)
- WP_{last} - WP_{first}	2.64	2.66	1.11	2.88	2.54	2.46

Table 3.2 continued

Juvenile sample	1		2		3	
	Leaf, *n=2*	Stem, *n=2*	Leaf, *n=2*	Stem, *n=2*	Leaf, *n=2*	Stem, *n=2*
- $P_{88} - P_{50}$	1.11	0.33	0.81	0.68	1.16	1.15
- *b*	0.25	0.16	0.16	0.20	0.3	0.44

3.4 Discussion

By analysing visual changes in the xylem associated with embolism formation, we found that adult *E. globulus* leaves were less vulnerable to hydraulic failure by > 1MPa when comparing the xylem tension associated with a 12% and 50% increase in embolised conduits. We found no significant difference in vulnerability between juvenile and adult stems. The vulnerability of juvenile *E. globulus* has not been reported in the literature, but the P_{12}, P_{50}, and P_{88} of adult leaves measured here is consistent with reported values (Brodribb et al. 2016).

To our knowledge this is the first assessment of ontogenetic changes in xylem vulnerability in *Eucalyptus,* and the only ontogenetic study to compare both leaf and stem vulnerability.

Indeed, remarkably few studies have assessed drought effects in the early life history of plants, and most are restricted to tropical forest species (Delissio and Primack, 2003; Engelbrecht and Kursar, 2003; Bunker and Carson, 2005; Engelbrecht, Kursar and Tyree, 2005; Yavitt and Wright, 2008; Chaturvedi, Raghubanshi and Singh, 2013; Song et al., 2016) with some exceptions in maize (Khan et al., 2004), temperate woody species (Sack, 2004) and chaparral shrubs (Pratt et al., 2010).

In contrast to our results, in one of the few studies that have measured xylem vulnerability in juvenile and adult plants, Sperry and Saliendra (1994) found no difference in P_{50} between juvenile and adult *Betula occidentalis* when comparing roots, trunks and twigs, although they did note that significant differences in the shapes of the vulnerability curves above the P_{50} could confer an advantage to juveniles.

Differences in vulnerability in *Betula occidentalis* are unsurprising given that selective pressure for drought adaptation among riparian species is likely to be weak. Indeed, *Betula occidentalis* is not particularly known for drought tolerance (Gucker, 2012), and the reported P_{50} (Sperry and Saliendra, 1994) is among the weakest of known values (Choat et al., 2012). Conversely, Australian phyllodineous Acacia species exemplify xeromorphic drought adaptation to arid environments (Boughton, 1986), and in the closely related Hawaiian endemic *Acacia koa* (Brown et al., 2012;

Le Roux et al., 2014), a heteroblastic species, the bi-pinnate compound leaves of juveniles were found to be more vulnerable than adult phyllodes (Pasquet-Kok, Creese and Sack, 2010). However, in that study vulnerability was assessed using transpiring leaves and phyllodes, and as such any loss of conductance could be the result of changes in the extra-xylary pathway and not embolism formation (Scoffoni et al., 2017), as measured here, and therefore may not be directly comparable. Nonetheless, the suite of contrasting traits between juvenile and adult *Acacia koa* strongly suggests that water stress, growth and shade are key selection pressures maintaining heteroblasty in the species (Pasquet-Kok, Creese and Sack, 2010). Indeed, in closely related heteroblastic *Acacia melanoxylon* (Murphy et al., 2010; Brown et al., 2012) analysis of gas exchange and photosynthesis over a range of vapour pressure deficits demonstrates that the morphology and anisohydric behaviour of the juvenile compound bi-pinnate leaves help to minimise costs associated with light capture, allowing them to maximise growth in stems, trading off the relative safety of the isohydric adult phyllodes (Brodribb and Hill, 1993).

In *E. globulus* field trials, slow growth is associated with increased mortality (Chambers, Borralho and Potts, 1996), suggesting strong selection for growth traits. However, quantitative genetic analysis of growth and the timing of phase change among natural populations of *E. globulus* indicates a complex relationship across its broad distribution (Jordan et al., 2000). At exposed coastal sites (Wilsons Promontory in South East Australia and Cape Tourville in North-Eastern Tasmania) where high winds and salt spray are likely to cause high evaporative demand and water stress, early phase change is associated with slow growth, and indeed significant local genetic differentiation can be expressed over a remarkably short distance (~500m) in association with proximity to exposure (i.e. cliff base to exposed top; Jordan et al. 2000). In a separate study, broad-scale genetic analysis of drought damage in *E. globulus* confirms these populations are drought adapted (Dutkowski and Potts, 2012). However, this apparent trade-off between growth and drought tolerance is confounded at the wetter end of the distribution where *faster* growth can be associated with *early* phase change, although this appears to be related to pathogen preference for juvenile foliage and an increase in pathogens at wet sites (Jordan et al., 2000). In this context early phase change provides a means of escape from pathogen attack (Jordan et al., 2000). Presumably this would also have

impacted growth during the juvenile phase resulting in the relative increase in growth associated with the shift to adult foliage. In terms of mean annual precipitation and temperature (Table 3) our sampling site (near Hobart, Tasmania) falls roughly in the middle of the distribution for *E. globulus* (Kirkpatrick, 1975; Jordan et al., 1993) and is unlikely to be pathogen-affected, nor is the site particularly exposed.

Broad-scale analysis of trade-offs in efficiency for safety indicate the relationship is complex, as evidenced above, with strong evidence for and against a trade-off among and within clades (Gleason et al., 2016; Hacke et al., 2017). In *Eucalyptus* (not represented in the previous analyses), variation in stem vessel diameters appears to be adaptive and driven by climate and aridity more than growth (Pfautsch et al., 2016). Our results suggest that this apparent trade-off in safety and efficiency among stem hydraulic traits may only extend to the species level and that during ontogeny, leaf traits provide the critical means of adjusting to the prevailing conditions. Both adaptation and plasticity of leaf xylem vulnerability have been demonstrated in closely-related *Corymbia calophylla* in response to temperature (Blackman et al., 2017).

The lack of significant differences between juvenile and adult stem xylem is unsurprising given that much of the juvenile stem xylem will continue to supply leaves through the juvenile, transitional, and into the initial adult phase, until secondary growth replaces the bulk of functional conduits.

The cause of the observed differences in xylem vulnerability between juvenile and adult leaves is difficult to determine, but the contrast in P_{12}, and the consistency in the slope of the relationship between *WP* and embolism formation between juvenile and adult leaves, suggests a systematic difference in the air-seeding threshold of pit pores (probably due to membrane thickness (Li et al., 2016)), or changes in the total pit area per conduit (Wheeler et al., 2005; Hacke et al., 2006) are most likely.

In Australia, where Eucalypt-dominated vegetation is particularly susceptible to climate change (Butt, Pollock and Mcalpine, 2013), a better understanding of plasticity and adaptation to drought in both stem and leaves is needed to improve the accuracy of climate vegetation models. Indeed, the representation of juvenile and early-life history traits may better serve the accuracy of models than those of the

adult vegetative and reproductive phases. Seedling and juvenile plants are generally considered to be more susceptible to drought because their limited rooting depth restricts access to deeper reserves of soil water, but if this is also coupled with a more vulnerable xylem then the effect of increased drought and heat may be compounded, leading to an underestimate of drought impacts. This may be especially important given the critical role of juvenile plants in establishment, regeneration and species community composition (Barber, 1965; Bunker and Carson, 2005; Engelbrecht, Kursar and Tyree, 2005; Pratt et al., 2014). Eucalypts are well known for their capacity to recover from damage by re-sprouting at their base from specialised structures called lignotubers (Noble, 2001). Coppice and juvenile shoots do not share the same issue of rooting depth, but they do share the same morphology (Noble, 2001) and possibly the same vulnerability to hydraulic failure, with implications for regeneration under future climate scenarios (Pratt et al., 2014).

The CaviScan program worked well and reduced the complexity of scanner configuration, enabling both leaves and stems to be scanned on the same scanner with multiple scanners able to be controlled using a single computer. By integrating with the VueScan scanning software the CaviScan program has the capacity to interface most, if not all, desktop scanners, thus providing a widely available and consistent approach for automated scanning.

Although CaviScan demonstrated a significant capacity for use in a high-throughput setup using multiple scanners, the approach could be limited. Although CaviScan can maximise the use of the available scanning area, I found the procedure for fitting samples into the scanner difficult and time-consuming. Often branches had to be supported in awkward positions to achieve the right orientation of samples in the scanner. For leaves where one side may have better imaging than the other (for example if the vascular bundle or xylem is nearer one of the surfaces) this could be particularly challenging. Additionally I also encountered a number of scanning artefacts that manifest as patterns of banding in the image differences. The issue came and went and there did not seem to be a particular pattern that would help identify the cause. Possibly it might be the result of inconsistent speed in the movement of the scanner head perhaps caused by heating of the belt that connects the stepper motor.

Chapter 4 - CaviCam and OpenSourceOV.org: a new device and online resource for assessing drought tolerance in plants

4.1 Introduction

In the previous chapters I explored a new approach for reducing the number of measurements required for conductance-based measurements (chapter 2) and developed CaviScan for increasing the usability and for maximising the number of measurements that can be made using a desktop scanner (chapter 3). To an extent these approaches were successful; the single-point technique can reduce the number of measurements when applied at scale, and CaviScan proved its potential for controlling multiple scanners and efficacy in maximising the scannable area and reducing the scan time. However, both approaches presented a number of limitations. The single-point technique requires a pre-assessment of vulnerability, is only useful at scale, and the accuracy depends on measurement under stable environmental conditions. Although the use of document scanners and the optical technique provide a significant improvement on the single-point conductance-based approach, not only because of the accuracy and reliability afforded by the optical technique, but also in the potential for scaling, automation, and broad accessibility, it nonetheless has fundamental issues with usability, susceptibility to artefacts possibly because of the mechanical nature of image capture (Fig. 4.1), and is cumbersome and difficult to use with a large number of samples (Fig. 4.2).

The benefits of using the optical technique are clear given the limitations of other methods (chapter 1), but current methods of applying the optical technique are also limited.

Three methods exist for capturing images of the xylem to use with the optical method: a microscope, document scanner, or point-and-shoot type camera. Microscopes are awkwardly shaped, expensive and require additional, and often expensive, camera attachments and imaging software, and do not have appropriate illumination for stems, which must be provided using additional lighting that can be difficult and awkward to setup (Fig. 4.3). Digital single lens reflex (DSLR) or other

point-and-shoot type cameras require an involved setup with additional stands and lights to fix the camera in position and provide suitable illumination (Fig. 4.4) – a setup that can be expensive, not easily portable, and despite best efforts to ensure the camera, sample and lights are all securely fixed in position, is still often highly susceptible to movement from bumps, knocks and vibrations. Document scanners, as discussed, have a number of limitations related to bulk and the mechanism of image capture.

Figure 4.1 An example of a banding artefact caused by a document scanner. The image shown is the result of subtracting pixel values between two consecutive scans of the same leaf using a document scanner. Dark areas indicate pixel differences between scans, white areas indicate no difference. Horizontal banding is possibly caused by imperfect coordination between the movement of the scanner head and the read out from the light sensors.

Continuous illumination is also an issue. Depending on the species and the rate of dry down, images of the xylem may need to be captured continually over several days. In a microscope or camera setup where the illumination is typically always on this can mean the sample is illuminated for extended periods of time causing sample heating.

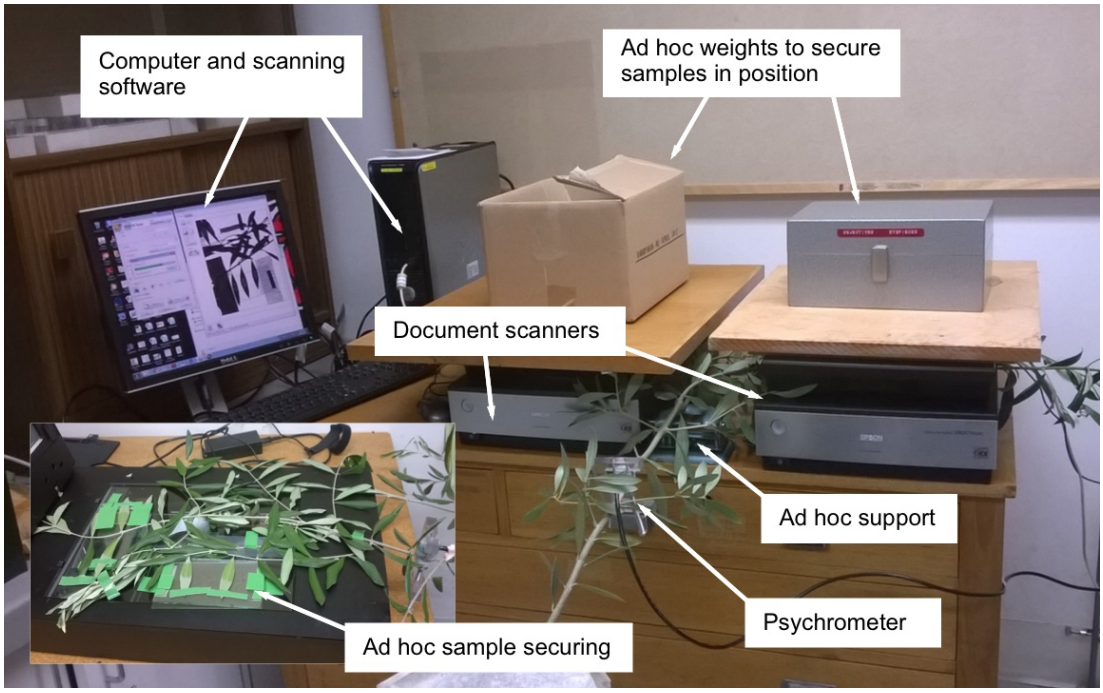

Figure 4.2 A scanner setup to assess olive leaves. This figure illustrates the typical ad hoc measures required for a scanner setup, including ad hoc weights used to force the lid of the scanner shut to reduce the amount of external light entering the scanning area and to clamp the sample in position, and ad hoc support of the main stem (a hole punch in this case). The inset image shows the sample preparation in the scanner and illustrates the difficulty in securing and arranging multiple samples. The overall bulk of the setup with the two scanners and the computer is apparent.

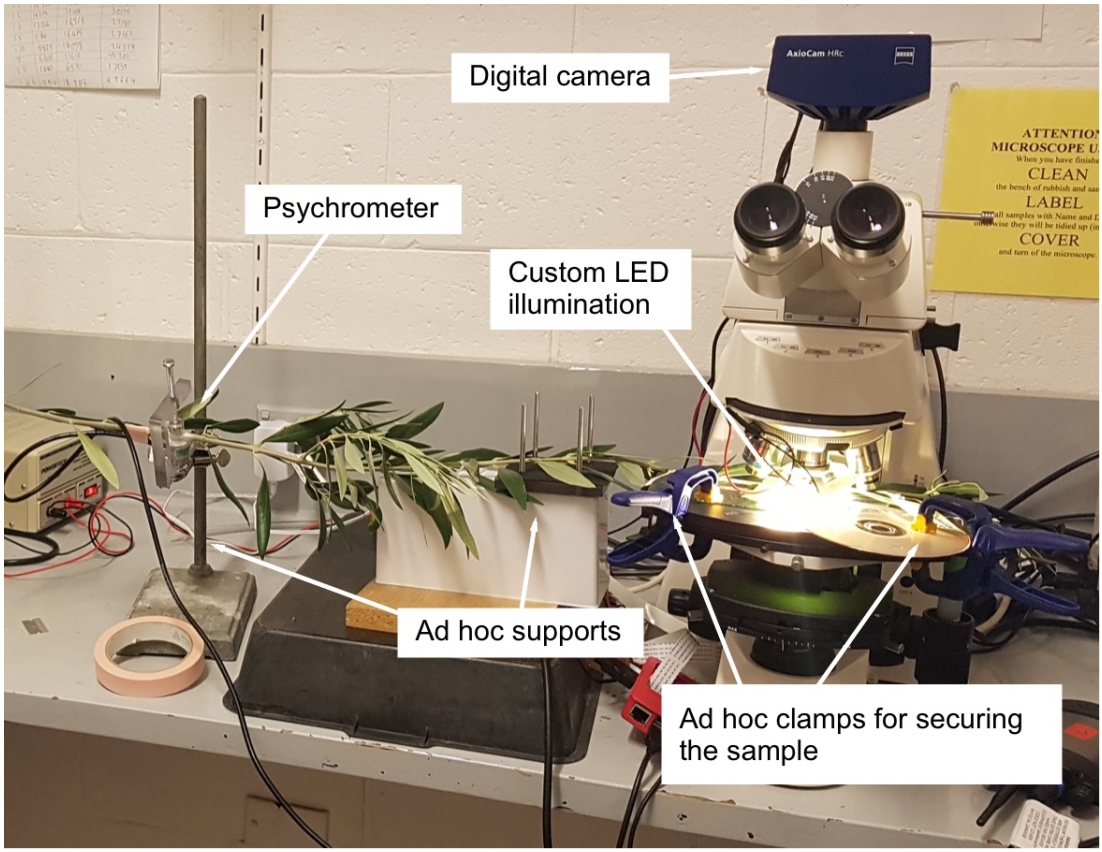

Figure 4.3 A typical microscope setup involving ad hoc supports to raise the sample to the level of the microscope stage. Clamps and a compact disc illustrate the ad hoc measures often needed to secure the sample in position. Compound microscopes such this do not have suitable lighting for stems, thus a custom-designed 3D-printed LED mount was constructed (not visible) to attach to the lens and provide the necessary illumination. A psychrometer is used to measure the sample water potential and a digital camera is mounted on the microscope to record images of the xylem under magnification.

Wrangling software to successfully control of the capture sequence is also an issue. For document scanners this necessitated the development of CaviScan and the VueScan scanning software, and although similar generic software exists for digital cameras (e.g. digiCamControl, http://digicamcontrol.com/) for which an alternative version of CaviScan could be developed (CaviPhoto?), it is limited to DSLR or point-and-shoot type cameras, not for cameras mounted on or integrated into a microscope, which would require yet another solution.

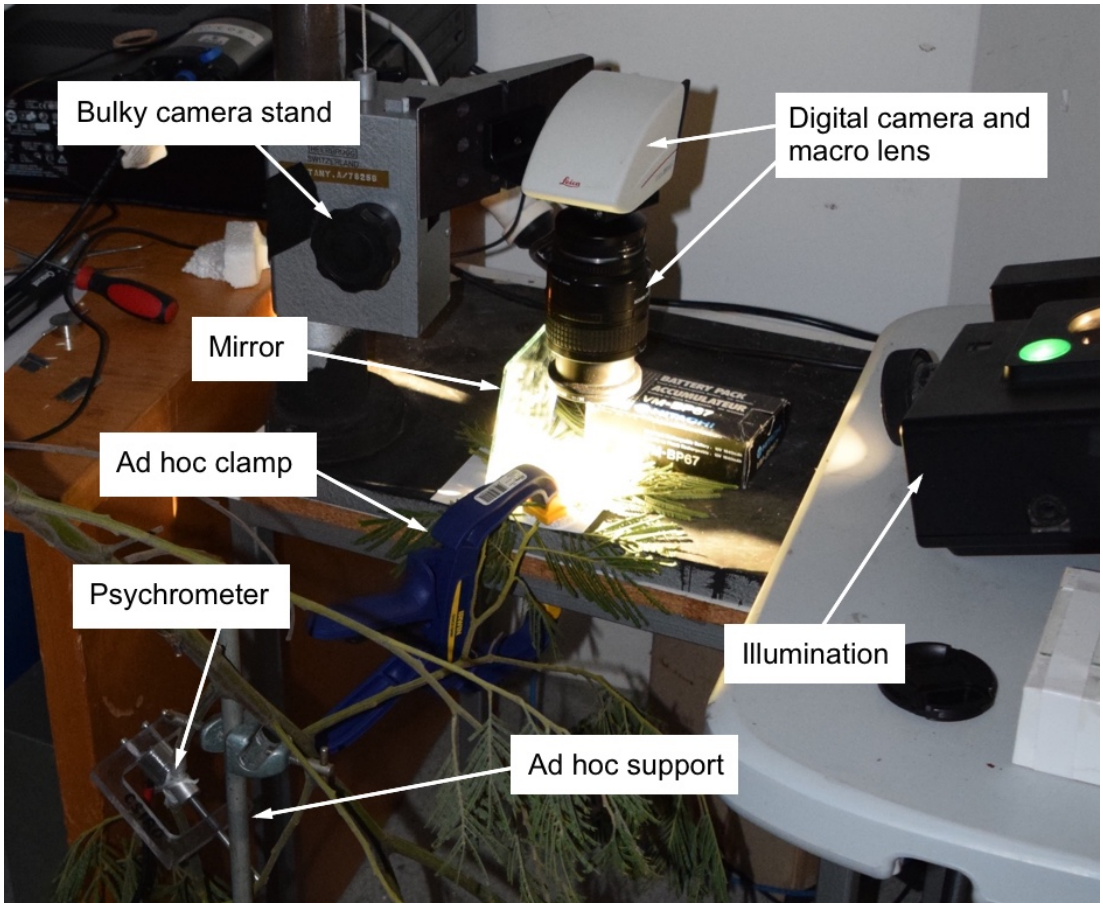

Figure 4.4 A typical camera setup that illustrates the ad hoc supports and clamps necessary to secure the sample in position. Ensuring sufficiently bright illumination can be a challenge with a camera setup. Here a mirror and propped up projector are used to illuminate the sample. A psychrometer is used to log sample water potential.

Given these limitations it became clear that a new device was needed, something that was affordable, portable, robust against knocks and bumps, and integrated a digital camera, data storage, illumination, magnification, and software control. I hypothesised that such a device (hereafter called the 'CaviCam') could be developed using recent advances in inexpensive electronics and 3D printing technology.

In this chapter I describe the development of the CaviCam and OpenSourceOV.org - an online repository of support materials, guides and information necessary to build and operate the system.

4.2 Methods

4.2.1 Data storage and digital camera

In the last decade there have been a proliferation of inexpensive and compact 'single-board' computers (micro-computers) and micro-controllers developed by organisations such as Arduino (https://www.arduino.cc/), Beagle Bone (https://beagleboard.org/), Adafruit (New York, United States), and the Raspberry Pi foundation (Cambridge, United Kingdom; Fig. 4.5) that offer storage options and considerable flexibility for integrating and controlling numerous different types of sensors and electronic components, including small digital cameras. The fundamental difference between a micro-computer and a micro-controller is that a micro-computer runs an entire stand-alone operating system based on a version of Linux or Windows, whereas a micro-controller requires specific instructions programmed on a separate computer that are compiled to lower-level machine code and transferred to the controller for execution. There are advantages and disadvantages to both, micro-controllers have less overhead, are more efficient and use less energy, but are less intuitive to use and configure - in effect they are a 'bare-bones' setup where only essential functionality is added to a rudimentary system. In comparison micro-computers are less efficient in energy use and processing capability, but are more user-friendly, require less expertise to setup and use, and tend to come with a broader suite of hardware already built in, such as Wi-Fi, Bluetooth, USB and ethernet ports, plus all the capabilities of a standard operating system, including a web browser, programming frameworks and a visual interface for system configuration.

Most tasks can be achieved in one way or another in both and both have general purpose input/output (GPIO) connectors through which other electrical components and devices can be connected. And indeed, through GPIO ports a micro-controller can be connected to micro-computer.

I opted to use a Raspberry Pi micro-computer (http://www.raspberrypi.org) for the CaviCam because: 1) has on-board and external storage options (e.g. USB stick and MicroSD card), 2) the on-board operating system and ease of setup make it a low-level entry to the technology which contributes to the general accessibility of the

system, 2) although all single-board computers and micro-controllers can be connected to a range of cameras, the Raspberry Pi Foundation (Cambridge, United Kingdom) develop an 8MP camera module, the Raspberry Pi Camera (Fig. 4.6), with a Sony IMX219 image sensor (Sony, 2018) that integrates with the Raspberry Pi hardware and has an excellent, well-documented Python library (PiCamera; https://github.com/waveform80/picamera) for programmatically controlling and configuring the camera, 3) the Raspberry Pi, like most micro-computers, can use any standard computer monitor for the display, and a mouse and keyboard can be attached using the standard USB ports, making the system inherently more flexible than a micro-controller setup, which requires a second computer or a screen display (and custom programming) to create a readout display, 4) the Raspberry Pi operating system (Raspbian) comes with many programming languages pre-installed and is therefore already primed for the development of custom programs in the user's language of choice, thus immediately improving the extensibility of the system. 5) The Raspberry Pi has a considerable following and there are numerous online communities and resources providing guidance and support to learn the Raspberry Pi platform and resolve issues.

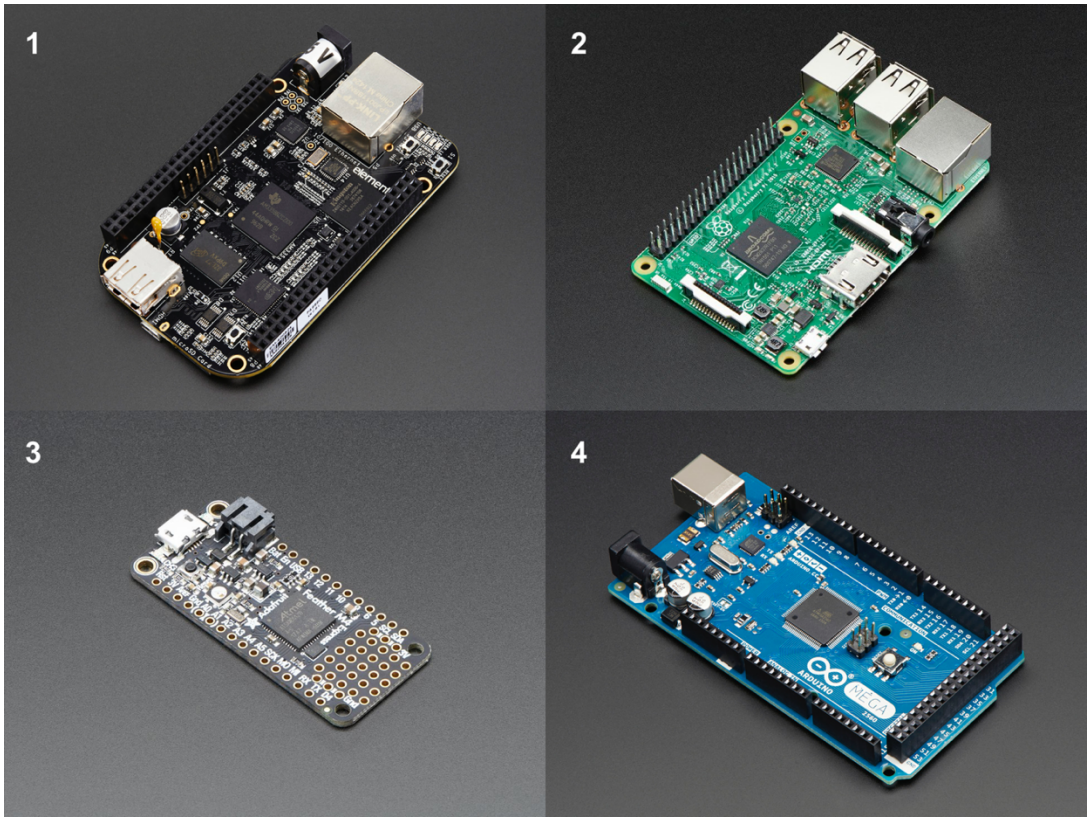

Figure 4.5 Two micro-computer examples: the BeagleBone Black Rev C (1) and Raspberry Pi Model B+ (2), and two commonly used micro-processors; the Adafruit Feather M4 Express (3) and Arduino Mega 2560 micro-processors. The devices are not shown to scale.

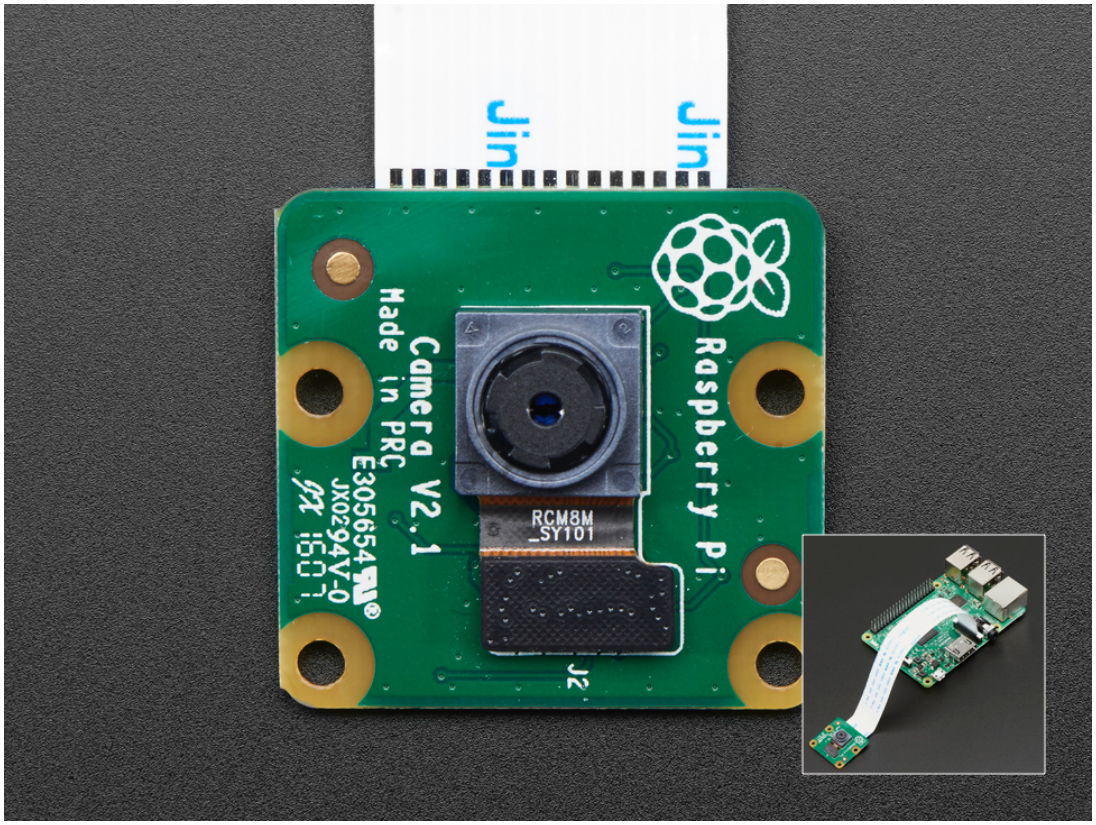

Figure 4.6 A close-up of the the Raspberry Pi Camera V2. Inset image shows the camera connected with ribbon cable to a Raspberry Pi. The camera is not to scale.

4.2.2 Magnification lens

I initially opted for a 10x macro lens from Moment (https://www.shopmoment.com/; Fig. 4.7). This is a high-end lens specifically designed to attach to a smartphone camera and is able to mate with the Raspberry Pi Camera light sensor mount, plus the optics produce excellent quality images with low distortion and a wide full field of view. Additionally the shape and low profile of the lens helped to reduce the overall profile of the CaviCam and made it relatively simple to integrate the lens into the CaviCam body. Although the lens is priced at the high-end of smartphone lenses it is still relatively inexpensive (<$140 AUD) compared to traditional lenses of similar quality, plus it can be bought online and shipped worldwide.

However, for thicker leaves and stems I found that 10x magnification was not generally sufficient to capture embolism events and I was unable to find a 20x mobile phone lens of equivalent quality to the Moment 10x lens. Instead I tested a number of hand/loupe lenses ranging from cheap and unbranded lenses sourced

primarily from eBay, to mid-range lenses, such as the BelOMO (Minsk, Belarus) range of lenses, to high-end lenses from manufacturers such as Eschenbach (Nurnberg, Germany) and Zeiss (Oberkochen, Germany). This list was far from exhaustive, the aim was to get a general idea of the features that were most appropriate for the clamp. An interesting aside is that I found a number of the unbranded lenses from eBay and Amazon purporting to be 20x magnification were in fact only 10x magnification or less. Of the true 20x lenses I found the most limiting factor was the working distance - the minimum distance from the base of the lens to the object sufficient to bring the object into focus. For example, the BelOMO 20x lens is a very popular and inexpensive (~$35 AUD) hand lens (Fig. 4.7) that incorporates multiple achromatic lenses, something typically only found in higher-end hand lenses, that improves image quality and clarity by correcting for colour and lens distortion, but I found the working distance to be only ~5mm. This provided very little clearance for manoeuvring a sample beneath the lens, and did not allow enough room for parts to securely fix the sample in position. Instead I found that a more expensive (~$170 AUD) 20x achromatic hand lens from Eschenbach (Fig. 4.7), which also has multiple lenses for correction, delivered the right combination of superior image quality, clarity and usable working distance (~12mm). I settled with the Eschenbach because it was the first to meet all the requirements, but there are undoubtedly other suitable lenses available, and the CaviCam was designed to accommodate, within reason, a range of different sized hand lenses.

4.2.2 Illumination

Bright illumination is essential to maximise light penetration through the sample and obtain a good signal from embolism events. I tested various light sources including custom-built circuits with a diversity of LED types, but for simplicity and flexibility I opted for sections of LED strip lighting. These are used in a broad variety of applications but mostly to provide accent lighting in home or commercial settings. They are widely available, come in a range of brightness and integrate all the necessary circuitry to connect the LEDs directly to a power source, plus they have an adhesive backing making it easy to attach to the clamp body. I chose LED strips that can be connected to a 12v DC supply rather than AC mains to minimise the risk of LED flicker due to fluctuating AC current, an issue I had seen with other LED light

sources, and created a very simple transistor-based circuit for controlling the power to the LED strips using a low-current output from one of the Raspberry Pi's GPIO pins.

Figure 4.7 The Moment 10x macro lens (1), the BelOMO 20x hand lens (2) and the Eschenbach 20x achromatic hand lens (3). The Moment 10x macro lens was used in version 1 of the CaviCam and the Eschenbach 20x hand lens was used in version 2. The BelOMO 20x hand lens provides an example of a cheaper 20x hand lens (~$35 AUD) compared to the Eschenbach 20x hand lens (~$170 AUD), however the working distance of the Eschenbach model (~12mm) was better suited for the CaviCam than the BelOMO model (~5mm).

4.2.3 Device housing

There were four main components that needed to be integrated into the CaviCam: 1) Raspberry Pi Camera, 2) magnification lens, 3) above-sample illumination for stems, and 4) below-sample illumination for leaves. The Raspberry Pi can be connected via long cables, so to keep the device as compact as possible I chose not to integrate the Raspberry Pi in the clamp body. These components could only be arranged in one particular order and this defined the basic organisation of the device (Fig 4.8).

Two versions of the CaviCam were developed – an initial version that incorporated the moment lens, and a second version for integrating a hand lens to increase the

magnification and to improve on various aspects of the first version. Each of these versions are discussed in more detail below.

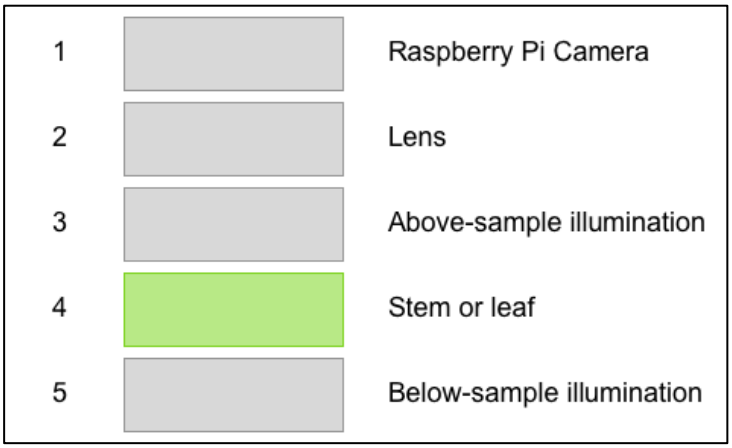

Figure 4.8 The basic components of the CaviCam: the Raspberry Pi Camera, magnification lens, above-sample and below-sample illumination.

For the fabrication of parts I opted to use 3D printed materials. The meteoric rise of 3D printing technology in recent years has revolutionised prototyping and small-scale production (Dimitrov, Schreve and De Beer, 2006), and indeed now seems set to move into the realm of large scale part production (Bak, 2003). The technology has matured quickly bringing down the cost of 3D printers while increasing the accuracy and quality of the 3D prints (Bogue, 2013). Indeed, even some of the moderately priced consumer-level 3D printers currently available for less than $1000 AUD, such as the i3 MK2S 3D printer from Prusa (Prague, Czech Republic), can fabricate parts to an accuracy of 0.05mm in a range of materials, including acrylonitrile butadiene styrene (ABS), polyethylene terephthalate (PET), polylactic acid (PLA) and nylon plastics, plus a growing range of 'speciality' materials that can produce flexible, rubbery, glowing, transparent, or extremely tough and durable parts by incorporating a range of additives, from ceramic and metal powders to wood and carbon fibres, among many others (including more exotic substances like beer by-products and algae).

For these reasons, plus increasing access to 3D printing services online and in universities, schools, libraries and public 'maker' workshops, 3D-printed parts for the device was an obvious choice to maximise accessibility and reduce the overall cost of the system.

Parts were designed using Tinkercad (https://www.tinkercad.com/), a free online 3D modelling program, and various iterations were printed and tested using a range of 3D printing materials and printers, including VeroClear, a transparent resin-based material using a high-end StrataSys (Minnesota, United States) Objet Eden260VS 3D printer, nylon using a high-end commercial Trump Precision Machinery (Zhongshan, China) Elite P3600 selective laser sintering (SLS) machine, and PLA and ABS using a mid-range 'consumer' Prusa i3 MK2S 3D printer. I found that all of these materials were suitably strong for the CaviCam construction and, surprisingly, the inexpensive Prusa desktop 3D printer was more than capable of producing parts for the device that were sufficiently accurate and robust (Fig. 4.9).

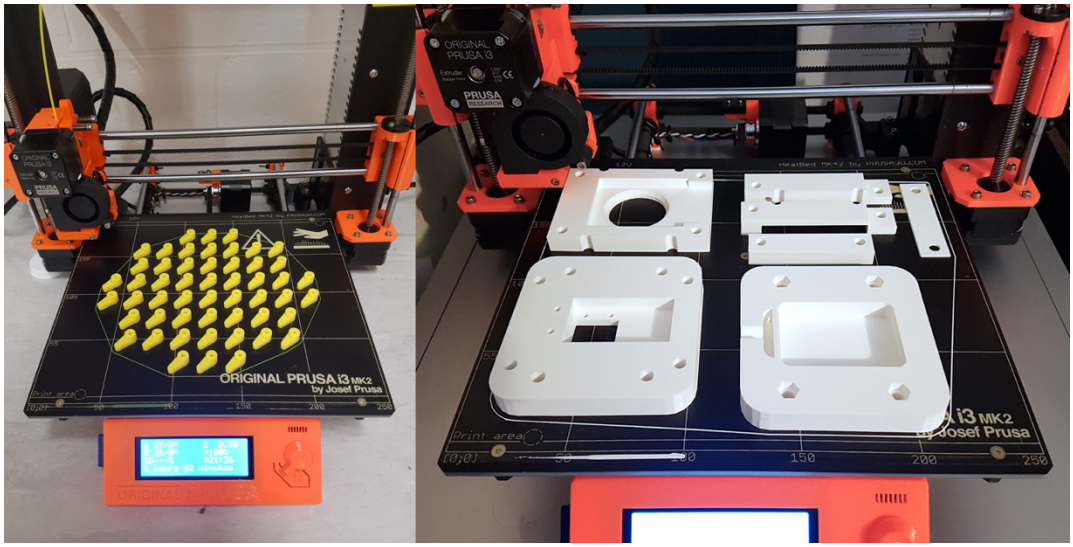

Figure 4.9 3D parts for the CaviCam printed on the Prusa i3 MK2S consumer 3D printer. *Left panel* A bulk number of prints of a single part illustrating the capacity of 3D printing for high-volume fabrication. *Right panel* All parts for a single CaviCam device (version 2) printed at the same time. The parts were printed overnight and took approximately 13 hours.

4.2.4 CaviCam Version 1

Version 1 consisted of four main components: 1) a layer for mounting the camera, 2) a layer enclosing the Moment lens and mounting two 50mm sections of LED strip lights, 3) a spacer for fixing the sample in position and setting the working distance between the camera and the sample, thus acting as a focusing component, 4) an

illumination base providing both a platform for the sample and below-sample illumination via a cavity (painted white if necessary to increase reflectance) with space to fit two LED strip sections (Fig. 4.10). A 3-5mm opaque acrylic section sits over the base to act as a light diffuser and surface to mount the sample.

Top layers were combined as one assembly using four bolts and recessed nuts, and four larger bolts secured the illumination base to the top assembly. Separating the top and bottom assembly provided the greatest flexibility for manoeuvring the sample in place and clamping it in position. I experimented with an alternative configuration where the top and bottom assemblies were held together using a hinge and spring configuration (Fig. 4.11), and although this provided a faster and more convenient method of inserting and securing the sample in position it significantly increased the overall bulk of the device.

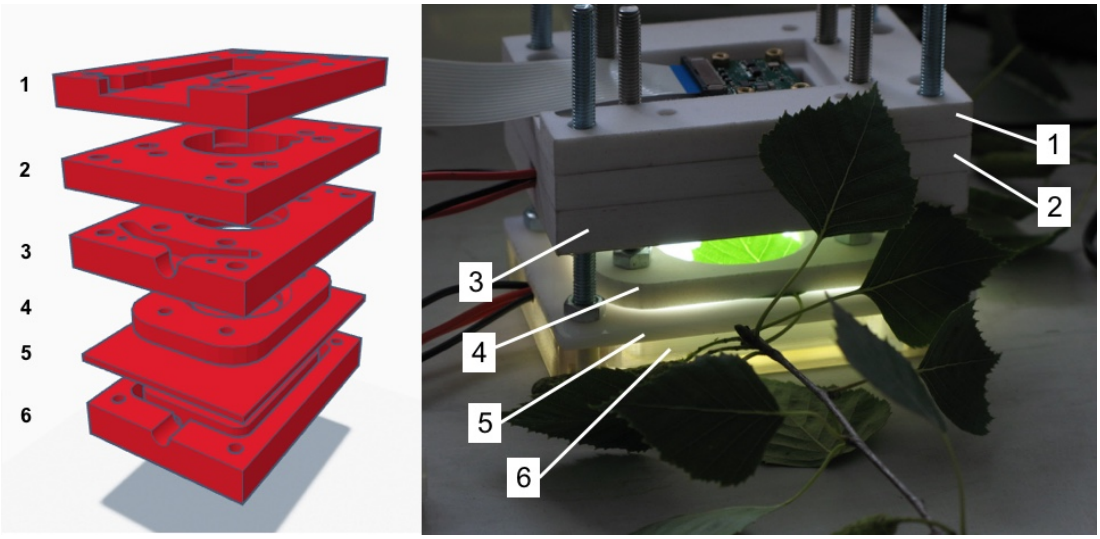

Figure 4.10 *Left panel* Schematic of CaviCam version 1. *Right panel* Picture of CaviCam version 1 fully constructed. Components are indicated by the following numbers: 1) Camera mount; 2 and 3) Lens mount that encloses the Moment lens (using part 2 and 3) and a mount for two LED strips (part 3); 4) Spacer for setting the working distance between the sample and the lens; 5) Acrylic cover for a sample platform and as a light diffuser for the illumination base; 6) Illumination base with a cavity for two LED strips.

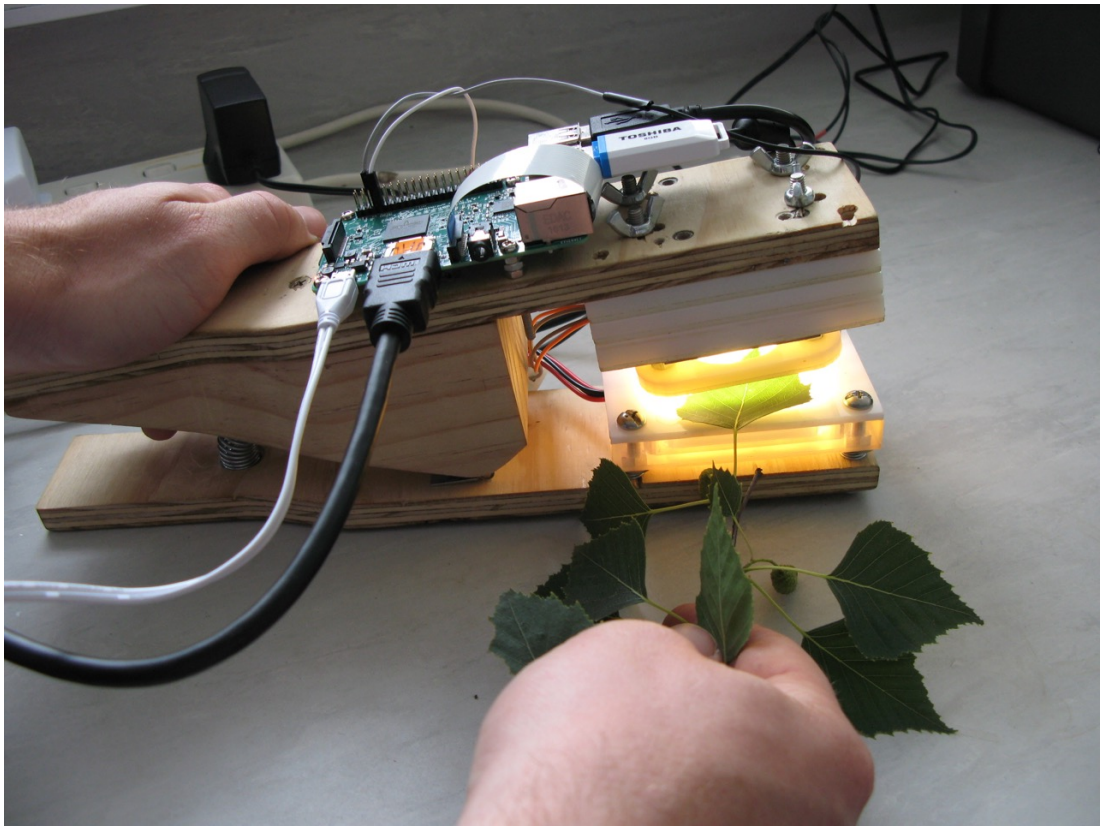

Figure 4.11. An early prototype with a hinge and spring configuration to clamp the sample in position. In this version the Raspberry Pi was fixed to the top of the clamp. Although this version provided an easy way of inserting the sample (as pictured) and clamping it in position, it was more bulky than the other CaviCam versions.

4.2.5 CaviCam Version 2

Version 2 has the following components (Fig. 4.12): 1) Camera mount, 2) lens spacers for setting the distance between the top of the lens and the camera via the lens cover, 3) lens clamp for fixing the lens vertically using the lens cover. This part sits underneath the top section of the lens case and when the top assembly is bolted together the top section of the lens case is clamped between the lens clamp and the camera mount (or lens spacer if using an alternative configuration, more details below) thus fixing it in position. 4) Lens locks to horizontally fix the lens in position, 5) wide right and left LED mounts that provide space in-between for a thinner hand lens, 6) thinner right and left LED mounts providing a space in-between for a wider hand lens. Separating the LED mounts into two separate components was an essential innovation on the first clamp to bring the higher magnification lens with a shallower working distance closer to the sample. 7) Spacer to set the distance

between the sample and the bottom of the lens, and to provide a base with recessed bolt holes to secure the top assembly parts in position, 8) foam pad to adjust the focus and secure the sample in place without damaging the sample. One of the main limitations of Version 1 was a limited ability to adjust the focus beyond the distance of the fixed spacer. The foam pad provides a simple way of fixing the sample in position without damage while providing an additional range of focus equivalent to a portion of the pad compression. Thus the focus can be easily adjusted by tightening or loosening nuts that fix the top and bottom assemblies. 9) Illuminated base. This has a similar construction to version 1 and integrates two 50mm LED strip sections fixed to the walls of a cavity and an opaque acrylic cover 3mm thick that acts as a diffuser and mounting surface for the sample.

As mentioned, the main driver for version 2 was the ability to fit a hand lens. To provide flexibility to mount different makes and models of hand lenses a number of features had to be incorporated, including: 1) different sized lens spacers - the bolt that fixes the lens to the lens cover of most hand lenses tends to sit proud such that if the lens is positioned directly against the camera mount it causes the lens to deflect. The lens spacers provide an adjustable clearance between the camera mount and the top of the hand lens. 2) The LED lights were positioned as close to the lens as possible so that the lens intercepts as much of the reflected light as possible. Wider lens mounts bring the LED lights closer to the lens but only allow for a narrower lens, thus thinner lens mounts accommodate wider lenses. 3) The parts of the top assembly were fixed together using a bolt at each corner. These allow for flexibility in positioning the components of the top assembly by using nuts/washers as spacers. For example, additional washers/nuts can be added between the spacer and/or LED mounts and lens clamp to accommodate a 10x magnification lens with a larger working distance (Fig. 4.13).

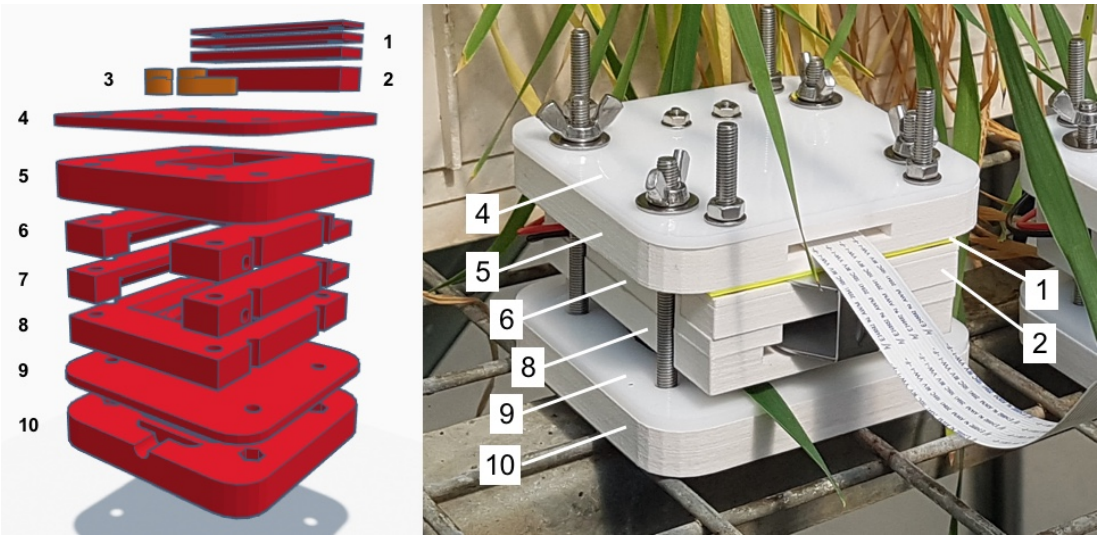

Figure 4.12 *Left panel* Schematic of CaviCam version 2. *Right panel* Picture of CaviCam version 2 fully constructed. Components are indicated by the following numbers: 1) Lens spacers for setting the distance between the top of the lens (not shown) and the camera (not shown); 2) Lens clamp for fixing the lens against the lens; 3) Lens locks to secure the lens in position (not visible on right panel); 4) Acrylic cover to protect the camera; 5) Camera mount; 6) Wide LED mounts; 7) Narrow LED mounts to be used with a wider lens (not shown); 8) Spacer to set the distance between the lens and the sample, to secure the sample, and to provide a base for the top assembly; 9) Acrylic cover for the base to provide a platform for the sample and to act as a light diffuser; 10) Base with LED strip lights for illumination. Note that the foam pad is not shown but is attached to the underside of the spacer (8).

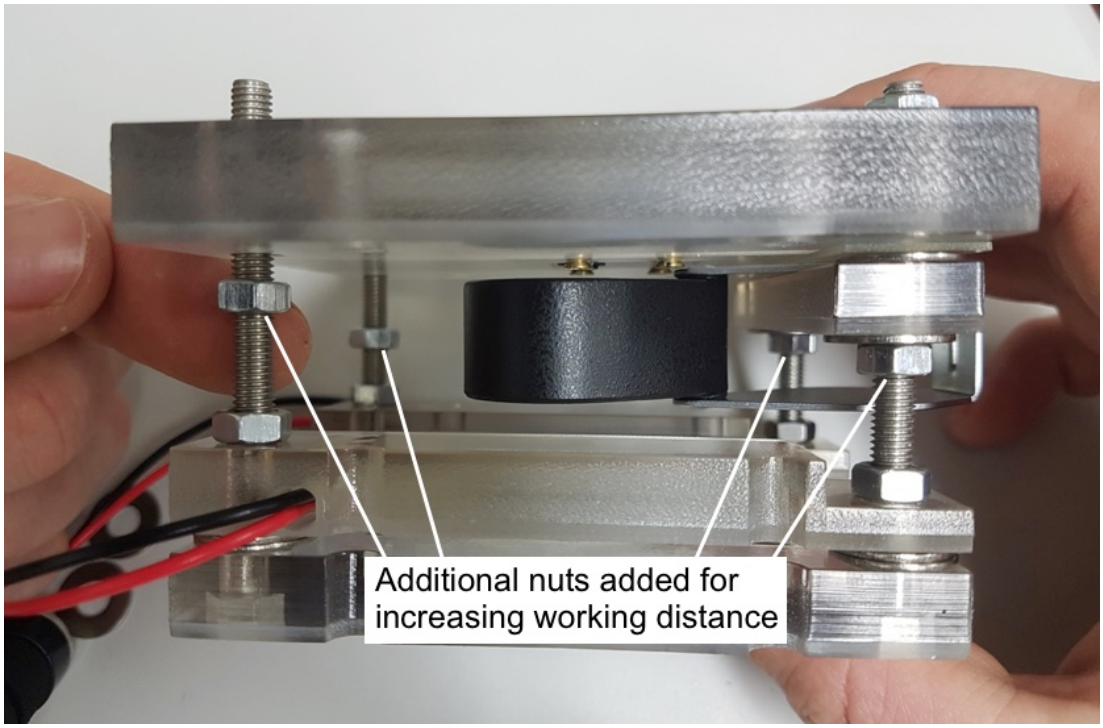

Figure 4.13. Example of an alternative configuration of CaviCam version 2 where the larger working distance of a 10x magnification lens is accommodated by repositioning layers using additional nuts.

4.2.6 Software control

For software control two command-line programs were developed to run on the Raspberry Pi: CaviCapture for controlling image capture and illumination, and CaviProcess for processing the images and extracting the data. Initially CaviCapture was developed just to capture images and save them to storage. Thus to process the images and extract the data it was necessary to transfer the images to a separate computer so that they could be processed using ImageJ. To aid this process a toolbox of newly developed and existing ImageJ functions and plugins was developed (CaviTools). The toolbox is also necessary for processing difficult images from the device, for example to remove the presence of artefacts caused by insects, or if embolism events are particularly faint. CaviProcess was developed so that images could be automatically processed on the Raspberry Pi. Not only did this significantly reduce the speed and complexity of the assessment process but enabled, for the first time, near real-time tracking of embolism events.

To maximise the extensibility of the CaviProcess program it was developed in such a way so that it could be interfaced with other programs and processes. This necessitated an upgrade to the CaviCapture script and consequently there are two versions of CaviCapture. The development of CaviProcess and the upgrade to CaviCapture enabled the creation of a graphical user interface (GUI), CaviConsole, for controlling image capture and processing, and for viewing the results of processing.

The command-line programs, the GUI and the ImageJ toolbox are now presented.

4.2.7 CaviCapture

CaviCapture is a program developed in Python 2.7 (http://www.python.org) to control the Raspberry Pi Camera and the LED illumination via terminal commands on the Raspberry Pi. The program uses the PiCamera python library (https://github.com/waveform80/picamera) to interface with the camera and the RPi.GPIO library (https://pypi.org/project/RPi.GPIO/) to control illumination via a Raspberry Pi GPIO port. A simple transistor circuit connects a 12v power source (e.g. a car battery), a NPN-type transistor and two GPIO pins on the Raspberry Pi (ground and a designated 'output' pin) to supply power to the LEDs and to turn them on or off via a small current from a GPIO output pin. The LEDs are wired in pairs above and below the sample using Molex-type connectors. Only one set can be connected to the transistor circuit at any one time and this provides the means of selecting the illumination source for the sample.

In the first CaviCapture version configuration settings were passed to the program via command-line options (Table 4.1). Version 2 has more configuration options (Table 4.2) which are accessed from a INI-based configuration file. This provides a simpler and more extensible approach for storing configuration values. Version 2 also writes a text-based log file of events and errors for information and debugging, and stores details about captured images in a local SQLite database. The advantage of using a database for results and the use of an external configuration file is that it provides easy access for other applications or processes to read the database and use the results and read/write configuration settings. Version 2 uses the SafeConfigParser (https://docs.python.org/2/library/configparser.html) and SQLite3

(https://docs.python.org/2/library/sqlite3.html) libraries for writing/reading INI configuration files and for managing a SQLite database. A crop function is provided via the OpenCV2 library (http://opencv.org).

The camera shutter speed, capture duration (the total time to capture images) and the interval between captures are mandatory settings in both versions. The camera ISO can also be configured, but rarely needs to be changed from the default value of 100.

In version 1 the entire area visible to the camera is captured at the maximum resolution of 2592x1944 pixels. In version 2 the resolution is configurable (640x480 pixels to a maximum of 2592x1944 pixels), and an ROI can be set to crop the image to smaller portion of the visible area. This reduces the file size and image processing times.

A 'setup' command line option (renamed 'preview' in version 2) opens a window showing a live preview from the camera with the device illumination turned on. This allows the user to position the sample and adjust the focus before initiating a capture sequence. In the setup/preview mode an automatically determined shutter speed is reported to the user to help set an appropriate value in the configuration.

Using CaviCapture version 1 the procedure for capturing sample images is as follows: 1) the sample is placed in the clamp, 2) the CaviCapture program is run from the Raspberry Pi command line by entering the command 'cavicapture.py' followed by the configuration options. Initially the program is run in setup mode using the command 'cavicapture.py –setup true' and the sample is re-positioned and focus adjusted as required. The automatic shutter speed value is noted. 3) cavicapture.py is re-run in setup mode but this time with a shutter speed value provided using the –shutterspeed option e.g. 'cavicapture.py –setup true –shutterspeed 1500'. If the user sees that the image is over or underexposed the program is re-run with an adjusted shutterspeed and the procedure continues until an optimum shutter speed has been determined. 4) The capture sequence is initiated by running cavicapture.py without the setup option, and with the interval, duration and shutter speed options provided, for example 'cavicapture.py –interval 300 –duration 30000 –shutterspeed 1500'. 5) Images are captured every interval for the total duration and then the program terminates. Captured images are saved in the same

directory from which the program is executed and file names are set to the timestamp of image capture.

For version 2 the procedure is similar: 1) the sample is placed in the clamp, 2) cavicapture.py is run in setup mode with the 'preview' option and with the location of the configuration file is provided via the 'config' option, for example 'cavicapture.py –config /location/of/config.ini –preview'. The user adjusts the focus, re-positions the sample as necessary and notes the reported automatic shutter speed. 3) The shutter speed is modified as required in the configuration file and the program is re-run so the user can check for correct exposure and adjust the shutter speed in the configuration file accordingly. The process repeats until an optimum shutterspeed has been determined. 4) The user sets the interval, duration, shutter speed, resolution and crop settings (if using) in the config file. 5) The capture sequence is initiated by running the program without the 'preview' option. 6) Files are saved in the output directory defined in the configuration file and as each image is captured a record of the capture including the filename, date and time, and a unique ID is added to the local SQLite database. File names are set to the date and time of capture. On first-run the database is created if it is not found in the output directory.

Table 4.1. CaviCapture version 1 configuration settings. Settings are passed to the cavicapture.py program via command line switches e.g. 'cavicapture.py –ISO 100'

Setting	Description	Default Value
ISO	Sets the camera ISO	100
shutterspeed	Sets the camera shutterspeed (ms)	No default
setup	Initiates a live preview window from the CaviCam with the LED illumination ON.	n/a
interval	Sets the interval between captures.	No default
duration	Sets the maximum capturing time (seconds)	No default

Table 4.2. CaviCapture version 2 INI file configuration settings.

Setting	Description	Default Value
ISO	Sets the camera ISO	100
shutter_speed	Sets the camera shutterspeed (ms)	1500
output_dir	Sets the base output directory for captured images	No default
sequence_name	Sets the output directory for captured images in the base output directory	No default
verbose	Enables additional logging of capture events to the log file	Off
resolution	Sets the image resolution (pixels). Settings available: Small (640x480), Medium (1296x972), Large (1920x1080), Max (2592x1944)	Medium
crop	ROI to crop the captured image to. Value is given as (x1, y1, x2, y2) corresponding to the top left and bottom right coordinates of the image.	No default
crop_enabled	Enables/disables the crop function	Off
processor	Location of the CaviProcess processing script	No default

4.2.8 CaviProcess

CaviProcess is a Python (version 2.7; http://www.python.org) program I developed for automatically processing images captured using CaviCapture version 2. The program is executed using terminal commands from the Raspberry Pi and can be run concurrently with the CaviCapture program to process files as they become available. The settings for the program are stored and loaded from the INI configuration file shared with CaviCapture v2.

Once activated CaviProcess interfaces with the database created by CaviCapture using the SQLite3 library and begins processing when a minimum of two files are available.

Images are processed in sequential pairs using a seven step procedure to identify differences between the images and to remove noise. The procedure for image processing is as follows: Step 1) Images are converted to 8-bit grayscale images such that each pixel has a value from 0 (black) to 255 (white). Step 2) Differences between images are revealed by subtracting pixel values from corresponding pixel positions in each image, for example the pixel value at row 1 column 1 of the first image is subtracted from the pixel value at row 1 column 1 of the second image, and then values at row 1 column 2 are subtracted, and so on. The results of subtraction are saved in a new image (the 'difference image'). If a pixel is the same in both images then the result pixel in the difference image will be 0 (black); the higher the value, the more different the pixels. The order of subtraction is important. If the sample is illuminated from above, as is required for stems, then more light is reflected back to the camera when a vessel embolises causing xylem pixels to become lighter (higher pixel values). For leaves, the sample is illuminated from below, causing a conduit to appear darker (lower pixel values) as it embolises, the result of more light reflected away from the camera sensor. An 8-bit image does not support negative values so the order of subtraction is set according to the source of illumination, defined as a setting in the configuration file. Step 3) Stage one of noise removal is to filter pixels in the difference image that have a value below a configurable filter threshold. Noise results in a bulk of low-value pixels in the difference image caused by small differences in pixel values between the original images, thus by simply removing pixels within this narrow range most of the noise can be quickly and efficiently removed. However, some or all of the pixels relating to embolism may also fall within this range of small differences, so the filter threshold must be set appropriately to maximise the removal of noise while retaining the signal of 'real' differences. If embolism events are strong and result in large pixel value differences then a high threshold can be set and the majority of noise can be removed. Conversely, if embolism events are weak then the filter threshold must be set low and more of the noise will remain and must be removed using additional steps. At this stage it is not necessary for all the noise to be removed, the focus is on removing as much noise as possible while retaining the structure of embolism events. Step 4) Stage two of noise removal. The bulk of remaining noise is now removed using outlier removal. One by one pixels are evaluated in the context of the pixels that surround them (up to a radius of three pixels) and if the median value of the

surrounding pixels is less than the central pixel value then the central pixel is replaced with the median value. Outlier removal works because a noisy pixel is more likely to be at odds with its surrounding and replaced, whereas a pixel that forms part of an embolism event will be surrounded by similar pixels and will be kept. Thus the more noise that can be filtered out at stage one the lower the density of noise at this stage and the more effective outlier removal will be. Step 6) All non-zero pixels are summed across the whole image or within a ROI defined in the configuration file. The total count is saved to the database and to a CSV file in the sample directory. The total count represents the total of embolism events, artefacts, and any noise that remains from the previous steps. Step 7) The difference image is saved in an output directory with all non-zero pixels set to 255 (bright white) to increase the prominence of differences for post-processing visual inspection.

CaviProcess has additional options to reprocess images and to recalculate the sum of non-zero pixels across all images without reprocessing. This is useful if the ROI is changed.

CaviProcess uses the Numpy (http://www.numpy.org) and OpenCV2 (http://opencv.org) libraries for image processing.

CaviProcess is activated from the command line by running the command ‘caviprocess.py’ and passing the location of the configuration file using the ‘config’ option e.g. ‘cavicapture.py –config /location/of/config.ini’.

On execution CaviProcess accesses the database created by CaviCapture and processes a minimum of two files that are available. Once complete it continually monitors the database for new files and processes them as they are added to the database. In this way the CaviProcess and CaviCapture processes can run concurrently to process images in near-real time or independently, without affecting each other.

Processed files are only processed once, but can be reprocessed by rerunning the CaviProcess program with a ‘reprocess’ option i.e. ‘cavicapture.py –config /location/of/config.ini –reprocess’.

CaviProcess has a number of configuration options for setting the noise removal filter threshold, the ROI filter, and a number of options for debugging, including enabling/disabling each of the processing steps and saving a copy of the image after each of processing steps has been executed (Table 4.3). The ROI is useful for excluding regions of the image where artefacts or excessive noise may be prominent, and for evaluating the consistency of the embolism signal in different parts of the viewable area. ROI areas can be recalculated without images being reprocessed by passing the 'roiareas' option e.g. 'cavicapture.py –config /location/of/config.ini –roiareas'.

Processing takes between 1-2 seconds depending on the resolution of the image i.e. in near real-time, and cropping the images can significantly reduce processing times further.

Table 4.3. CaviProcess configuration settings. These are defined in an INI-based configuration that shares settings with the CaviCapture program.

Setting	Description	Default Value
intermediates_enabled	If enabled a copy of the image is saved after each step in the processing procedure. Useful for debugging	Off
outlier_removal_enabled	Enables/disables the outlier removal routine	On
filter_enabled	Enables/disables the filtering routine	On
thresholding_enabled	Enables/disables the thresholding routine	On
difference_enabled	Enables/disables the difference routine	On
roi_enabled	Enables/disables the data ROI function	Off
roi	Data ROI region. Only pixels within this region are counted as part of the total embolism area. Value is given as (x1, y1, x2, y2) corresponding to the top left and bottom right coordinates of the image.	Off
filter_threshold	Sets the pixel filter threshold	10
GPIO_light_channel	Sets the GPIO 'output' port that controls the illumination	7
verbose	Enables additional logging of processing events to the log file	Off

4.2.9 CaviTools ImageJ Plugin Toolbox

Manual processing of captured images using ImageJ is aided by the CaviTools toolbox of plugins and scripts. The toolbox contains functions for creating the image

difference using an imported stack of captured images, for manually removing difficult artefacts or noise from the difference images where standard noise removal techniques have not been effective, and for generating composite coloured images that represent the progression of embolism events in the sequence and are useful for figures for publication.

The toolbox is installed in ImageJ and can be added to the toolbar for easy access to the various functions, listed below:

Image Difference

Captured images are imported into ImageJ as a 'stack' and the Image Difference function is applied to reveal the differences between sequential pairs of stack 'slices'. The Image Difference function provides an option for selecting the sample type (Leaf or Stem) which determines the order of pixel subtraction. Differences are revealed using a four step procedure: 1) images in the original stack are converted to 8-bit images, 2) two duplicates of the original stack are generated, 2) the duplicate stacks are offset by removing the first slice from one and the last slice from the other such that the same slice number in each stack represents a pair of sequential slices in the original stack. The direction of offset depends on the sample type. 3) Using the ImageJ 'Image Calculator' function the stacks are subtracted from each other slice by slice to produce a result stack of image differences (the 'difference image stack') used for subsequent processing. 4) the duplicate stacks are removed and the difference image stack is presented to the user.

Colour Slices

I developed the colour slices function to colour slices in a stack according to a selection of scales and colour schemes. This function was based on the figures produced by Brodribb et al. (2016).

Clear Slices, Clear Slice, Clear Outside, and Save Slices

I developed these functions to aid the manual removal of artefacts or noise. All non-zero pixels can be removed (set to zero) across a range of slices (Clear Slices), in the

current slice (Clear Slice), or outside of the current selection (Clear Outside). Save Slices removes pixels in slices other than those provided.

Z Project, Cumulative Z Project

Provides a shortcut to the ImageJ 'Z Project' function which can be used to create a composite image of all non-zero pixels across the sequence, thus providing a spatial map of all events (Fig. 4.14). Cumulative Z Project is a custom plugin I developed that creates a new stack of cumulative z-projections from the difference image stack i.e. for each slice in the original stack the Z Project function is applied to give a Z projection of all slices preceding. This can be useful for illustrating how events have progressed by creating a montage of slices for a selection of time periods or water potential. Used in combination with the Colour Slices function this can produce useful images for publication (e.g. Brodribb et al. (2017) and Rodriguez-Dominguez et al. (2018)).

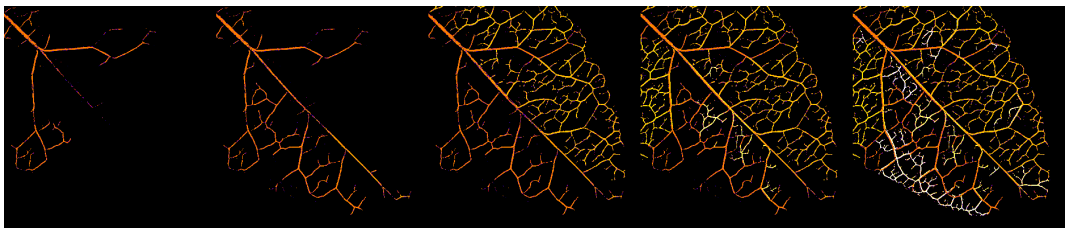

Figure 4.14 Sequence colouring used in combination with the Cumulative Z Project function to illustrate the progression of embolism events at a selection of time periods in the sequence. Image shows the progression of embolism events that occurred at five arbitrary times during a dry-down sequence of a passion flower leaf.

Remove Outliers

Provides a short-cut to the ImageJ 'Remove Outliers' function used for noise removal.

4.2.10 CaviConsole

CaviConsole was developed using Angular (https://angular.io/), a JavaScript framework for developing web-based applications, and Node.js (https://nodejs.org/), which provides server-side JavaScript programming and a means of interfacing with the Raspberry Pi operating system and the CaviCapture and CaviProcess programs.

The advantage of a web-based application is that it can be easily accessed via the internet browser on the Raspberry Pi or on a browser on a remote machine connected to the same network.

The interface was built using Bootstrap (https://getbootstrap.com/), a html-based framework of user interface components and functions for layout. One advantage of applications built using this framework is that they are 'responsive', meaning they can adapt to the size of the screen on which they are being viewed, thus allowing CaviConsole to be controlled via the small screen of a mobile device, such as a smartphone or tablet. In combination with remote desktop control this provides many options for checking on the progress of sequences or configuring sequences in the lab, out in the field or in the glasshouse.

The user interface has five main sections: i) Config – for selecting/creating a sequence INI configuration file, ii) Capture – for controlling and configuring CaviCapture and the capture process, iii) Process – for controlling and configuring CaviProcess and image processing, iv) Results – displays the results of image processing, v) Advanced – for controlling various Raspberry Pi and CaviConsole settings.

Config

CaviConsole uses the INI configuration file shared between the CaviCapture and CaviProcess programs to read/write settings. The config section provides an option for entering the path of an existing configuration file or for creating a new configuration file (Fig. 4.15) Once a configuration file has been loaded or created the other sections become visible and are preloaded with the settings from the configuration file.

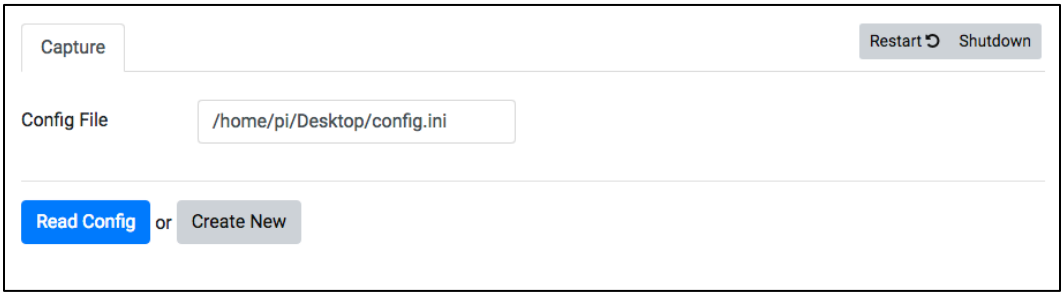

Figure 4.15. The CaviConsole configuration screen. The user enters the location of an existing configuration file or chooses to create a new file. Once the new/existing file is loaded the other sections of the interface become visible.

Capture

The capture section sets the configuration settings for CaviCapture (Fig. 4.16), including the camera ISO, shutterspeed, image resolution, capture interval, capture total duration, sample type (i.e. stem or leaf) and output directory for images. CaviConsole forces the user to select an external device (e.g. a USB memory stick) for the output directory. Storing images on the same memory as the Raspbian operating system can cause the system to become inaccessible once the on-board memory is full. Using an external memory also makes it easier to transfer the images from the Raspberry Pi. The user can force the system to use local storage by directly editing the CaviConsole configuration file. Indeed, any of the settings can be changed manually in the configuration file and then reloaded into the GUI via the 'Reload Config' button.

The crop option provides functionality for setting the crop area. Once enabled the user is presented with a still from the camera over which they can drag a marquee to select the region of interest, thus cropping unwanted image space (Fig. 4.17). The crop dimensions are saved to the configuration file.

A 'Live' button provides the functionality of the CaviCapture 'setup' mode to position and focus the sample using a live feed from the camera (Fig. 4.18). Illumination is controlled using a 'Light' button that toggles the lights on or off.

Once all the relevant options are set and configured the user can initiate a dry-run using the 'Preview' button which captures an image using the current settings and displays the output image to the user (Fig. 4.19). To initiate the capture sequence the user presses a 'Start' button which can be pressed again to stop the capture. The 'View Log' button opens a window with a live feed of capture events and errors.

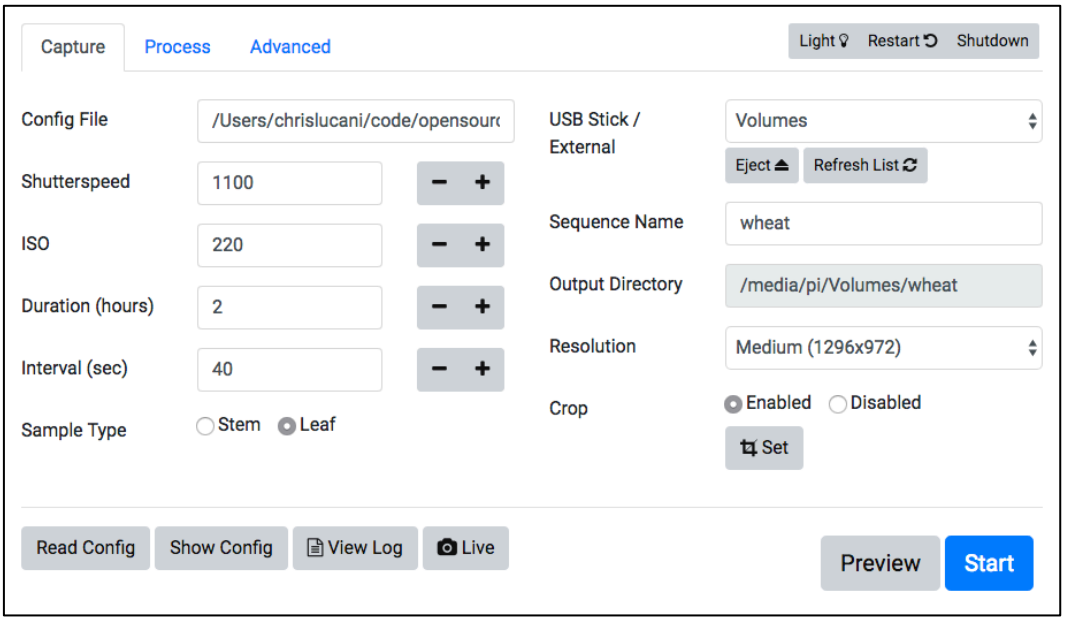

Figure 4.16 The CaviConsole 'Capture' section provides options to configure the CaviCapture program and start/stop image capture.

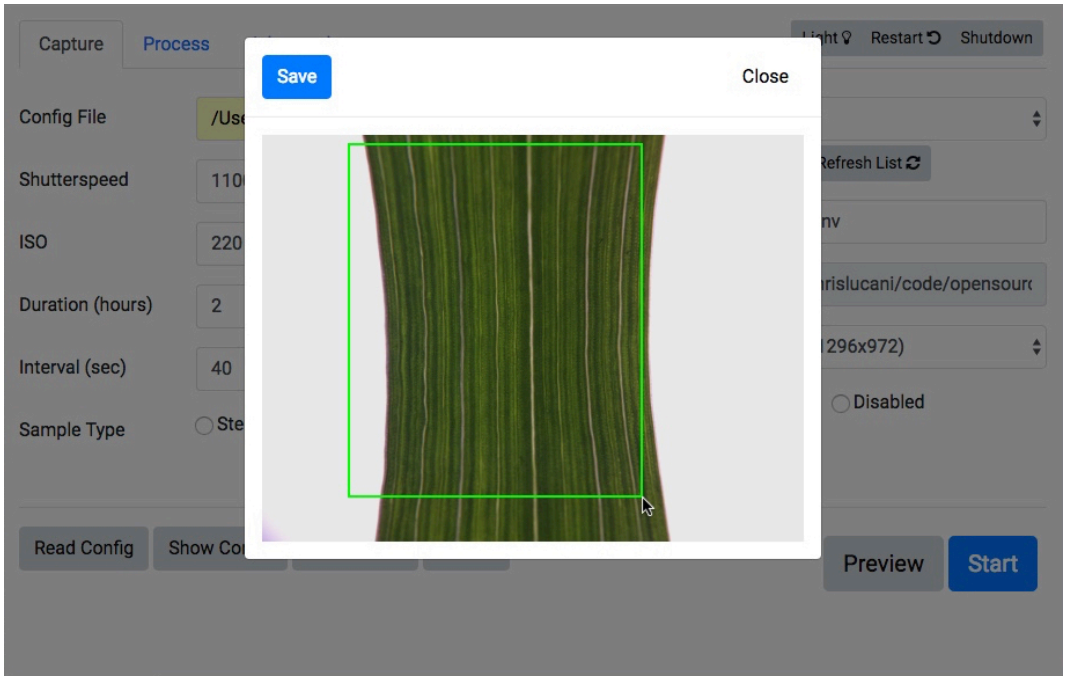

Figure 4.17 A smaller region of the camera field of view is defined using the crop function. The green marquee defines the dimensions of the crop area and is set by dragging the mouse around the preview. Once the region has been defined the user clicks the 'Save' button and is returned to the Capture screen.

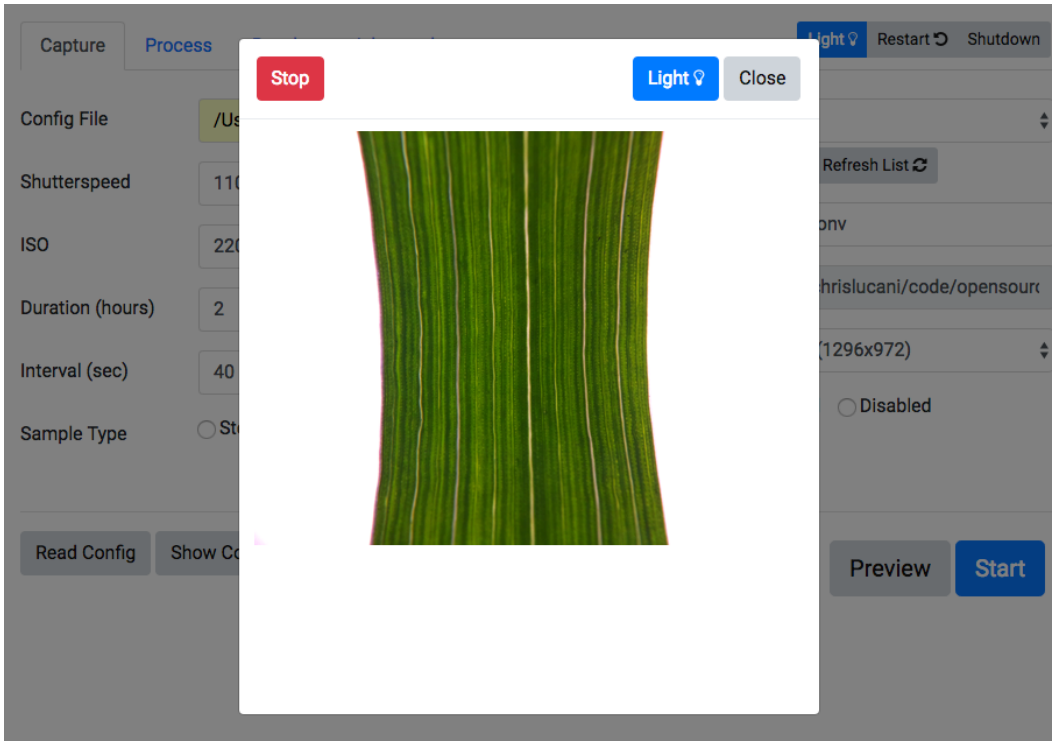

Figure 4.19 The sample is positioned and the focus adjusted using a live feed from the camera. The 'Light' button toggles the CaviClamp illumination on or off.

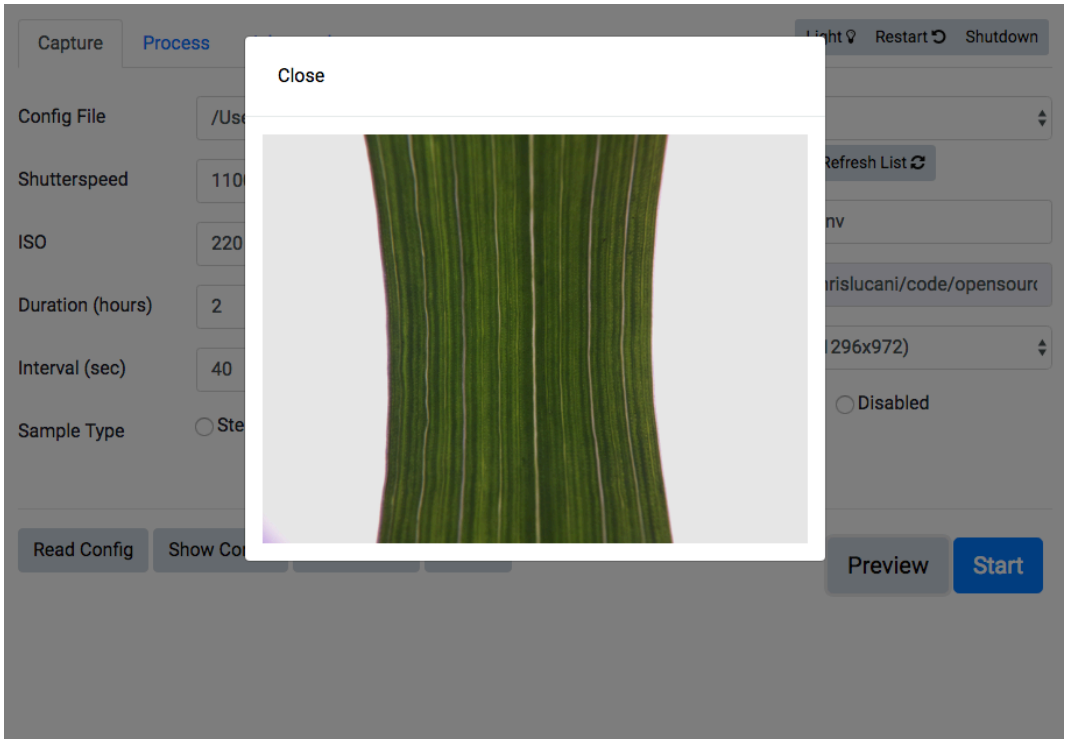

Figure 4.20 The 'Preview' function captures a single image using the settings from the Capture screen and displays the result to the user to check before initiating the capture sequence.

Process

The process section provides functions for starting, stopping and configuring CaviProcess, including options for enabling/disabling image processing steps, setting the pixel filter threshold, and for setting the ROI ('Set ROI') (Fig. 4.20). By enabling the ROI the user is presented with a still from the camera where they can drag a marquee to define the ROI (Fig. 4.21). Enabling the 'Intermediates' option saves the result of each step of processing as a separate file.

The 'Start' button is used to stop/start automated processing and the 'View Log' button shows a live feed of processing events and errors. The 'Queue' button provides a live summary of the number of images processed and the total number of images. The 'Export Data' function generates a CSV download of the embolism areas.

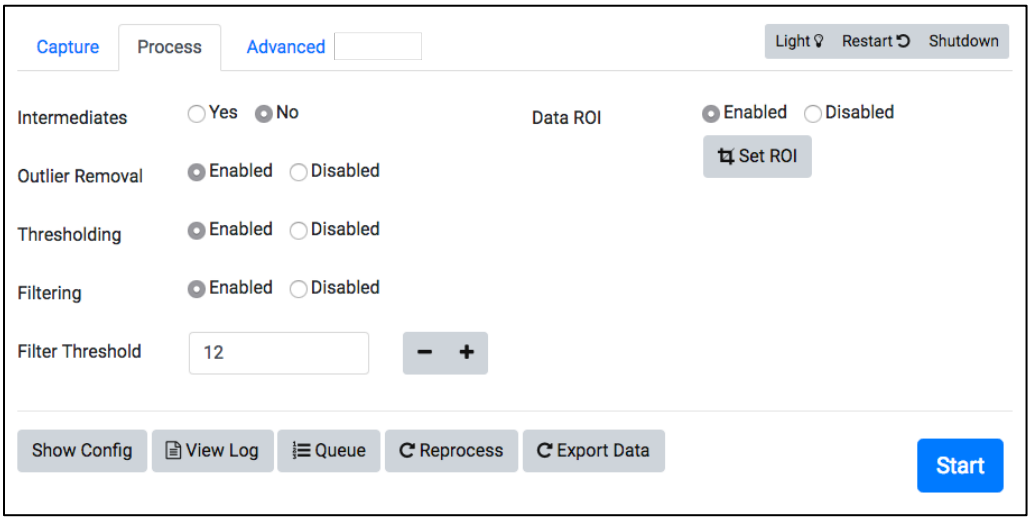

Figure 4.20 The CaviConsole 'Process' section provides options to configure the CaviProcess program and to start/stop automated image processing.

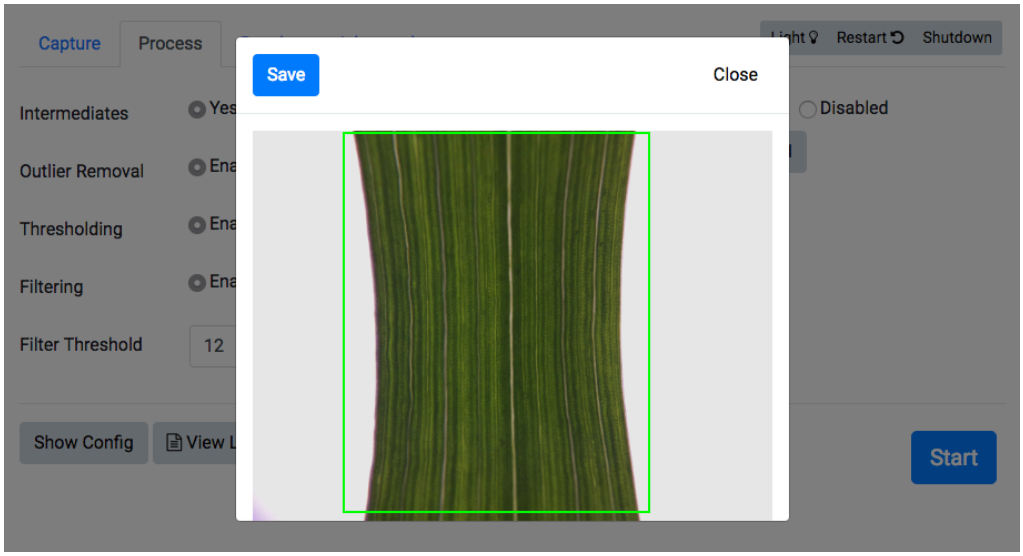

Figure 4.21 The final step of processing is to count the number of non-zero pixels that remain after procedures to remove noise. The remaining pixels represent the differences between images i.e. the embolism events or artefacts. The Data ROI tool enables the user to limit the count of pixels to a sub region of the image (the ROI).

Results

The results section is visible after image processing is initiated for the first time. Results displays a running timeline of total embolism area per image (sum of non-zero pixels) with time on the *x* axis and embolism area on the *y* axis (Fig. 4.22). As images are processed the areas are automatically added to the plot. Depending on the

degree of synchronisation between capture and processing this plot can provide near-real time tracking of embolism events within 80 seconds of an embolism event plus the interval between captures. Data can be displayed as a running total by toggling a 'Cumulative' button at the top of the plot area (Fig. 4.23).

To check for artefacts and to validate the pixel threshold value the user can click (or tap if on a mobile device) any of the plot data points and see the original captured image, the processed result and the total embolism area (Fig. 4.24). An option to edit the total pixel count allows the user to adjust the area to zero if it is obvious that none of the pixels are related to embolism. By using the left and right cursor keys or by swiping left and right with a finger the user can navigate through the previous and next 10 captured images.

The data ROI, processing queue and the processing log are also accessible from this section, as well as a button to initiate re-processing. When the ROI is changed CaviProcess is stopped and then re-started using the 'roiareas' option. The plot updates with the new values as they are amended and once complete processing is resumed by the user. If time synchronisation between image capture and processing is important then ROI queries are performed after the capture sequence is complete.

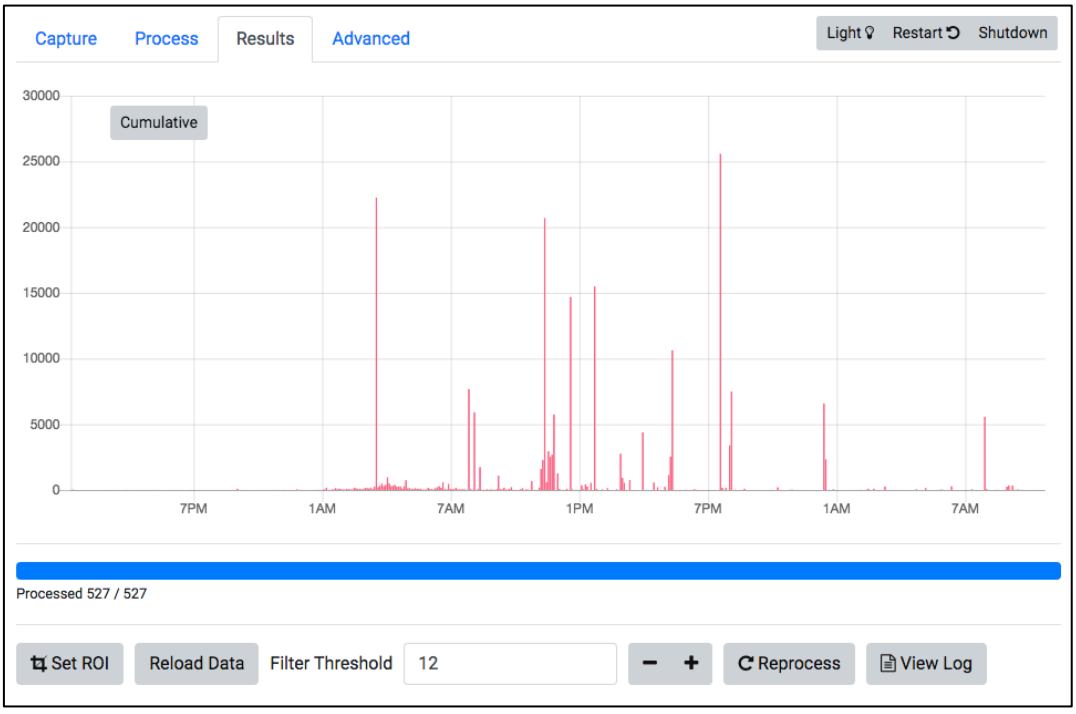

Figure 4.22 As images are captured using CaviCapture and then processed using the CaviProcess program the results of processing – the counts of non-zero pixels – is plotted on a graph. On this screenshot counts of non-zero pixels are shown for a wheat plant imaged over several hours. On the y-axis is the sum of pixels and the x-axis is time. Larger peaks can indicate that a larger or more numerous embolism events have occurred.

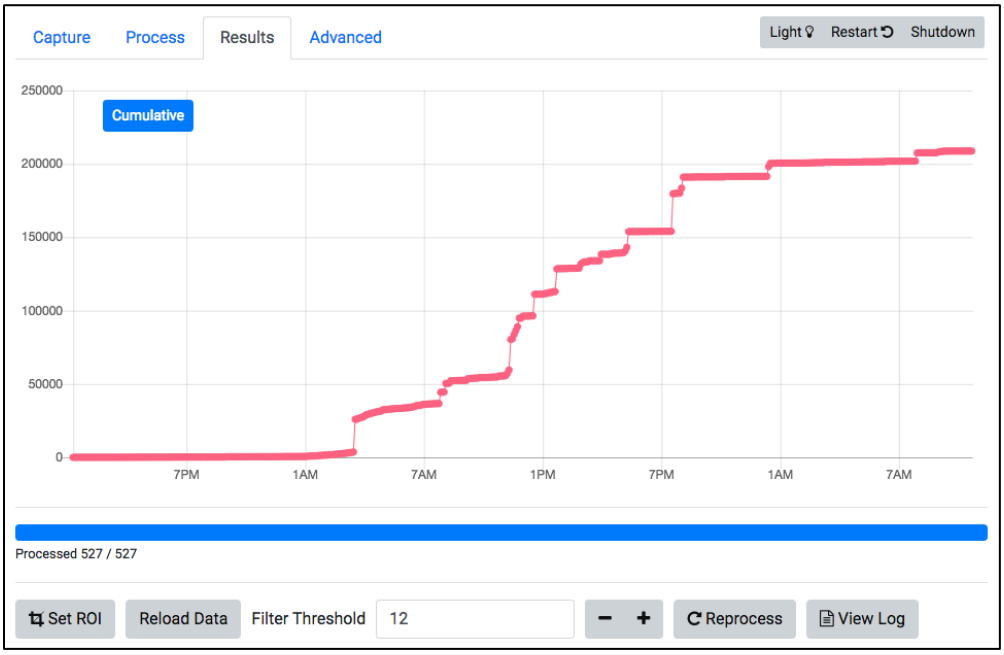

Figure 4.23 The plot of non-zero pixels can also be shown as a cumulative count. Here the same data from Fig. 4.2.2 is shown using the cumulative function.

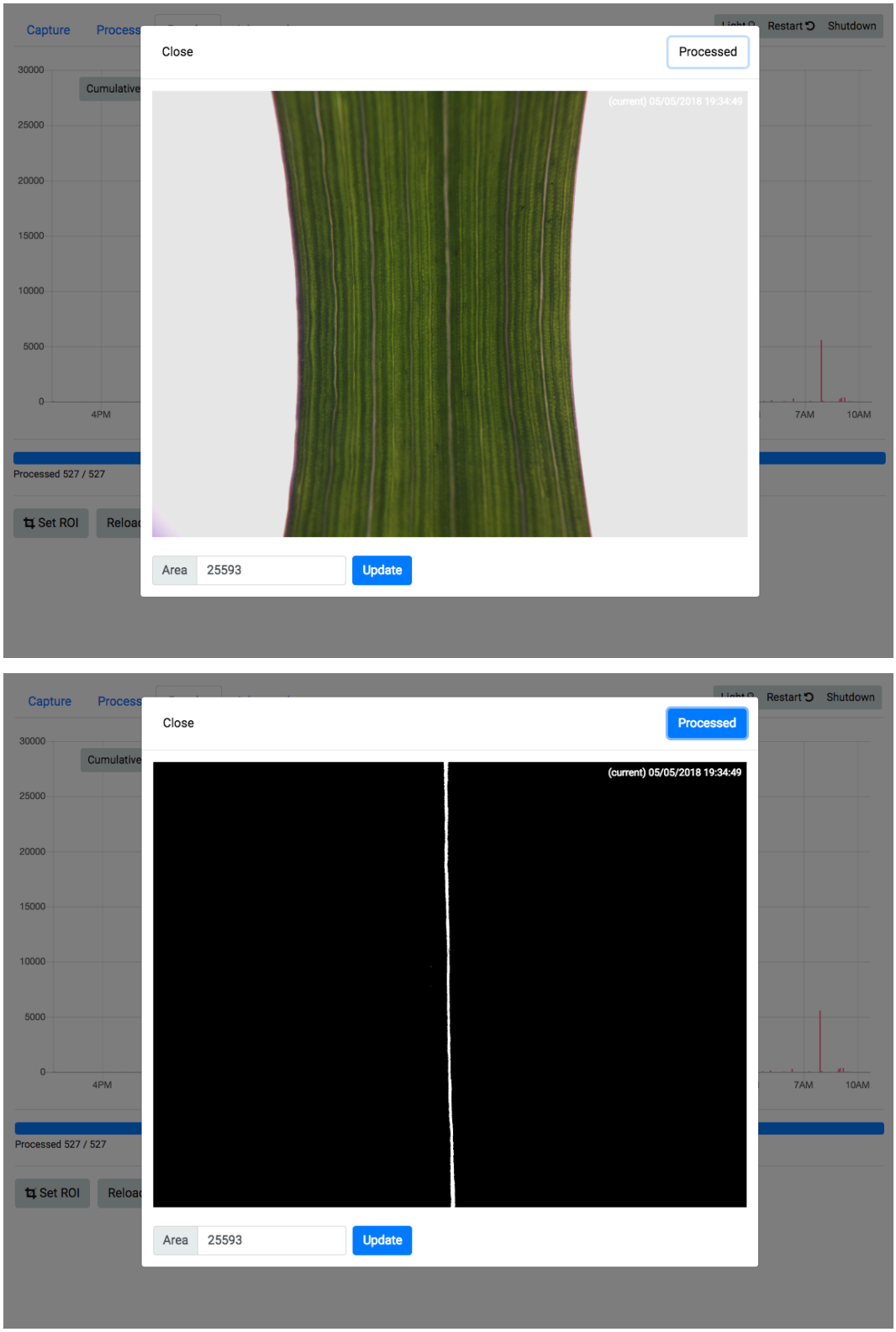

Figure 4.24 By clicking (or tapping if using a touch screen device) any of the data points on the results plot (Fig. 4.22) the user can see the original captured image (top) and the processed image (bottom). The pixel count (Area) can be adjusted to

zero using a form at the bottom of the image. In the bottom image a clear embolism event is seen in the mid-vein of the wheat leaf.

Advanced

The advanced section provides options for setting the location of the CaviCapture and CaviProcess programs, the GPIO pin used to connect the Raspberry Pi to the CaviClamp illumination via the transistor circuit, and a network configuration option for toggling the Raspberry Pi between 'Access Point' and 'Network' mode (Fig. 4.25). 'Access Point' mode configures the Raspberry Pi to run as a router that creates a wireless network for other computers to join. This is useful for connecting to the Raspberry Pi where other networks may not be available, such in the field or in a glasshouse, but it also offers a simple way of remotely controlling the Pi in the lab by using any available computer with Wi-Fi capabilities (including mobile devices). 'Network' mode configures the Raspberry Pi to connect to an existing wireless network.

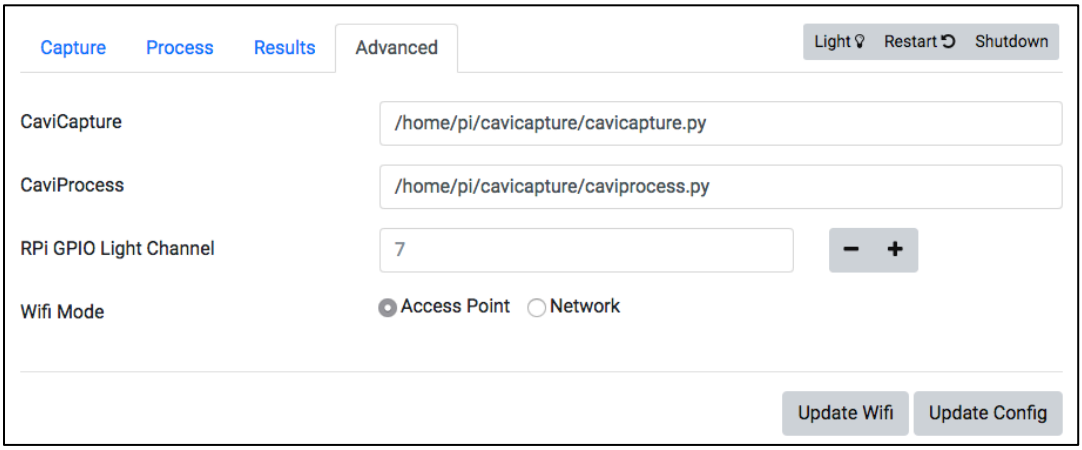

Figure 4.25 The advanced section of CaviConsole provides options for setting the CaviCapture and CaviProcess programs to use and the Raspberry Pi GPIO 'output' pin used to control the illumination. 'Wifi mode' enables the user to choose whether the Raspberry Pi should run as an 'access point' or be connected to a Wi-Fi network. In access mode the Raspberry Pi creates a wireless network that other computers can join. This is useful for remotely connecting to the Raspberry Pi without an internet connection.

4.2.11 OpenSourceOV.org

OpenSourceOV.org was developed to provide the necessary resources for promoting, building and using the device, including parts and supplier lists, learning materials, 3D printable files and resources, processing and analysis instructions, and ImageJ plugins. The site also provides a gallery for user-contributed capture sequences, a general guide for sample selection and preparation, and a repository of published articles that use the device or the optical technique.

CaviCam build instructions, processing and analysis instructions, parts and supplier lists and ImageJ plugins are hosted as git repositories on GitHub, an online collaborative platform for community-driven development of open source resources. Appendix 1 provides an overview and screenshots of OpenSourceOV.org. Details of the GitHub repositories can be found in Appendix 2.

4.3 Results

I have developed a cheap, effective, portable and widely accessible system for assessing stem and leaf xylem vulnerability in short and long vesseled species. The CaviCam system comprises: 1) the CaviCam - a time-lapse device for capturing images of the xylem over time, 2) A Raspberry Pi micro-computer, 3) CaviCapture – a command line program for capturing images using the CaviCam, 4) CaviProcess – a command line program for processing captured images to reveal embolism events, 5) CaviTools – an ImageJ plugin toolbox of plugins and scripts for manually processing captured images and generating figures for publication using ImageJ, 6) CaviConsole – a GUI for controlling the CaviCapture and CaviProcess programs and displaying the results from processing.

Support materials for the CaviCam system, including detailed CaviCam build instructions, programs, supplier and parts lists, learning materials, details about the optical vulnerability method, and processing and analysis guides and instructional videos, are available online through a new website OpenSourceOV.org (http://www.opensourceov.org).

4.4 Discussion

The CaviCam is an affordable, easy to build and widely accessible device for measuring xylem vulnerability, a primary determinant of the drought tolerance of plants. By employing a non-invasive visual technique for identifying embolism formation the system is immune to artefacts present in other techniques associated with using excised material, and can measure leaf and stem xylem in both short- and long-vesseled species. Automated image processing has the ability to provide, for the first time, near real-time tracking of embolism events throughout a cycle of dehydration.

All the necessary programs, 3D models and support materials are freely available online and can be adapted to suit different components, applications and experimental setups. The CaviCam is constructed using 3D-printed parts that can be modified using CAD software and reprinted as necessary, and the Raspberry Pi was designed ‘out-of-the-box’ to integrate with a diversity of sensors and electronic components that can be controlled using a wide variety of programming languages. The Raspberry Pi platform is well supported by numerous suppliers, a wealth of online guides and learning resources, and a large community of enthusiasts to help resolve problems. Image capture and processing are controlled via extensible programs that can be integrated into other software and processes. This was demonstrated in the development of CaviConsole, an advanced software GUI for on-board and remote control of the CaviCam system.

The platform is expected to have a broad appeal among plant physiologists, ecologists, geneticists, plant breeders, and educators, and in doing so has the potential to boost the number of vulnerability assessments while filling a gap for a robust, accurate and reliable system for measuring all species including herbaceous and long-vesseled species which are notoriously difficult to measure with other methods.

For educators the system is an excellent resource popular among students because of the combination of new technologies such as 3D printing and modern electronics and the immediacy and visual nature of the results.

For geneticists and plant breeders the system has application in phenotyping, and indeed the affordability and flexibility of a Raspberry Pi-based system is already being realised in a new generation of affordable 'DIY' phenotyping platforms such as Phenotiki (Minervini et al., 2017), PYM (Valle et al., 2017) and others (Tovar et al., 2018). Directly measuring xylem vulnerability is faster and more accurate than current approaches for quantifying drought tolerance which typically involve growing plants under drought conditions and monitoring a suite of traits over a period of growth to identify signs of susceptibility. In comparison, an assessment of xylem vulnerability can be completed in one cycle of dehydration. The limiting factor in affordable xylem vulnerability phenotyping is measurement of water potential. New approaches that use spectral signatures as a proxy for water status might provide one solution (Rapaport et al., 2017).

For ecologists the system provides a more accessible, portable and low power means of assessing an important trait in the lab or in the field that can otherwise be difficult and time-consuming to measure accurately with traditional methods. The CaviConsole has a shallower learning curve. By following the instructions provided online it can be setup and used very quickly with results appearing virtually as they happen.

For physiologists the system provides a convenient, affordable and easy to use device for applying the optical method of assessing xylem vulnerability. Additionally, because of its low cost and size it provides new opportunities to understand the spatial and temporal distribution of drought damage in plants. For example, multiple CaviCams can be fitted to several leaves and stems on the same plant to simultaneously monitor and evaluate embolism formation among and between organs in response to water stress. Such an approach would be impossible with other techniques and could provide, for example, valuable insight into our understanding of hydraulic segmentation.

By integrating other sensors, such as spectral and hyperspectral analysers (Khan et al., 2018; Mohd Asaari et al., 2018), fluorometers, porometers, sap flow sensors, and gas exchange analysers, the system provides new opportunities for evaluating drought damage in the context of other physiological processes. For example, in

combination with real-time identification of embolism events this offers a new way of exploring relationships between xylem vulnerability, gas exchange, and sap flow.

Chapter 5 - Conclusion

Developing accurate models to predict vegetation response to climate change is critical to planning and managing the impact of global warming on biodiversity (Sykes et al., 2005; Bellard et al., 2012), ecosystem integrity (Lenton et al., 2008), agriculture (Nelson et al., 2014), and associated implications for animal and human populations (IPCC, 2007).

Climate vegetation models based on functional trait such as the P_{50} and HSM can significantly improve the ability to predict vegetation mortality and changes in species distribution due to changes in temperature and the occurrence, severity and intensity of droughts under climate change (Buckley and Kingsolver, 2012; Soudzilovskaia et al., 2013; Anderegg, 2014; Skelton, West and Dawson, 2015; Yang et al., 2015).

To achieve these outcomes, a substantial increase in the number of xylem vulnerability measurements are required. Current approaches for measuring vulnerability are either limited in capacity to measure a large number of plants, or are limited to short-vesseled species, thus the broad aim of the thesis was to find a technique that could be used for accurately measuring vulnerability in large number of species or individuals.

5.1 Increasing capacity by reducing the number of measurements

The initial approach was to reduce the overall number of measurements required to undertake a conductance-based evaluation of vulnerability (chapter 2). In comparison with other approaches, conductance-based methods offer the right combination of broad accessibility, affordability, and capacity to measure a range of species, but are limited because they are sample-intensive and time consuming. Thus I attempted to reduce the sample size required by exploring an alternative approach where differences in vulnerability are revealed by measuring and comparing conductance at a single common water potential (the reference water potential), instead of across a range of water potentials that are necessary to generate a full vulnerability curve.

The approach demonstrated a capacity to identify significant phenotypic variation, however it was limited in ability to meet the aim of the thesis because of two factors. The first is that the efficiency of the system is limited by the number of water potential measurements that are made to precisely dry the samples down to a common water potential. Although the software I developed for tracking and predicting drying times can reduce the number of water potential measurements required, the precision of the software, and therefore the efficacy of reducing measurements by predicting drying times, relies on stable conditions of temperature and humidity. In a lab these are relatively easy to control, but less so, or impossible, in a glasshouse or the field. Using a psychrometer instead of a pressure chamber to measure water potential would resolves these issues, but a separate psychrometer would be required for each sample (since they have to be in constant contact with the xylem), and this would impact affordability and/or limit the capacity to measure a large number of samples. Secondly, the approach requires pre-assessment of the likely range in water potential to identify a suitable reference water potential. This requires a dataset of full vulnerability curves, thus the approach is only beneficial at scale where the overall number of samples is more than what is necessary to determine the reference water potential.

The approach can deliver savings in time and effort, especially if a psychrometer is used to continually log water potential, but towards the aim of generating a significant number of assessments across a broad number of species, the approach has limited application.

5.2 Improving the accessibility of an optical method

The innovation of an optical technique for assessing xylem vulnerability (Brodribb et al. 2016) provided new opportunities to increase capacity for vulnerability assessments. The use of document scanners had already proved useful in capturing high resolution images of multiple samples (Brodribb et al. 2017), but the procedure for setting up automated scanning of different regions and specific time intervals was difficult and restricted to OEM (original equipment manufacturer) scanner software, which limited the procedure to scanner models from a particular brand. I realised that by simplifying this procedure and developing an approach that would work across all common desktop scanners, there was significant potential for a broadly-accessible

procedure with potential for scaling. To this end I developed a highly customisable script (CaviScan) that integrated with a widely-available scanner control software product (VueScan) that was capable of interfacing with an extensive list of common desktop scanners. Using the script, multiple scanners can be controlled using a single computer, thus allowing the system to be scaled-up. In theory this could enable a farm of scanners to image a significant number of samples.

I tested the system by evaluating differences in vulnerability between juvenile and adult leaves and stems (chapter 3), thus demonstrating the capacity to simultaneously measure different organs and multiple samples, while answering an important question about variation in vulnerability associated with ontogeny. In that regard I was able to demonstrate that juvenile leaves are more vulnerable than adult leaves of *Eucalyptus globulus*, a result that indicates the critical need to measure and represent variation associated with age and development. But in terms of leveraging desktop scanners to boost capacity for vulnerability measurements, I realised two things that led to the conclusion that they are not the ideal solution. The first was that despite the software system working well in maximising the scannable area for simultaneously measuring multiple samples, actually fitting multiple samples in the scanner was a difficult and time-consuming procedure, one that often involved wrangling large branches into awkward and unstable positions. The second was the common occurrence of banding artefacts in the scanned images, presumably caused by imperfect coordination between the movement of the scanner head and the read out from the light sensors. This highlighted to me a fundamental limitation in the application of desktop scanners: that image quality will always depend on a mechanical process that can be subject to wear, quality of construction, product age, and the eccentricities of certain makes and models. These issues would likely compound with age and use, and be a source of considerable time, effort, and frustration in a high volume setup like a scanner farm.

Nonetheless, desktop scanners are still useful in applying the optical technique because they offer high resolution over a large area, and provide the only method for scanning larger leaves. They are also broadly and immediately accessible since most laboratories have access to a scanner for measurement of traits such as leaf area. For these reasons the CaviScan script is still useful. Indeed, translating the procedures for

automated processing that were later developed for the CaviCam system such that they could also be used with desktop scanners could significantly increase the overall usability and speed of the scanning workflow.

5.3 A new device

To circumvent the issues related to mechanically-aided capture, returning to the original method of image capture, a digital camera, was the obvious solution. However, as shown in chapter 4, a camera setup can also be particularly awkward, cumbersome, immobile, and susceptible to its own particular set of artefacts caused by knocks and bumps. Plus a camera setup requires a separate solution for illumination, which adds another layer of complexity and difficulty. As such it can require a similar degree of wrangling and time to the scanner approach to orientate and securely fix a leaf or stem in position.

In regarding the significant amount of unnecessary physical and technological overhead in a typical camera setup, it was clear that a far simpler device could be designed and constructed that incorporated just the basic elements of illumination, magnification, a digital camera, software control, and a means of securely fixing the sample in position. I eventually achieved this in the development of the CaviCam device by using custom-designed 3D-printed parts, and the integration of widely available electronic components and a cheap micro-computer (chapter 4). I also developed computer programs and GUI to control and orchestrate illumination and image capture, and for automatically processing images to identify and quantify embolism events in near real-time.

The resulting platform is accurate, cheap, user friendly, compact and portable. Combining these features with the extensibility of the software and hardware provides an innovative and adaptable platform that meets the basic requirement of vulnerability assessment, while offering new opportunities for investigating embolism events in the context of other physiological processes.

To support and promote the system I developed OpenSourceOV.org and created detailed and extensive guides and resources for building, using and adapting the CaviCam device and contributing to its continued development. All resources were

made available on GitHub, a collaborative online platform that provides an easy way for users to download resources and keep up to date with fixes and improvements, while also allowing users to upload their own improvements, adaptations, and variants for the benefit of others.

The extensibility of the hardware and the software architecture lends itself to integration with other sensors and systems such as gas exchange and spectral analysers, sap flow meters and temperature and humidity sensors. This significantly increases the potential applications for the device in investigating drought stress in the context of a raft of other physiological processes. For example, combining measurements of chlorophyll fluorescence with optical measurements of xylem vulnerability has already proved useful in analysing drought recovery in wheat plants (Johnson, Jordan and Brodribb, 2018).

Integration with spectral and hyperspectral analysers would offer an extra dimension of insight into drought stress and related physiology. As plants dehydrate a number of physiological and structural changes occur (Scoffoni et al., 2014) that alter the spectral signature of the plant (Mahlein et al., 2013). Analysis of spectral signatures have been used to identify drought stress (Mahlein et al., 2013), but have not, to my knowledge, been assessed in context of embolism formation.

A significant innovation of the system is near real-time tracking of embolism events in excised segments and shoots and intact plants. Not only does this significantly reduce the time required to complete an assessment of vulnerability – post-capture processing often causes a bottleneck when measuring multiple samples - but it also provides exciting new opportunities for monitoring and probing the dynamic physiology of drought stress.

5.1 Summary

By providing a system that is widely accessible and capable of accurately measuring a diversity of species, I believe the CaviCam has the potential to meet the research aim of this thesis. Time will tell whether it has achieved this goal, but as at the date of thesis submission I have personally built a total of 40 CaviCams, 10 of which are being used in the Department of Natural Sciences at the University of Tasmania in

Australia, 3 are being loaned to other universities in Australia and France, and the remaining CaviCams were acquired by various institutions and research departments in Australia, France, Spain, Israel, Italy, North and South America, and China. These are being used in a range of studies which are starting to appear in the literature (e.g. Rodriguez-Dominguez et al. 2018). I am also aware of at least another 49 CaviCams that were built and modified to use different electronic components and lens configurations (C. Barton, S. Gleason, *pers. comms.*). How many other CaviCams have been constructed using the resources provided through OpenSourceOV.org is impossible to determine, but in the 16 months since the website went online in May 2017, there have been 2000 visitors to the site, just over 3500 sessions (a session being a user entering the site, looking at various pages and then leaving) and an average of just over 200 new users each month since January 2018, a figure increasing by an average of 10% per month. This indicates a significant and growing interest in the platform.

It is an exciting time for innovation. A number of key technologies are converging in maturity, affordability, and accessibility: 3D printing, micro-computers, micro-controllers, a diversity of sensors, smartphones, machine learning and artificial intelligence (AI), advanced image processing, fast and wireless internet, and cloud-based high-performance processing. Together this means that cutting-edge technology and capability can be leveraged by the individual, and *vice versa* that networks of individuals can be mobilised in the application of cutting-edge technology. In this second capacity through application of devices such as the CaviCam I believe we have the necessary capability to achieve a global assessment of vegetation drought tolerance.

References

Aasamaa, K., Sõber, A. and Rahi, M. (2001) 'Leaf anatomical characteristics associated with shoot hydraulic conductance, stomatal conductance and stomatal sensitivity to changes of leaf water status in temperate deciduous trees', *Functional Plant Biology*, 28(8), p. 765. doi: 10.1071/PP00157.

Adams, H. D., Guardiola-Claramonte, M., Barron-Gafford, G. A., Villegas, J. C., Breshears, D. D., Zou, C. B., Troch, P. A. and Huxman, T. E. (2009) 'Temperature sensitivity of drought-induced tree mortality portends increased regional die-off under global-change-type drought', *Proceedings of the National Academy of Sciences*, 106(17), pp. 7063–7066. doi: 10.1073/pnas.0901438106.

Aitken, S. N. and Bemmels, J. B. (2016) 'Time to get moving: Assisted gene flow of forest trees', *Evolutionary Applications*, 9(1), pp. 271–290. doi: 10.1111/eva.12293.

Aitken, S. N. and Whitlock, M. C. (2013) 'Assisted Gene Flow to Facilitate Local Adaptation to Climate Change', *Annual Review of Ecology, Evolution, and Systematics*, 44, pp. 367–88. doi: 10.1146/annurev-ecolsys-110512-135747.

Alder, N. N. (1997) 'Use of centrifugal force in the study of xylem cavitation', *Journal of Experimental Botany*, 48(308), pp. 665–674. doi: 10.1093/jxb/48.3.665.

Allen, C. D., Breshears, D. D. and McDowell, N. G. (2015) 'On underestimation of global vulnerability to tree mortality and forest die-off from hotter drought in the Anthropocene', *Ecosphere*, 6(8), p. art129. doi: 10.1890/ES15-00203.1.

Allen, C. D., Macalady, A. K., Chenchouni, H., Bachelet, D., McDowell, N., Vennetier, M., Kitzberger, T., Rigling, A., Breshears, D. D., Hogg, E. H. (Ted), Gonzalez, P., Fensham, R., Zhang, Z., Castro, J., Demidova, N., Lim, J.-H., Allard, G., Running, S. W., Semerci, A. and Cobb, N. (2010) 'A global overview of drought and heat-induced tree mortality reveals emerging climate change risks for forests', *Forest Ecology and Management*, 259(4), pp. 660–684. doi: 10.1016/j.foreco.2009.09.001.

Anderegg, W. R. L. (2014) 'Spatial and temporal variation in plant hydraulic traits and their relevance for climate change impacts on vegetation', *New Phytologist*, pp.

1008–1014. doi: 10.1111/nph.12907.

Anderegg, W. R. L., Flint, A., Huang, C. Y., Flint, L., Berry, J. A., Davis, F. W., Sperry, J. S. and Field, C. B. (2015) 'Tree mortality predicted from drought-induced vascular damage', *Nature Geoscience*, 8(5), pp. 367–371. doi: 10.1038/ngeo2400.

Anderegg, W. R. L., Hicke, J. A., Fisher, R. A., Allen, C. D., Aukema, J., Bentz, B., Hood, S., Lichstein, J. W., Macalady, A. K., McDowell, N., Pan, Y., Raffa, K., Sala, A., Shaw, J. D., Stephenson, N. L., Tague, C. and Zeppel, M. (2015) 'Tree mortality from drought, insects, and their interactions in a changing climate', *New Phytologist*, 208(3), pp. 674–683. doi: 10.1111/nph.13477.

Anderegg, W. R. L., Klein, T., Bartlett, M., Sack, L., Pellegrini, A. F. A. and Choat, B. (2016) 'Meta-analysis reveals that hydraulic traits explain cross-species patterns of drought-induced tree mortality across the globe', *Proceedings of the National Academy of Sciences*, 113(18), pp. 2–7. doi: 10.1073/pnas.1525678113.

Bak, D. (2003) 'Rapid prototyping or rapid production? 3D printing processes move industry towards the latter', *Assembly Automation*, 23(4), pp. 340–345. doi: 10.1108/01445150310501190.

Barber, H. N. (1965) 'Selection in natural populations', *Heredity*, 20(August), pp. 551–572. doi: 10.1038/hdy.1965.68.

Bellard, C., Bertelsmeier, C., Leadley, P., Thuiller, W. and Courchamp, F. (2012) 'Impacts of climate change on the future of biodiversity', *Ecology Letters*, 15, pp. 365–377. doi: 10.1111/j.1461-0248.2011.01736.x.

Blackman, C. J., Aspinwall, M. J., Tissue, D. T. and Rymer, P. D. (2017) 'Genetic adaptation and phenotypic plasticity contribute to greater leaf hydraulic tolerance in response to drought in warmer climates', *Tree Physiology*, pp. 1–10. doi: 10.1093/treephys/tpx005.

Blackman, C. J., Brodribb, T. J. and Jordan, G. J. (2009) 'Leaf hydraulics and drought stress: response, recovery and survivorship in four woody temperate plant species.', *Plant, Cell and Environment*, 32(11), pp. 1584–95. doi: 10.1111/j.1365-3040.2009.02023.x.

Blackman, C. J., Brodribb, T. J. and Jordan, G. J. (2012) ‘Leaf hydraulic vulnerability influences species’ bioclimatic limits in a diverse group of woody angiosperms.’, *Oecologia*, 168(1), pp. 1–10. doi: 10.1007/s00442-011-2064-3.

Bogue, R. (2013) ‘3D printing: The dawn of a new era in manufacturing?’, *Assembly Automation*, 33(4), pp. 307–311. doi: 10.1108/AA-06-2013-055.

Booth, T. H., Broadhurst, L. M., Pinkard, E., Prober, S. M., Dillon, S. K., Bush, D., Pinyopusarerk, K., Doran, J. C., Ivkovich, M. and Young, A. G. (2015) ‘Native forests and climate change: Lessons from eucalypts’, *Forest Ecology and Management*. Elsevier B.V., 347, pp. 18–29. doi: 10.1016/j.foreco.2015.03.002.

Boughton, V. H. (1986) ‘Phyllode structure, taxonomy and distribution in some Australian Acacias’, *Australian Journal of Botany*, 34(6), pp. 663–674. doi: 10.1071/BT9860663.

Breda, N., Cochard, H., Dreyer, E. and Granier, a (1993) ‘Field Comparison of Transpiration, Stomatal Conductance and Vulnerability To Cavitation of Quercus-petraea and Quercus-robur Under Water-stress’, *Annales Des Sciences Forestieres*, 50(6), pp. 571–582. doi: 10.1051/forest:19930606.

Brennan, E. B., Weinbaum, S. a., Rosenheim, J. a. and Karban, R. (2001) ‘Heteroblasty in Eucalyptus globulus (Myricales : Myricaceae) affects ovipositonal and settling preferences of Ctenarytaina eucalypti and C-spatulata (Homoptera : Psyllidae)’, *Environmental Entomology*, 30(6), pp. 1144–1149. doi: 10.1603/0046-225X-30.6.1144.

Breshears, D. D., Cobb, N. S., Rich, P. M., Price, K. P., Allen, C. D., Balice, R. G., Romme, W. H., Kastens, J. H., Floyd, M. L., Belnap, J., Anderson, J. J., Myers, O. B. and Meyer, C. W. (2005) ‘Regional vegetation die-off in response to global-change-type drought’, *Proceedings of the National Academy of Sciences*, 102(42), pp. 15144–15148. doi: 10.1073/pnas.0505734102.

Brodersen, C. R., Mcelrone, A. J., Choat, B., Lee, E. F., Shackel, K. A. and Matthews, M. A. (2013) ‘In Vivo Visualizations of Drought-Induced Embolism’, *Plant Physiology*, 161(April), pp. 1820–1829. doi: 10.1104/pp.112.212712.

Brodribb, T. and Feild, T. (2000) ‘Stem hydraulic supply is linked to leaf photosynthetic capacity: evidence from New Caledonian and Tasmanian rainforests’, *Plant, Cell and Environment*, pp. 1381–1388. Available at: http://onlinelibrary.wiley.com/doi/10.1046/j.1365-3040.2000.00647.x/full (Accessed: 15 April 2013).

Brodribb, T. and Hill, R. (1999) ‘The importance of xylem constraints in the distribution of conifer species’, *New Phytologist*, 143(2), pp. 365–372. Available at: http://onlinelibrary.wiley.com/doi/10.1046/j.1469-8137.1999.00446.x/abstract (Accessed: 13 June 2013).

Brodribb, T. and Hill, R. S. (1993) ‘A physiological comparison of leaves and phyllodes in Acacia melanoxylon’, *Australian Journal of Botany*, 41(3), pp. 293–305. doi: 10.1071/BT9930293.

Brodribb, T. and Holbrook, N. (2003) ‘Stomatal closure during leaf dehydration, correlation with other leaf physiological traits’, *Plant Physiology*, 132(August), pp. 2166–2173. doi: 10.1104/pp.103.023879.sensitive.

Brodribb, T. and Holbrook, N. (2005) ‘Leaf hydraulic capacity in ferns, conifers and angiosperms: impacts on photosynthetic maxima’, *New Phytologist*, 165(3), pp. 839–846. Available at: http://onlinelibrary.wiley.com/doi/10.1111/j.1469-8137.2004.01259.x/full (Accessed: 18 June 2013).

Brodribb, T. J. (2009) ‘Xylem hydraulic physiology: The functional backbone of terrestrial plant productivity’, *Plant Science*, 177(4), pp. 245–251. doi: 10.1016/j.plantsci.2009.06.001.

Brodribb, T. J., Bienaimé, D. and Marmottant, P. (2016) ‘Revealing catastrophic failure of leaf networks under stress’, *Proceedings of the National Academy of Sciences*, 113(17), p. 201522569. doi: 10.1073/pnas.1522569113.

Brodribb, T. J., Carriqui, M., Delzon, S. and Lucani, C. (2017) ‘Optical Measurement of Stem Xylem Vulnerability’, *Plant Physiology*, 174(4), pp. 2054–2061. doi: 10.1104/pp.17.00552.

Brodribb, T. J. and Cochard, H. (2009) ‘Hydraulic failure defines the recovery and

point of death in water-stressed conifers.', *Plant Physiology*, 149(1), pp. 575–84. doi: 10.1104/pp.108.129783.

Brodribb, T. J., Feild, T. S. and Jordan, G. J. (2007) 'Leaf maximum photosynthetic rate and venation are linked by hydraulics.', *Plant Physiology*, 144(4), pp. 1890–8. doi: 10.1104/pp.107.101352.

Brodribb, T. J., Feild, T. S. and Sack, L. (2010) 'Viewing leaf structure and evolution from a hydraulic perspective', *Functional Plant Biology*, 37(6), p. 488. doi: 10.1071/FP10010.

Brodribb, T. J., McAdam, S. A. M., Jordan, G. J. and Martins, S. C. V (2014) 'Conifer species adapt to low-rainfall climates by following one of two divergent pathways.', *Proceedings of the National Academy of Sciences*, 111(40), pp. 14489–93. doi: 10.1073/pnas.1407930111.

Brodribb, T. J., McAdam, S. A. M., Jordan, G. J. and Feild, T. S. (2009) 'Evolution of stomatal responsiveness to CO(2) and optimization of water-use efficiency among land plants.', *New Phytologist*, 183(3), pp. 839–47. doi: 10.1111/j.1469-8137.2009.02844.x.

Brodribb, T. J., Skelton, R. P., Mcadam, S. A. M., Bienaimé, D., Lucani, C. J. and Marmottant, P. (2016) 'Visual quantification of embolism reveals leaf vulnerability to hydraulic failure', *New Phytologist*, 209(4), pp. 1403–1409. doi: 10.1111/nph.13846.

Brodribb, T., McAdam, S. A. M. and Carins Murphy, M. R. (2017) 'Xylem and stomata, coordinated through time and space', *Plant, Cell and Environment*, 40(6), pp. 872–880. doi: 10.1111/pce.12817.

Brown, G. K., Murphy, D. J., Kidman, J. and Ladiges, P. Y. (2012) 'Phylogenetic connections of phyllodinous species of Acacia outside Australia are explained by geological history and human-mediated dispersal', *Australian Systematic Botany*, 25(6), pp. 390–403. doi: 10.1071/SB12027.

Buckley, L. B. and Kingsolver, J. G. (2012) 'Functional and Phylogenetic Approaches to Forecasting Species' Responses to Climate Change', *Annual Review*

of Ecology, Evolution, and Systematics, 43(1), pp. 205–226. doi: 10.1146/annurev-ecolsys-110411-160516.

Bunker, D. E. and Carson, W. P. (2005) 'Drought stress and tropical forest woody seedlings: Effect on community structure and composition', *Journal of Ecology*, 93(4), pp. 794–806. doi: 10.1111/j.1365-2745.2005.01019.x.

Butt, N., Pollock, L. J. and Mcalpine, C. A. (2013) 'Eucalypts face increasing climate stress', *Ecology and Evolution*, 3(15), pp. 5011–5022. doi: 10.1002/ece3.873.

Canny, M. J. (1997) 'Vessel contents during transpiration- Embolisms and refilling', *American Journal of Botany*, 84(9), pp. 1223–1230. doi: 10.2307/2446046.

Carnegie, A. J. and Ades, P. K. (2005) 'Variation in Eucalyptus globulus LABILL. and E. nitens DEAN and MAIDEN in Susceptibility of Adult Foliage to Disease Caused by Mycosphaerella cryptica (COOKE) HANSF', *Silvae Genetica*, 54(1–6), pp. 174–184. doi: 10.1515/sg-2005-0026.

Carter, J. L. and White, D. A (2009) 'Plasticity in the Huber value contributes to homeostasis in leaf water relations of a mallee Eucalypt with variation to groundwater depth.', *Tree Physiology*, 29(11), pp. 1407–18. doi: 10.1093/treephys/tpp076.

Caupin, F. and Herbert, E. (2006) 'Cavitation in water: a review', *Comptes Rendus Physique*, 7(9–10), pp. 1000–1017. doi: 10.1016/j.crhy.2006.10.015.

Chambers, P. G. S., Borralho, N. M. G. and Potts, B. M. (1996) 'Genetic analysis of survival in Eucalyptus globulus ssp. globulus', *Silvae Genetica*, 45(2–3), pp. 107–112.

Charrier, G., Delzon, S., Domec, J. C., Zhang, L., Delmas, C. E. L., Merlin, I., Corso, D., King, A., Ojeda, H., Ollat, N., Prieto, J. A., Scholach, T., Skinner, P., Van Leeuwen, C. and Gambetta, G. A. (2018) 'Drought will not leave your glass empty: Low risk of hydraulic failure revealed by long-term drought observations in world's top wine regions', *Science Advances*, 4(1), pp. 1–10. doi: 10.1126/sciadv.aao6969.

Chaturvedi, R. K., Raghubanshi, A. S. and Singh, J. S. (2013) 'Growth of tree seedlings in a tropical dry forest in relation to soil moisture and leaf traits', *Journal of Plant Ecology*, 6(2), pp. 158–170. doi: 10.1093/jpe/rts025.

Choat, B., Badel, E., Burlett, R., Delzon, S., Cochard, H. and Jansen, S. (2016) 'Noninvasive Measurement of Vulnerability to Drought-Induced Embolism by X-Ray Microtomography', *Plant Physiology*, 170(1), pp. 273–282. doi: 10.1104/pp.15.00732.

Choat, B., Cobb, A. R. and Jansen, S. (2008) 'Structure and function of bordered pits: new discoveries and impacts on whole-plant hydraulic function.', *New Phytologist*, 177(3), pp. 608–25. doi: 10.1111/j.1469-8137.2007.02317.x.

Choat, B., Jansen, S., Brodribb, T. J., Cochard, H., Delzon, S., Bhaskar, R., Bucci, S. J., Feild, T. S., Gleason, S. M., Hacke, U. G., Jacobsen, A. L., Lens, F., Maherali, H., Martínez-Vilalta, J., Mayr, S., Mencuccini, M., Mitchell, P. J., Nardini, A., Pittermann, J., Pratt, R. B., Sperry, J. S., Westoby, M., Wright, I. J. and Zanne, A. E. (2012) 'Global convergence in the vulnerability of forests to drought.', *Nature*, 491(7426), pp. 752–5. doi: 10.1038/nature11688.

Choat, B., Lahr, E. C., Melcher, P. J., Zwieniecki, M. I. A. and Holbrook, N. M. (2005) 'The spatial pattern of air seeding thresholds in mature sugar maple trees', *Plant, Cell and Environment*, 28(9), pp. 1082–1089. doi: 10.1111/j.1365-3040.2005.01336.x.

Choat, B. and Pittermann, J. (2009) 'New insights into bordered pit structure and cavitation resistance in angiosperms and conifers', *New Phytologist*, 182(3), pp. 557–560. Available at: http://onlinelibrary.wiley.com/doi/10.1111/j.1469-8137.2009.02847.x/full (Accessed: 30 July 2013).

Choat, B., Sack, L. and Holbrook, N. M. (2007) 'Diversity of hydraulic traits in nine Cordia species growing in tropical forests with contrasting precipitation', *New Phytologist*, 175(4), pp. 686–698. doi: 10.1111/j.1469-8137.2007.02137.x.

Cochard, H., Badel, E., Herbette, S., Delzon, S., Choat, B. and Jansen, S. (2013) 'Methods for measuring plant vulnerability to cavitation: a critical review', *Journal*

of Experimental Botany, 64(15), pp. 4779–4791. doi: 10.1093/jxb/ert193.

Cochard, H., Bodet, C., Améglio, T. and Cruiziat, P. (2015) 'Cryo-scanning electron microscopy observations of vessel content during transpiration in walnut petioles. Facts or artifacts?', *Plant Physiology*, 124(3), pp. 1191–202. Available at: http://www.pubmedcentral.nih.gov/articlerender.fcgi?artid=59218&tool=pmcentrez&rendertype=abstract.

Cochard, H., Coll, L., Le Roux, X., Ameglio, T., Roux, X. Le and Améglio, T. (2002) 'Unraveling the effects of plant hydraulics on stomatal closure during water stress in walnut', *Plant Physiology*, 128(1), pp. 282–290. doi: 10.1104/pp.010400.

Cochard, H., Cruiziat, P. and Tyree, M. T. (1992) 'Use of Positive Pressures to Establish Vulnerability Curves : Further Support for the Air-Seeding Hypothesis and Implications for Pressure-Volume Analysis', *Plant Physiology*, 100(1), pp. 205–209. doi: 10.1104/pp.100.1.205.

Cochard, H., Damour, G., Bodet, C., Tharwat, I., Poirier, M. and Améglio, T. (2005) 'Evaluation of a new centrifuge technique for rapid generation of xylem vulnerability curves', *Physiologia Plantarum*, 124(4), pp. 410–418. doi: 10.1111/j.1399-3054.2005.00526.x.

Cochard, H. and Delzon, S. (2013) 'Hydraulic failure and repair are not routine in trees', *Annals of Forest Science*, 70, pp. 659–661. doi: 10.1007/s13595-013-0317-5.

Cochard, H., Holtta, T., Herbette, S., Delzon, S. and Mencuccini, M. (2009) 'New Insights into the Mechanisms of Water-Stress-Induced Cavitation in Conifers', *Plant Physiology*, 151(2), pp. 949–954. doi: 10.1104/pp.109.138305.

Cochard, H. and Tyree, M. T. (1990) 'Xylem dysfunction in Quercus: vessel sizes, tyloses, cavitation and seasonal changes in embolism', *Tree Physiology*, 6(4), pp. 393–407. doi: 10.1093/treephys/6.4.393.

Crombie, D. S. (1983) *The Physiology of the Cavitation of Xylem Sap*, *PhD Thesis*. University of Glasgow.

Crombie, D. S., Hipkins, M. F. and Milburn, J. A. (1985) 'Gas Penetration of Pit

Membranes in the Xylem of Rhododendron as the Cause of Acoustically Detectable Sap Cavitation', *Australian Journal of Plant Physiology*, 12, pp. 445–453. doi: 10.1071/PP9850445.

Delissio, L. J. and Primack, R. B. (2003) 'The impact of drought on the population dynamics of canopy-tree seedlings in an aseasonal Malaysian rain forest', *Journal of Tropical Ecology*, 19(5), pp. 489–500. doi: 10.1017/S0266467403003547.

Delzon, S. and Cochard, H. (2014) 'Recent advances in tree hydraulics highlight the ecological significance of the hydraulic safety margin', *New Phytologist*, 203(2), pp. 355–358. doi: 10.1111/nph.12798.

Delzon, S., Douthe, C., Sala, A. and Cochard, H. (2010) 'Mechanism of water-stress induced cavitation in conifers: bordered pit structure and function support the hypothesis of seal capillary-seeding.', *Plant, Cell and Environment*, 33(12), pp. 2101–11. doi: 10.1111/j.1365-3040.2010.02208.x.

Dimitrov, D., Schreve, K. and De Beer, N. (2006) 'Advances in three dimensional printing - State of the art and future perspectives', *Rapid Prototyping Journal*, 12(3), pp. 136–147. doi: 10.1108/13552540610670717.

Dixon, H. and Joly, J. (1895) 'The path of the transpiration-current', *Annals of Botany*, IX(Xxxv). Available at: http://aob.oxfordjournals.org/content/os-9/3/403.full.pdf (Accessed: 20 August 2013).

Dungey, H. S., Potts, B. M., Carnegie, a J. and Ades, P. K. (1997) 'Mycosphaerella leaf disease: genetic variation in damage to Eucaliptus nitens, Eucalyptus globulus, and ther F1 hybrid.', *Canadian Journal of Forest Research*, 759, pp. 750–759.

Dutkowski, G. and Potts, B. (1999) 'Geographic patterns of genetic variation in Eucalyptus globulus ssp. globulus and a revised racial classification', *Australian Journal of Botany*, 47. Available at: http://www.publish.csiro.au/?paper=BT97114 (Accessed: 4 October 2013).

Dutkowski, G. W. and Potts, B. M. (2012) 'Genetic variation in the susceptibility of Eucalyptus globulus to drought damage', *Tree Genetics & Genomes*, 8(4), pp. 757–773. doi: 10.1007/s11295-011-0461-8.

Edwards, D. (2003) ‘Xylem in early tracheophytes’, *Plant, Cell and Environment*, 26(1), pp. 57–72. doi: 10.1046/j.1365-3040.2003.00878.x.

Edwards, D., Kerp, H. and Hass, H. (1998) ‘Stomata in early land plants: an anatomical and ecophysiological approach’, *Journal of Experimental Botany*, 49(March), pp. 255–278. doi: 10.1093/jxb/49.Special_Issue.255.

Engelbrecht, B. M. J. and Kursar, T. A. (2003) ‘Comparative drought-resistance of seedlings of 28 species of co-occurring tropical woody plants’, *Oecologia*, 136(3), pp. 383–393. doi: 10.1007/s00442-003-1290-8.

Engelbrecht, B. M. J., Kursar, T. A. and Tyree, M. T. (2005) ‘Drought effects on seedling survival in a tropical moist forest’, *Trees*, 19(3), pp. 312–321. doi: 10.1007/s00468-004-0393-0.

Ennajeh, M., Simões, F., Khemira, H. and Cochard, H. (2011) ‘How reliable is the double-ended pressure sleeve technique for assessing xylem vulnerability to cavitation in woody angiosperms?’, *Physiologia Plantarum*, 142(3), pp. 205–210. doi: 10.1111/j.1399-3054.2011.01470.x.

Fick, A. (1855) ‘Über Diffusion’, *Poggendorffs Annalen*, (94), pp. 59–86.

Fick, S. E. and Hijmans, R. J. (2017) ‘WorldClim 2: new 1-km spatial resolution climate surfaces for global land areas’, *International Journal of Climatology*, 37(12), pp. 4302–4315. doi: 10.1002/joc.5086.

Freeman, J. S., Jackson, H. D., Steane, D. a., McKinnon, G. E., Dutkowski, G. W., Potts, B. M. and Vaillancourt, R. E. (2001) ‘Chloroplast DNA phylogeography of Eucalyptus globulus’, *Australian Journal of Botany*, 49(5), pp. 585–596. doi: 10.1071/BT00094.

Givnish, T. J., Wong, S. C., Stuart-Williams, H., Holloway-Phillips, M. and Farquhar, G. D. (2014) ‘Determinants of maximum tree height in Eucalyptus species along a rainfall gradient in Victoria, Australia’, *Ecology*, 95(11), pp. 2991–3007. doi: 10.1890/14-0240.1.

Gleason, S. M., Westoby, M., Jansen, S., Choat, B., Hacke, U. G., Pratt, R. B.,

Bhaskar, R., Brodribb, T. J., Bucci, S. J., Cao, K., Cochard, H. H., Delzon, S., Domec, J., Fan, Z., Feild, T. S., Jacobsen, A. L., Johnson, D. M., Lens, F., Maherali, H., Mart?nez-Vilalta, J., Mayr, S., McCulloh, K. A., Mencuccini, M., Mitchell, P. J., Morris, H., Nardini, A., Pittermann, J., Plavcov?, L., Schreiber, S. G., Sperry, J. S., Wright, I. J. and Zanne, A. E. (2016) 'Weak tradeoff between xylem safety and xylem-specific hydraulic efficiency across the world's woody plant species', *New Phytologist*, 209(1), pp. 123–136. doi: 10.1111/nph.13646.

Granier, A. (1985) 'Une nouvelle méthode pour la mesure du flux de sève brute dans le tronc des arbres', *Annales Des Sciences Forestieres*, 42(2), pp. 193–200. doi: 10.1051/forest:19850204.

Gucker, C. (2012) 'Betula occidentalis', *Fire Effects Information System, [Online]. U.S. Department of Agriculture, Forest Service, Rocky Mountain Research Station, Fire Sciences Laboratory (Producer)*. U.S. Department of Agriculture, Forest Service, Rocky Mountain Research Station, Fire Sciences Laboratory (Producer). Available at: www.fs.fed.us/database/feis/plants/tree/betocc/all.html (Accessed: 10 May 2018).

Hacke, U. G. and Sperry, J. S. (2001) 'Functional and ecological xylem anatomy', *Perspectives in Plant Ecology, Evolution and Systematics*, 4(2), pp. 97–115. doi: 10.1078/1433-8319-00017.

Hacke, U. G., Sperry, J. S., Wheeler, J. K. and Castro, L. (2006) 'Scaling of angiosperm xylem structure with safety and efficiency.', *Tree Physiology*, 26(6), pp. 689–701. Available at: http://www.ncbi.nlm.nih.gov/pubmed/16510385.

Hacke, U. G., Spicer, R., Schreiber, S. G. and Plavcová, L. (2017) 'An ecophysiological and developmental perspective on variation in vessel diameter', *Plant, Cell & Environment*, 40(6), pp. 831–845. doi: 10.1111/pce.12777.

HAINES, F. M. (1935) 'Observations on the Occurrence of Air in Conducting Tracts', *Annals of Botany*, os-49(2), pp. 367–379. doi: 10.1093/oxfordjournals.aob.a090511.

Hajek, P., Kurjak, D., von Wühlisch, G., Delzon, S. and Schuldt, B. (2016)

‘Intraspecific Variation in Wood Anatomical, Hydraulic, and Foliar Traits in Ten European Beech Provenances Differing in Growth Yield’, *Frontiers in Plant Science*, 7(June), pp. 1–14. doi: 10.3389/fpls.2016.00791.

Hales, S. (1727) *Vegetable staticks*, *Oldbourne*. London. Available at: http://www.cabdirect.org/abstracts/19630300223.html.

Haworth, M., Elliott-Kingston, C. and McElwain, J. C. (2011) ‘Stomatal control as a driver of plant evolution.’, *Journal of Experimental Botany*, 62(8), pp. 2419–23. doi: 10.1093/jxb/err086.

Hietz, P., Rosner, S., Sorz, J. and Mayr, S. (2008) ‘Comparison of methods to quantify loss of hydraulic conductivity in Norway spruce’, *Annals of Forest Science*, 65(5), pp. 502–502. doi: 10.1051/forest:2008023.

Hochberg, U., Windt, C. W., Ponomarenko, A., Zhang, Y.-J., Gersony, J., Rockwell, F. E. and Holbrook, N. M. (2017) ‘Stomatal Closure, Basal Leaf Embolism, and Shedding Protect the Hydraulic Integrity of Grape Stems’, *Plant Physiology*, 174(2), pp. 764–775. doi: 10.1104/pp.16.01816.

Holbrook, N. M., Ahrens, E. T., Burns, M. J. and Zwieniecki, M. a (2001) ‘In vivo observation of cavitation and embolism repair using magnetic resonance imaging.’, *Plant Physiology*, 126(1), pp. 27–31. Available at: http://www.pubmedcentral.nih.gov/articlerender.fcgi?artid=1540104&tool=pmcentrez&rendertype=abstract.

Holbrook, N. M., Burns, M. J. and Field, C. B. (1995) ‘Negative Xylem Pressures in Plants: A Test of the Balancing Pressure Technique’, *Science*, 270(5239), pp. 1193–1194. doi: 10.1126/science.270.5239.1193.

IPCC (2007) *Climate Change 2007 : Synthesis Report*. Available at: http://www.ipcc.ch/publications_and_data/publications_ipcc_fourth_assessment_report_synthesis_report.htm.

Jacobsen, A. L. and Pratt, R. B. (2012) ‘No evidence for an open vessel effect in centrifuge-based vulnerability curves of a long-vesselled liana (Vitis vinifera)’, *New Phytologist*, 194(4), pp. 982–990. doi: 10.1111/j.1469-8137.2012.04118.x.

Jacobsen, A. L., Pratt, R. B., Ewers, F. W. and Davis, S. D. (2007) 'Cavitation resistance among 26 chaparral species of southern california', *Ecological Monographs*, 77(1), pp. 99–115. doi: 10.1890/05-1879.

Jacobsen, A. L., Rodriguez-Zaccaro, F. D., Lee, T. F., Valdovinos, J., Toschi, H. S., Martinez, J. A. and Pratt, R. B. (2015) 'Grapevine Xylem Development, Architecture, and Function', in *Functional and Ecological Xylem Anatomy*. Cham: Springer International Publishing, pp. 133–162. doi: 10.1007/978-3-319-15783-2_5.

James, S. A. and Bell, D. T. (2000a) 'Influence of light availability on leaf structure and growth of two Eucalyptus globulus ssp. globulus provenances.', *Tree Physiology*, 20(15), pp. 1007–1018. doi: 10.1093/treephys/20.15.1007.

James, S. A. and Bell, D. T. (2000b) 'Leaf orientation, light interception and stomatal conductance of Eucalyptus globulus ssp. globulus leaves', *Tree Physiology*, 20(12), pp. 815–823. doi: 10.1093/treephys/20.12.815.

James, S. A. and Bell, D. T. (2001) 'Leaf morphological and anatomical characteristics of heteroblastic Eucalyptus globulus ssp. globulus (Myrtaceae)', *Australian Journal of Botany*, 49(2), pp. 259–269. doi: 10.1071/BT99044.

James, S. A., Smith, W. K. and Vogelmann, T. C. (1999) 'Ontogenetic differences in mesophyll structure and chlorophyll distribution in Eucalyptus globulus ssp. globulus (Myrtaceae)', *American Journal of Botany*, 86(2), pp. 198–207. doi: 10.2307/2656937.

Johnson, E. D. (1926) 'A comparasion of the juvenile and adult leaves of Eucalyptus globulus', *New Phytologist*, 25(3), pp. 202–212.

Johnson, K. M., Jordan, G. J. and Brodribb, T. J. (2018) 'Wheat leaves embolised by water stress do not recover function upon rewatering', *Plant, Cell and Environment*. doi: 10.1111/pce.13397.

Jones, C. S. (1999) 'An Essay on Juvenility, Phase Change, and Heteroblasty in Seed Plants', *International Journal of Plant Sciences*, 160(S6), pp. S105–S111. doi: 10.1086/314215.

Jones, H. and Sutherland, R. (1991) 'Stomatal control of xylem embolism', *Plant, Cell and Environment*, (August 1990), pp. 607–612. Available at: http://onlinelibrary.wiley.com/doi/10.1111/j.1365-3040.1991.tb01532.x/abstract (Accessed: 13 June 2013).

Jordan, G. J., Potts, B. M., Chalmers, P. and Wiltshire, R. J. E. (2000) 'Quantitative genetic evidence that the timing of vegetative phase change in Eucalyptus globulus ssp. globulus is an adaptive trait', *Australian Journal of Botany*, 48(5), p. 561. doi: 10.1071/BT99038.

Jordan, G. J., Potts, B. M. K. J. B., Kirkpatrick, J. B. and Gardiner, C. (1993) 'Variation in the Eucalyptus globulus complex revisited', *Australian Journal of Botany*, 41(6), pp. 763–785. doi: 10.1071/BT9930763.

Jordan, G. J., Potts, B. M. and Wiltshire, R. J. E. (1999) 'Strong, independent, quantitative genetic control of the timing of vegetative phase change and first flowering in Eucalyptus globulus ssp. globulus (Tasmanian Blue Gum)', *Heredity*, 83(2), pp. 179–187. doi: 10.1046/j.1365-2540.1999.00570.x.

Kathiravan, S. (2013) 'A Review of Magnetic Resonance Imaging Techniques', *The Smart Computing Review*, 3(5). doi: 10.6029/smartcr.2013.05.006.

Kattge, J., Díaz, S., Lavorel, S., Prentice, I. C., Leadley, P., Bönisch, G., Garnier, E., Westoby, M., Reich, P. B., Wright, I. J., Cornelissen, J. H. C., Violle, C., Harrison, S. P., Van Bodegom, P. M., Reichstein, M., Enquist, B. J., Soudzilovskaia, N. a., Ackerly, D. D., Anand, M., Atkin, O., Bahn, M., Baker, T. R., Baldocchi, D., Bekker, R., Blanco, C. C., Blonder, B., Bond, W. J., Bradstock, R., Bunker, D. E., Casanoves, F., Cavender-Bares, J., Chambers, J. Q., Chapin, F. S., Chave, J., Coomes, D., Cornwell, W. K., Craine, J. M., Dobrin, B. H., Duarte, L., Durka, W., Elser, J., Esser, G., Estiarte, M., Fagan, W. F., Fang, J., Fernández-Méndez, F., Fidelis, a., Finegan, B., Flores, O., Ford, H., Frank, D., Freschet, G. T., Fyllas, N. M., Gallagher, R. V., Green, W. a., Gutierrez, a. G., Hickler, T., Higgins, S. I., Hodgson, J. G., Jalili, a., Jansen, S., Joly, C. a., Kerkhoff, a. J., Kirkup, D., Kitajima, K., Kleyer, M., Klotz, S., Knops, J. M. H., Kramer, K., Kühn, I., Kurokawa, H., Laughlin, D., Lee, T. D., Leishman, M., Lens, F., Lenz, T., Lewis, S. L., Lloyd, J., Llusià, J., Louault, F., Ma, S., Mahecha, M. D., Manning, P., Massad,

T., Medlyn, B. E., Messier, J., Moles, a. T., Müller, S. C., Nadrowski, K., Naeem, S., Niinemets, Ü., Nöllert, S., Nüske, a., Ogaya, R., Oleksyn, J., Onipchenko, V. G., Onoda, Y., Ordoñez, J., Overbeck, G., Ozinga, W. a., Patiño, S., Paula, S., Pausas, J. G., Peñuelas, J., Phillips, O. L., Pillar, V., Poorter, H., Poorter, L., Poschlod, P., Prinzing, a., Proulx, R., Rammig, a., Reinsch, S., Reu, B., Sack, L., Salgado-Negret, B., Sardans, J., Shiodera, S., Shipley, B., Siefert, a., Sosinski, E., Soussana, J. F., Swaine, E., Swenson, N., Thompson, K., Thornton, P., Waldram, M., Weiher, E., White, M., White, S., Wright, S. J., Yguel, B., Zaehle, S., Zanne, a. E. and Wirth, C. (2011) 'TRY - a global database of plant traits', *Global Change Biology*, 17, pp. 2905–2935. doi: 10.1111/j.1365-2486.2011.02451.x.

Kenrick, P. and Crane, P. R. (1997) 'The origin and early evolution of plants on land', *Nature*, 389, pp. 33–39. doi: 10.1038/37918.

Kenrick, P. and Strullu-Derrien, C. (2014) 'The Origin and Early Evolution of Roots', *Plant Physiology*, 166(2), pp. 570–580. doi: 10.1104/pp.114.244517.

Khan, I. A., Habib, S., Sadaqat, H. A., Hammad, M. and Tahir, N. (2004) 'Comparative evaluation and analysis of seedling traits for drought tolerance in maize', *International Journal of Agriculture & Biology*, 6(2), pp. 246–251. Available at: http://www.ijab.org.

Khan, M. J., Khan, H. S., Yousaf, A., Khurshid, K. and Abbas, A. (2018) 'Modern Trends in Hyperspectral Image Analysis: A Review', *IEEE Access*, 6(March), pp. 14118–14129. doi: 10.1109/ACCESS.2018.2812999.

Kikuta, S. B., Hietz, P. and Richter, H. (2003) 'Vulnerability curves from conifer sapwood sections exposed over solutions with known water potentials', *Journal of Experimental Botany*, 54(390), pp. 2149–2155. doi: 10.1093/jxb/erg216.

Kirkpatrick, J. B. (1975) 'Natural Distribution of Eucalyptus Globulus Labill', *Australian Geographer*, 13(1), pp. 22–35. doi: 10.1080/00049187508702675.

Kolb, K., Sperry, J. and Lamont, B. (1996) 'A method for measuring xylem hydraulic conductance and embolism in entire root and shoot systems', *Journal of Experimental Botany*, 47(304), pp. 1805–1810. Available at:

http://jxb.oxfordjournals.org/content/47/11/1805.short (Accessed: 13 June 2013).

Kramer, P. J. and Boyer, J. S. (1995) *Water relations of plants and soils*, *Water Relations of Plants and Soil*.

Lamy, J.-B., Delzon, S., Bouche, P. S., Alia, R., Vendramin, G. G., Cochard, H. and Plomion, C. (2014) 'Limited genetic variability and phenotypic plasticity detected for cavitation resistance in a Mediterranean pine', *New Phytologist*, 201(3), pp. 874–886. doi: 10.1111/nph.12556.

Larter, M., Pfautsch, S., Domec, J. C., Trueba, S., Nagalingum, N. and Delzon, S. (2017) 'Aridity drove the evolution of extreme embolism resistance and the radiation of conifer genus Callitris', *New Phytologist*, 215(1), pp. 97–112. doi: 10.1111/nph.14545.

Lenton, T. M., Held, H., Kriegler, E., Hall, J. W., Lucht, W., Rahmstorf, S. and Schellnhuber, H. J. (2008) 'Tipping elements in the Earth's climate system', *Proceedings of the National Academy of Sciences*, 105(6), pp. 1786–1793. doi: 10.1073/pnas.0705414105.

Lewis, A. M., Harnden, V. D. and Tyree, M. T. (1994) 'Collapse of Water-Stress Emboli in the Tracheids of Thuja occidentalis L.', *Plant Physiology*, 106(4), pp. 1639–1646. doi: 10.1104/pp.106.4.1639.

Li, S., Klepsch, M., Jansen, S., Schmitt, M., Lens, F., Karimi, Z., Schuldt, B., Espino, S. and Schenk, H. J. (2016) 'Intervessel Pit Membrane Thickness as a Key Determinant of Embolism Resistance in Angiosperm Xylem', *IAWA Journal*, 37(2), pp. 152–171. doi: 10.1163/22941932-20160128.

Li, Y., Sperry, J. S., Taneda, H., Bush, S. E. and Hacke, U. G. (2008) 'Evaluation of centrifugal methods for measuring xylem cavitation in conifers, diffuse- and ring-porous angiosperms', *New Phytologist*, 177(2), pp. 558–568. doi: 10.1111/j.1469-8137.2007.02272.x.

De Little, D. W., Foster, S. D. and Hingston, T. L. (2008) 'Temporal occurrence pattern of insect pests and fungal pathogens in youngTasmanian plantations of Eucalyptus globulus Lab ill. and E. nitens Maiden', *Papers and Proceedings of the*

Royal Society of Tasmania, 142(2), pp. 61–69. Available at: http://eprints.utas.edu.au/13286/%5Cnhttp://eprints.utas.edu.au/13286/1/2008_de_Little_insect_pests.pdf.

López de Heredia, U., Collada, C., Cano, F. J., Emerson, B. C., Cochard, H. and Gil, L. (2013) 'Vulnerability to cavitation, hydraulic efficiency, growth and survival in an insular pine (Pinus canariensis).', *Annals of Botany*, 111(6), pp. 1167–79. doi: 10.1093/aob/mct084.

Lucani, C. J. (2018a) *GitHub Repository - Analysis Instructions*. Available at: https://github.com/OpenSourceOV/analysis-instructions (Accessed: 13 July 2018).

Lucani, C. J. (2018b) *GitHub Repository - CaviScan*. Available at: https://github.com/OpenSourceOV/caviscan (Accessed: 13 July 2018).

Lucani, C. J. (2018c) *GitHub Repository - Clamp 3D Printing Resources*. Available at: https://github.com/OpenSourceOV/clamp-3d-printing-resources (Accessed: 13 July 2018).

Lucani, C. J. (2018d) *GitHub Repository - Clamp Build Instructions*. Available at: https://github.com/OpenSourceOV/clamp-build-instructions (Accessed: 13 July 2018).

Lucani, C. J. (2018e) *GitHub Repository - Clamp Image Capture Instructions*. Available at: https://github.com/OpenSourceOV/clamp-image-capture-instructions (Accessed: 13 July 2018).

Lucani, C. J. (2018f) *GitHub Repository - Contributing*. Available at: https://github.com/OpenSourceOV/contributing (Accessed: 13 July 2018).

Lucani, C. J. (2018g) *GitHub Repository - Image Processing Instructions*. Available at: https://github.com/OpenSourceOV/image-processing-instructions (Accessed: 13 July 2018).

Lucani, C. J. (2018h) *GitHub Repository - Raspberry Pi Setup*. Available at: https://github.com/OpenSourceOV/raspberry-pi-setup (Accessed: 13 July 2018).

Lucani, C. J. (2018i) *GitHub Repository - Resources*. Available at:

https://github.com/OpenSourceOV/resources (Accessed: 13 July 2018).

Lucani, C. J. (2018j) *GitHub Repository - Scanner Image Capture Instructions*. Available at: https://github.com/OpenSourceOV/scanner-image-capture-instructions (Accessed: 13 July 2018).

Lucani, C. J. (2018k) *OpenSourceOV.org - Analyze*. Available at: http://www.opensourceov.org/analyze/ (Accessed: 13 July 2018).

Lucani, C. J. (2018l) *OpenSourceOV.org - Capture*. Available at: http://www.opensourceov.org/overview/ (Accessed: 13 July 2018).

Lucani, C. J. (2018m) *OpenSourceOV.org - Contributing*. Available at: http://www.opensourceov.org/contributing/ (Accessed: 13 July 2018).

Lucani, C. J. (2018n) *OpenSourceOV.org - Gallery*. Available at: http://www.opensourceov.org/gallery/ (Accessed: 13 July 2018).

Lucani, C. J. (2018o) *OpenSourceOV.org - Homepage*. Available at: http://www.opensourceov.org/ (Accessed: 13 July 2018).

Lucani, C. J. (2018p) *OpenSourceOV.org - Overview*. Available at: http://www.opensourceov.org/overview/ (Accessed: 13 July 2018).

Lucani, C. J. (2018q) *OpenSourceOV.org - Posts*. Available at: http://www.opensourceov.org/posts/ (Accessed: 13 July 2018).

Lucani, C. J. (2018r) *OpenSourceOV.org - Process*. Available at: http://www.opensourceov.org/process/ (Accessed: 13 July 2018).

Lucani, C. J. (2018s) *OpenSourceOV.org - Resources*. Available at: http://www.opensourceov.org/resources/ (Accessed: 13 July 2018).

Lucani, C. J. and Nolf, M. (2018a) *GitHub Repository - CaviCapture*. Available at: https://github.com/OpenSourceOV/cavicapture (Accessed: 13 July 2018).

Lucani, C. J. and Nolf, M. (2018b) *GitHub Repository - ImageJ Scripts*. Available at: https://github.com/OpenSourceOV/imagej-scripts (Accessed: 13 July 2018).

Maherali, H. and DeLucia, E. H. (2000) ‘Xylem conductivity and vulnerability to cavitation of ponderosa pine growing in contrasting climates.’, *Tree Physiology*, 20(13), pp. 859–67. Available at: http://www.ncbi.nlm.nih.gov/pubmed/11303576.

Maherali, H., Pockman, W. T. W. and Jackson, R. B. R. (2004) ‘Adaptive variation in the vulnerability of woody plants to xylem cavitation’, *Ecology*, 85(8), pp. 2184–2199. doi: 10.1890/02-0538.

Mahlein, A. K., Rumpf, T., Welke, P., Dehne, H. W., Plümer, L., Steiner, U. and Oerke, E. C. (2013) ‘Development of spectral indices for detecting and identifying plant diseases’, *Remote Sensing of Environment*. Elsevier Inc., 128, pp. 21–30. doi: 10.1016/j.rse.2012.09.019.

Marshall, D. C. (1958) ‘Measurment of sap flow in conifers by heat transport’, *Plant Physiology*, 33(6), p. 385 396.

Martínez-Vilalta, J., Cochard, H., Mencuccini, M., Sterck, F., Herrero, a, Korhonen, J. F. J., Llorens, P., Nikinmaa, E., Nolè, a, Poyatos, R., Ripullone, F., Sass-Klaassen, U. and Zweifel, R. (2009) ‘Hydraulic adjustment of Scots pine across Europe.’, *New Phytologist*, 184(2), pp. 353–64. doi: 10.1111/j.1469-8137.2009.02954.x.

Matsushima, U., Herppich, W. B., Kardjilov, N., Graf, W., Hilger, A. and Manke, I. (2009) ‘Estimation of water flow velocity in small plants using cold neutron imaging with D2O tracer’, *Nuclear Instruments and Methods in Physics Research, Section A: Accelerators, Spectrometers, Detectors and Associated Equipment*, 605(1–2), pp. 146–149. doi: 10.1016/j.nima.2009.01.187.

Matusick, G. (2012) ‘Drought and Heat Triggers Sudden and Severe Dieback in a Dominant Mediterranean-Type Woodland Species’, *Open Journal of Forestry*, 02(04), pp. 183–186. doi: 10.4236/ojf.2012.24022.

McAdam, S. A. M. and Brodribb, T. J. (2012) ‘Stomatal innovation and the rise of seed plants’, *Ecology Letters*, 15(1), pp. 1–8. doi: 10.1111/j.1461-0248.2011.01700.x.

McDowell, N. G., Beerling, D. J., Breshears, D. D., Fisher, R. A., Raffa, K. F. and Stitt, M. (2011) ‘The interdependence of mechanisms underlying climate-driven

vegetation mortality', *Trends in Ecology and Evolution*, 26(10), pp. 523–532. doi: 10.1016/j.tree.2011.06.003.

McDowell, N., Pockman, W. T., Allen, C. D., Breshears, D. D., Cobb, N., Kolb, T., Plaut, J., Sperry, J., West, A., Williams, D. G. and Yepez, E. A (2008) 'Mechanisms of plant survival and mortality during drought: why do some plants survive while others succumb to drought?', *New Phytologist*, 178(4), pp. 719–39. doi: 10.1111/j.1469-8137.2008.02436.x.

McKinnon, G. E., Jordan, G. J., Vaillancourt, R. E., Steane, D. A and Potts, B. M. (2004) 'Glacial refugia and reticulate evolution: the case of the Tasmanian eucalypts.', *Philosophical Transactions of the Royal Society of London*, 359(1442), p. 275–284; discussion 284. doi: 10.1098/rstb.2003.1391.

McLean, E. H., Prober, S. M., Stock, W. D., Steane, D. A, Potts, B. M., Vaillancourt, R. E. and Byrne, M. (2014) 'Plasticity of functional traits varies clinally along a rainfall gradient in Eucalyptus tricarpa.', *Plant, Cell and Environment*, 37(6), pp. 1440–51. doi: 10.1111/pce.12251.

Melcher, P. J., Zwieniecki, M. A. and Michele Holbrook, N. (2003) 'Vulnerability of Xylem Vessels to Cavitation in Sugar Maple. Scaling from Individual Vessels to Whole Branches', *Plant Physiology*, 131(4), pp. 1775–1780. doi: 10.1104/pp.102.012856.

Milburn, J. A. (1973) 'Cavitation in Ricinus by acoustic detection: Induction in excised leaves by various factors', *Planta*, 110(3), pp. 253–265. doi: 10.1007/BF00387637.

Milburn, J. A. and Johnson, R. P. C. (1966) 'The conduction of sap', *Planta*, 69(1), pp. 43–52. doi: 10.1007/BF00380209.

Minervini, M., Giuffrida, M. V., Perata, P. and Tsaftaris, S. A. (2017) 'Phenotiki: an open software and hardware platform for affordable and easy image-based phenotyping of rosette-shaped plants', *The Plant Journal*, 90(1), pp. 204–216. doi: 10.1111/tpj.13472.

Mitchell, P. J., O'Grady, A. P., Hayes, K. R. and Pinkard, E. A. (2014) 'Exposure of

trees to drought-induced die-off is defined by a common climatic threshold across different vegetation types', *Ecology and Evolution*, 4(7), pp. 1088–1101. doi: 10.1002/ece3.1008.

Mohd Asaari, M. S., Mishra, P., Mertens, S., Dhondt, S., Inzé, D., Wuyts, N. and Scheunders, P. (2018) 'Close-range hyperspectral image analysis for the early detection of stress responses in individual plants in a high-throughput phenotyping platform', *ISPRS Journal of Photogrammetry and Remote Sensing*. International Society for Photogrammetry and Remote Sensing, Inc. (ISPRS), 138, pp. 121–138. doi: 10.1016/j.isprsjprs.2018.02.003.

Murphy, D. J., Brown, G. K., Miller, J. T. and Ladiges, P. Y. (2010) 'Molecular phylogeny of Acacia Mill. (Mimosoideae: Leguminosae): Evidence for major clades and informal classification', *Taxon*, 59(1), pp. 7–19. doi: 10.2307/27757046.

Nakanishi, T. M. and Matsubayashi, M. (1997) 'Nondestructive water imaging by neutron beam analysis in living plants', *Journal of Plant Physiology*. Gustav Fischer Verlag, Jena, 151(4), pp. 442–445. doi: 10.1016/S0176-1617(97)80009-0.

Nardini, A. and Luglio, J. (2014) 'Leaf hydraulic capacity and drought vulnerability: Possible trade-offs and correlations with climate across three major biomes', *Functional Ecology*, 28(4), pp. 810–818. doi: 10.1111/1365-2435.12246.

Nardini, A. and Salleo, S. (2000) 'Limitation of stomatal conductance by hydraulic traits: sensing or preventing xylem cavitation?', *Trees*, 15(1), pp. 14–24. doi: 10.1007/s004680000071.

Nelson, G. C., Valin, H., Sands, R. D., Havlík, P., Ahammad, H., Deryng, D., Elliott, J., Fujimori, S., Hasegawa, T., Heyhoe, E., Kyle, P., Von Lampe, M., Lotze-Campen, H., Mason d'Croz, D., van Meijl, H., van der Mensbrugghe, D., Müller, C., Popp, A., Robertson, R., Robinson, S., Schmid, E., Schmitz, C., Tabeau, A. and Willenbockel, D. (2014) 'Climate change effects on agriculture: Economic responses to biophysical shocks', *Proceedings of the National Academy of Sciences*, 111(9), pp. 3274–3279. doi: 10.1073/pnas.1222465110.

Newbanks, D., Bosch, a and Zimmermann, M. H. (1983) 'Evidence for xylem

dysfunction by embolization in Dutch elm disease.', *Phytopathology*, 73(7), pp. 1060–1063. doi: 10.1094/Phyto-73-1060.

Nicotra, A. B., Atkin, O. K., Bonser, S. P., Davidson, A. M., Finnegan, E. J., Mathesius, U., Poot, P., Purugganan, M. D., Richards, C. L., Valladares, F. and van Kleunen, M. (2010) 'Plant phenotypic plasticity in a changing climate.', *Trends in Plant Science*. Elsevier Ltd, 15(12), pp. 684–92. doi: 10.1016/j.tplants.2010.09.008.

Noble, J. C. (2001) 'Lignotubers and meristem dependence in mallee (Eucalyptus spp.) coppicing after fire', *Australian Journal of Botany*, 49(1), pp. 31–41. doi: 10.1071/BT00046.

Nolf, M., Beikircher, B., Rosner, S., Nolf, A. and Mayr, S. (2015) 'Xylem cavitation resistance can be estimated based on time-dependent rate of acoustic emissions', *New Phytologist*, 208(2), pp. 625–632. doi: 10.1111/nph.13476.

Nolf, M., Lopez, R., Peters, J. M. R. R., Flavel, R. J., Koloadin, L. S., Young, I. M. and Choat, B. (2017) 'Visualization of xylem embolism by X-ray microtomography: a direct test against hydraulic measurements', *New Phytologist*, 214(2), pp. 890–898. doi: 10.1111/nph.14462.

North, G. B. and Nobel, P. S. (1997) 'Root-soil contact for the desert succulent Agave deserti in wet and drying soil', *New Phytologist*, 135(1), pp. 21–29. doi: 10.1046/j.1469-8137.1997.00620.x.

North, G. B. and Nobel, P. S. (1998) 'Water uptake and structural plasticity along roots of a desert succulent during prolonged drought', *Plant, Cell and Environment*, 21(7), pp. 705–713. doi: 10.1046/j.1365-3040.1998.00317.x.

Oswald, S. E., Menon, M., Carminati, A., Vontobel, P., Lehmann, E. and Schulin, R. (2008) 'Quantitative Imaging of Infiltration, Root Growth, and Root Water Uptake via Neutron Radiography', *Vadose Zone Journal*, 7(3), p. 1035. doi: 10.2136/vzj2007.0156.

Parmesan, C. and Hanley, M. E. (2015) 'Plants and climate change: Complexities and surprises', *Annals of Botany*, 116(6), pp. 849–864. doi: 10.1093/aob/mcv169.

Pasquet-Kok, J., Creese, C. and Sack, L. (2010) 'Turning over a new "leaf": multiple functional significances of leaves versus phyllodes in Hawaiian Acacia koa.', *Plant, Cell and Environment*, 33(12), pp. 2084–100. doi: 10.1111/j.1365-3040.2010.02207.x.

Pereira, L., Bittencourt, P. R. L., Oliveira, R. S., Junior, M. B. M., Barros, F. V, Ribeiro, R. V. and Mazzafera, P. (2016) 'Plant pneumatics: stem air flow is related to embolism - new perspectives on methods in plant hydraulics', *New Phytologist*, 211(1), pp. 357–370. doi: 10.1111/nph.13905.

Perez-Donoso, A. G., Greve, L. C., Walton, J. H., Shackel, K. A. and Labavitch, J. M. (2006) 'Xylella fastidiosa Infection and Ethylene Exposure Result in Xylem and Water Movement Disruption in Grapevine Shoots', *Plant Physiology*, 143(2), pp. 1024–1036. doi: 10.1104/pp.106.087023.

Pfautsch, S., Harbusch, M., Wesolowski, A., Smith, R., Macfarlane, C., Tjoelker, M. G., Reich, P. B. and Adams, M. a. (2016) 'Climate determines vascular traits in the ecologically diverse genus Eucalyptus', *Ecology Letters*, pp. 240–248. doi: 10.1111/ele.12559.

Pickard, W. F. (1982) 'The ascent of sap in plants', *Progress in Biophysics and Molecular Biology*, 37(C), pp. 181–229. doi: 10.1016/0079-6107(82)90023-2.

Pratt, R. B., Jacobsen, A. L., Ramirez, A. R., Helms, A. M., Traugh, C. A., Tobin, M. F., Heffner, M. S. and Davis, S. D. (2014) 'Mortality of resprouting chaparral shrubs after a fire and during a record drought: Physiological mechanisms and demographic consequences', *Global Change Biology*, 20(3), pp. 893–907. doi: 10.1111/gcb.12477.

Pratt, R. B., North, G. B., Jacobsen, A. L., Ewers, F. W. and Davis, S. D. (2010) 'Xylem root and shoot hydraulics is linked to life history type in chaparral seedlings', *Functional Ecology*, 24(1), pp. 70–81. doi: 10.1111/j.1365-2435.2009.01613.x.

R Development Core Team, R. (2011) *R: A Language and Environment for Statistical Computing*, *R Foundation for Statistical Computing*. doi: 10.1007/978-3-

540-74686-7.

Rapaport, T., Hochberg, U., Cochavi, A., Karnieli, A. and Rachmilevitch, S. (2017) 'The potential of the spectral "water balance index" (WABI) for crop irrigation scheduling', *New Phytologist*, 1. doi: 10.1111/nph.14718.

Rapley, L. P., Allen, G. R. and Potts, B. M. (2004) 'Genetic variation of Eucalyptus globulus in relation to autumn gum moth Mnesampela privata (Lepidoptera: Geometridae) oviposition preference', *Forest Ecology and Management*, 194(1–3), pp. 169–175. doi: 10.1016/j.foreco.2004.02.019.

Raven, J. A. (1977) 'The Evolution of Vascular Land Plants in Relation to Supracellular Transport Processes', *Advances in Botanical Research*, 5(C), pp. 153–219. doi: 10.1016/S0065-2296(08)60361-4.

Raven, J. J. A. (2002) 'Selection pressures on stomatal evolution', *New Phytologist*, (131), pp. 371–386. Available at: http://onlinelibrary.wiley.com/doi/10.1046/j.0028-646X.2001.00334.x/full (Accessed: 13 June 2013).

Ritman, K. T. and Milburn, J. A. (1988) 'Acoustic emissions from plants: Ultrasonic and audible compared', *Journal of Experimental Botany*, 39(9), pp. 1237–1248. doi: 10.1093/jxb/39.9.1237.

Rodriguez-Dominguez, C. M., Carins Murphy, M. R., Lucani, C. and Brodribb, T. J. (2018) 'Mapping xylem failure in disparate organs of whole plants reveals extreme resistance in olive roots', *New Phytologist*, 218(3), pp. 1025–1035. doi: 10.1111/nph.15079.

Le Roux, J. J., Strasberg, D., Rouget, M., Morden, C. W., Koordom, M. and Richardson, D. M. (2014) 'Relatedness defies biogeography: The tale of two island endemics (Acacia heterophylla and A. koa)', *New Phytologist*, 204(1), pp. 230–242. doi: 10.1111/nph.12900.

Ryan, M. and Yoder, B. (1997) 'Hydraulic limits to tree height and tree growth', *Bioscience*, 47(4), pp. 235–242. Available at: http://www.jstor.org/stable/10.2307/1313077 (Accessed: 4 April 2013).

Sack, L. (2004) ‘Responses of temperate woody seedlings to shade and drought: Do trade-offs limit potential niche differentiation?’, *Oikos*, 107(1), pp. 110–127. doi: 10.1111/j.0030-1299.2004.13184.x.

Sack, L. and Holbrook, N. (2006) ‘Leaf hydraulics’, *Annual Review of Plant Biology*, 57, pp. 361–81. doi: 10.1146/annurev.arplant.56.032604.144141.

Sack, L. and Scoffoni, C. (2012) ‘Measurement of leaf hydraulic conductance and stomatal conductance and their responses to irradiance and dehydration using the Evaporative Flux Method (EFM).’, *Journal of visualized experiments : JoVE*, (70), pp. 1–7. doi: 10.3791/4179.

Salleo, S., Hinckley, T. M., Kikuta, S. B., Lo Gullo, M. A., Weilgnony, P., Yoon, T. M. and Richter, H. (1992) ‘A method for inducing xylem emboli in situ: experiments with a field-grown tree’, *Plant, Cell and Environment*, 15(4), pp. 491–497. doi: 10.1111/j.1365-3040.1992.tb01001.x.

Scholander, P. (1964) ‘Hydrostatic pressure and osmotic potential in leaves of mangroves and some other plants’, *Proceedings of the National Academy of Sciences*, 52(1), pp. 119–125. Available at: http://www.ncbi.nlm.nih.gov/pmc/articles/pmc300583/ (Accessed: 13 June 2013).

Schuldt, B., Knutzen, F., Delzon, S., Jansen, S., Müller-Haubold, H., Burlett, R., Clough, Y. and Leuschner, C. (2016) ‘How adaptable is the hydraulic system of European beech in the face of climate change-related precipitation reduction?’, *New Phytologist*, 210(2), pp. 443–458. doi: 10.1111/nph.13798.

Scoffoni, C., Albuquerque, C., Brodersen, C. R., Townes, S. V., John, G. P., Bartlett, M. K., Buckley, T. N., McElrone, A. J. and Sack, L. (2017) ‘Outside-xylem vulnerability, not xylem embolism, controls leaf hydraulic decline during dehydration’, *Plant Physiology*, 173(February), p. pp.01643.2016. doi: 10.1104/pp.16.01643.

Scoffoni, C., Vuong, C., Diep, S., Cochard, H. and Sack, L. (2014) ‘Leaf Shrinkage with Dehydration: Coordination with Hydraulic Vulnerability and Drought Tolerance’, *Plant Physiology*, 164(4), pp. 1772–1788. doi: 10.1104/pp.113.221424.

Skelton, R. P., Brodribb, T. J. and Choat, B. (2017) 'Casting light on xylem vulnerability in an herbaceous species reveals a lack of segmentation', *New Phytologist*, 214(2), pp. 561–569. doi: 10.1111/nph.14450.

Skelton, R. P., West, A. G. and Dawson, T. E. (2015) 'Predicting plant vulnerability to drought in biodiverse regions using functional traits', *Proceedings of the National Academy of Sciences*, 112(18), pp. 5744–5749. doi: 10.1073/pnas.1503376112.

Song, X., Li, J., Zhang, W., Tang, Y., Sun, Z. and Cao, M. (2016) 'Variant responses of tree seedling to seasonal drought stress along an elevational transect in tropical montane forests', *Scientific Reports*. Nature Publishing Group, 6(October), pp. 1–9. doi: 10.1038/srep36438.

Sony (2018) *IMX219PQ*. Available at: https://www.sony-semicon.co.jp/products_en/new_pro/april_2014/imx219_e.html (Accessed: 13 July 2018).

Soudzilovskaia, N. a, Elumeeva, T. G., Onipchenko, V. G., Shidakov, I. I., Salpagarova, F. S., Khubiev, A. B., Tekeev, D. K. and Cornelissen, J. H. C. (2013) 'Functional traits predict relationship between plant abundance dynamic and long-term climate warming.', *Proceedings of the National Academy of Sciences*, 110(45), pp. 18180–4. doi: 10.1073/pnas.1310700110.

Sperry, J. (1993) 'Winter xylem embolism and spring recovery in Betula cordifolia, Fagus grandifolia, Abies balsamea and Picea rubens', *Water transport in plants under climatic stress*. Available at: http://content.lib.utah.edu/utils/getfile/collection/uspace/id/1684/filename/2428.pdf (Accessed: 13 June 2013).

Sperry, J. S. (1985) 'Xylem Embolism in the Palm Rhapis Excelsa', *IAWA Journal*, 6(4), pp. 283–292. doi: 10.1163/22941932-90000956.

Sperry, J. S. (1986) 'Relationship of Xylem Embolism to Xylem Pressure Potential, Stomatal Closure, and Shoot Morphology in the Palm Rhapis excelsa.', *Plant Physiology*, 80(1), pp. 110–116. doi: 10.1104/pp.80.1.110.

Sperry, J. S., Donnelly, J. R. and Tyree, M. T. (1988) 'A method for measuring

hydraulic conductivity and embolism in xylem', *Plant, Cell and Environment*, 11(1), pp. 35–40. doi: 10.1111/j.1365-3040.1988.tb01774.x.

Sperry, J. and Saliendra, N. (1994) 'Intra-and inter-plant variation in xylem cavitation in Betula occidentalis', *Plant, Cell and Environment*, pp. 1233–1241. Available at: http://onlinelibrary.wiley.com/doi/10.1111/j.1365-3040.1994.tb02021.x/full (Accessed: 5 July 2013).

Sperry, J. and Tyree, M. (1988) 'Mechanism of water stress-induced xylem embolism', *Plant Physiology*, 88(3), pp. 581–587. Available at: http://www.plantphysiol.org/content/88/3/581.short (Accessed: 22 April 2013).

Sperry, J. and Tyree, M. (1990) 'Water-stress-induced xylem embolism in three species of conifers', *Plant, Cell and Environment*, pp. 427–436. Available at: http://onlinelibrary.wiley.com/doi/10.1111/j.1365-3040.1990.tb01319.x/abstract (Accessed: 9 July 2013).

Steinberg, S., van Bavel, C. and McFarland, M. (1989) 'A gauge to measure mass flow rate of sap in stems and trunks of woody plants', *Journal of the American Society for Horticultural Science*, 114(3), pp. 466–472.

Sykes, M. T., Prentice, I. C., Thuiller, W., Lavorel, S., Arau, M. B., Araújo, M. B., Sykes, M. T., Prentice, I. C., Thuiller, W., Lavorel, S. and Arau, M. B. (2005) 'Climate change threats to plant diversity in Europe.', *Proceedings of the National Academy of Sciences*, 102(23), pp. 8245–50. doi: 10.1073/pnas.0409902102.

Taiz, L. and Zeiger, E. (2006) *Plant Physiology*. 4th Editio. Sinauer Associates.

Tester, M. and Langridge, P. (2010) 'Breeding technologies to increase crop production in a changing world', *Science*, 327(5967), pp. 818–822. doi: 10.1126/science.1183700.

Thuiller, W., Albert, C., Araújo, M. B., Berry, P. M., Cabeza, M., Guisan, A., Hickler, T., Midgley, G. F., Paterson, J., Schurr, F. M., Sykes, M. T. and Zimmermann, N. E. (2008) 'Predicting global change impacts on plant species' distributions: Future challenges', *Perspectives in Plant Ecology, Evolution and Systematics*, 9(3–4), pp. 137–152. doi: 10.1016/j.ppees.2007.09.004.

Toro, M. A., Silió, L., Rodriguez, M. C., Soria, F. and Toval, G. (1998) 'Genetic analysis of survival to drought in Eucalyptus globulus in Spain', in *6th World Congress on Genetics Applied to Livestock Production*, pp. 499–502.

Torres-Ruiz, J. M., Cochard, H., Mayr, S., Beikircher, B., Diaz-Espejo, A., Rodriguez-Dominguez, C. M., Badel, E. and Fernández, J. E. (2014) 'Vulnerability to cavitation in Olea europaea current-year shoots: Further evidence of an open-vessel artifact associated with centrifuge and air-injection techniques', *Physiologia Plantarum*, 152(3), pp. 465–474. doi: 10.1111/ppl.12185.

Tötzke, C., Kardjilov, N., Manke, I. and Oswald, S. E. (2017) 'Capturing 3D Water Flow in Rooted Soil by Ultra-fast Neutron Tomography', *Scientific Reports*, 7(1), pp. 1–9. doi: 10.1038/s41598-017-06046-w.

Tötzke, C., Miranda, T., Konrad, W., Gout, J., Kardjilov, N., Dawson, M., Manke, I. and Roth-Nebelsick, A. (2013) 'Visualization of embolism formation in the xylem of liana stems using neutron radiography', *Annals of Botany*, 111(4), pp. 723–730. doi: 10.1093/aob/mct014.

Tovar, J. C., Hoyer, J. S., Lin, A., Tielking, A., Callen, S. T., Elizabeth Castillo, S., Miller, M., Tessman, M., Fahlgren, N., Carrington, J. C., Nusinow, D. A. and Gehan, M. A. (2018) 'Raspberry Pi–powered imaging for plant phenotyping', *Applications in Plant Sciences*, 6(3), pp. 1–12. doi: 10.1002/aps3.1031.

Tyree, M. T., Davis, S. D. and Cochard, H. (1994) 'Biophysical perspectives of xylem evolution: Is there a tradeoff of hydraulic efficiency for vulnerability to dysfunction?', *IAWA Journal*, pp. 335–360. doi: 10.1163/22941932-90001369.

Tyree, M. T., Patino, S., Bennink, J. and Alexander, J. (1995) 'Dynamic Measurements of Root hydraulic conductance using a high-pressure flowmeter in the laboratory and field', *Journal of Experimental Botany*, 46(282), pp. 83–94. doi: 10.1093/jxb/46.1.83.

Tyree, M. T. and Sperry, J. S. (1989) 'Vulnerability of Xylem to Cavitation and Embolism', *Annual Review of Plant Physiology and Plant Molecular Biology*, 40(1), pp. 19–36. doi: 10.1146/annurev.pp.40.060189.000315.

Tyree, M. T. and Yang, S. (1992) 'Hydraulic Conductivity Recovery versus Water Pressure in Xylem of Acer saccharum.', *Plant Physiology*, 100(2), pp. 669–76. doi: 10.1104/pp.100.2.669.

Tyree, M. T. and Zimmermann, M. H. (2002) *Xylem Structure and the Ascent of Sap*. Berlin, Heidelberg: Springer Berlin Heidelberg (Springer Series in Wood Science). doi: 10.1007/978-3-662-04931-0.

Urli, M., Porté, A. A. J. A., Cochard, H., Guengant, Y., Burlett, R. and Delzon, S. (2013) 'Xylem embolism threshold for catastrophic hydraulic failure in angiosperm trees', *Tree Physiology*, pp. 672–683. doi: 10.1093/treephys/tpt030.

Valle, B., Simonneau, T., Boulord, R., Sourd, F., Frisson, T., Ryckewaert, M., Hamard, P., Brichet, N., Dauzat, M. and Christophe, A. (2017) 'PYM: A new, affordable, image-based method using a Raspberry Pi to phenotype plant leaf area in a wide diversity of environments', *Plant Methods*. BioMed Central, 13(1), pp. 1–17. doi: 10.1186/s13007-017-0248-5.

Velikova, V., Loreto, F., Brilli, F., Stefanov, D. and Yordanov, I. (2008) 'Characterization of juvenile and adult leaves of Eucalyptus globulus showing distinct heteroblastic development: Photosynthesis and volatile isoprenoids', *Plant Biology*, 10(1), pp. 55–64. doi: 10.1055/s-2007-964964.

Venturas, M. D., Sperry, J. S. and Hacke, U. G. (2017) 'Plant xylem hydraulics: What we understand, current research, and future challenges', *Journal of Integrative Plant Biology*, 59(6), pp. 356–389. doi: 10.1111/jipb.12534.

West, D. W. and Gaff, D. F. (1976) 'Xylem cavitation in excised leaves of Malus sylvestris Mill. and measurement of leaf water status with the pressure chamber', *Planta*, 129(1), pp. 15–18. doi: 10.1007/BF00390906.

Wheeler, J. K., Huggett, B. A., Tofte, A. N., Rockwell, F. E. and Holbrook, N. M. (2013) 'Cutting xylem under tension or supersaturated with gas can generate PLC and the appearance of rapid recovery from embolism', *Plant, Cell and Environment*, 36(11), pp. 1938–1949. doi: 10.1111/pce.12139.

Wheeler, J. K., Sperry, J. S., Hacke, U. G. and Hoang, N. (2005) 'Inter-vessel pitting

and cavitation in woody Rosaceae and other vessel led plants: A basis for a safety versus efficiency trade-off in xylem transport', *Plant, Cell and Environment*, 28(6), pp. 800–812. doi: 10.1111/j.1365-3040.2005.01330.x.

Will, R. E., Wilson, S. M., Zou, C. B. and Hennessey, T. C. (2013) 'Increased vapor pressure deficit due to higher temperature leads to greater transpiration and faster mortality during drought for tree seedlings common to the forest-grassland ecotone', *New Phytologist*, 200(2), pp. 366–374. doi: 10.1111/nph.12321.

William, T., John, S., Leary, O., James, W., Pockman, W. T., Sperry, J. S., O'Leary, J. W. and O'leary, J. W. (1995) 'Sustained and significant negative water pressure in xylem', *Nature*, 378(6558), pp. 715–716. doi: 10.1038/378715a0.

Wolkerstorfer, S. V., Rosner, S. and Hietz, P. (2012) 'An improved method and data analysis for ultrasound acoustic emissions and xylem vulnerability in conifer wood', *Physiologia Plantarum*, 146(2), pp. 184–191. doi: 10.1111/j.1399-3054.2012.01605.x.

Yang, S. and Tyree, M. T. (1993) 'Hydraulic resistance in Acer saccharum shoots and its influence on leaf water potential and transpiration.', *Tree Physiology*, 12(3), pp. 231–42. doi: 10.1093/treephys/12.3.231.

Yang, Y., Zhu, Q., Peng, C., Wang, H. and Chen, H. (2015) 'From plant functional types to plant functional traits: A new paradigm in modelling global vegetation dynamics', *Progress in Physical Geography*, 39(4), pp. 514–535. doi: 10.1177/0309133315582018.

Yavitt, J. B. and Wright, S. J. (2008) 'Seedling growth responses to water and nutrient augmentation in the understorey of a lowland moist forest, Panama', *Journal of Tropical Ecology*, 24, pp. 19–26. doi: 10.1017/S0266467407004713.

Zimmermann, M. H. (1978) 'Hydraulic architecture of some diffuse-porous trees', *Canadian Journal of Botany*, 56(18), pp. 2286–2295. doi: 10.1139/b78-274.

Zimmermann, M. H. (1983) *Xylem Structure and the Ascent of Sap*. Springer Berlin Heidelberg (Springer Series in Wood Science). Available at: https://books.google.com.au/books?id=BWvsCAAAQBAJ.

Zolfaghar, S., Villalobos-Vega, R., Cleverly, J. and Eamus, D. (2015) ‘Co-ordination among leaf water relations and xylem vulnerability to embolism of Eucalyptus trees growing along a depth-to-groundwater gradient’, *Tree Physiology*, 35(7), pp. 732–743. doi: 10.1093/treephys/tpv039.

Appendix 1 - OpenSourceOV.org

The OpenSourceOV.org is divided into a number of sections (Table 1).

Table 1. The sections of the OpenSourceOV.org website

Section	Features	Figure; Reference
1. Homepage	Introduces the sections of the site and highlights the latest articles, news, and publications	1; (Lucani, 2018o)
2. Overview	Background and technical description of the optical technique and discusses the development of the CaviCam device and the OpenSourceOV.org website.	2; (Lucani, 2018p)
3. Capture	Overview of the methods and key components required to capture images of the xylem for optical measurement, links to CaviCam build and operating instructions, link to instructions for capturing images using a desktop scanner.	3; (Lucani, 2018l)
4. Process	Overview of the procedure for processing captured images and links to the processing instructions and ImageJ CaviTools toolbox.	4; (Lucani, 2018r)
5. Analyze	Link to the image analysis instructions	5; (Lucani, 2018k)
6. Posts	Articles and news about the optical method, the CaviCam system and OpenSourceOV.org, publications that use the optical method or the CaviCam system.	6; (Lucani, 2018q)
7. Resources	Links to electronics suppliers and online 3D printing services in addition to tutorials and community websites for learning electronics and 3D printing.	7; (Lucani, 2018s)
8. Gallery	User-contributed sequences of embolism events	8; (Lucani, 2018n)
9. Contributing	Details about the Open Source project and instructions for contributing.	9; (Lucani, 2018m)

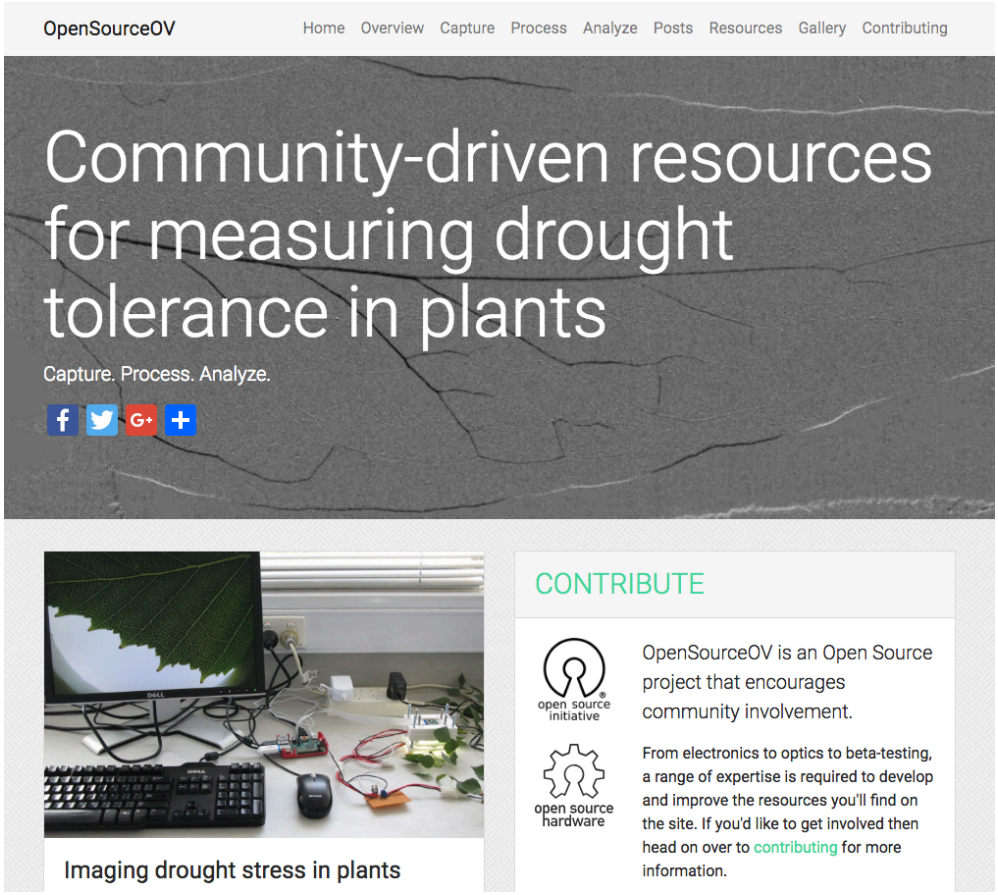

Fig. 1. The OpenSourceOV.org homepage

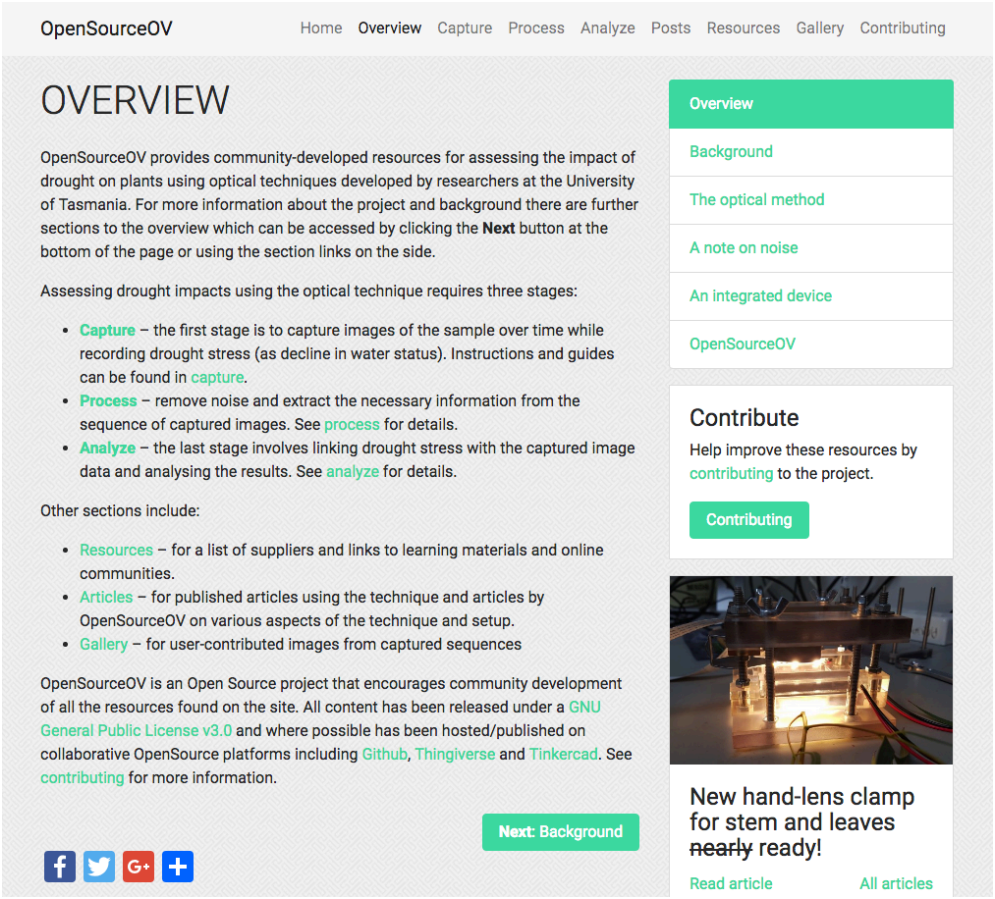

Fig. 2. The Overview section of the OpenSourceOV.org website.

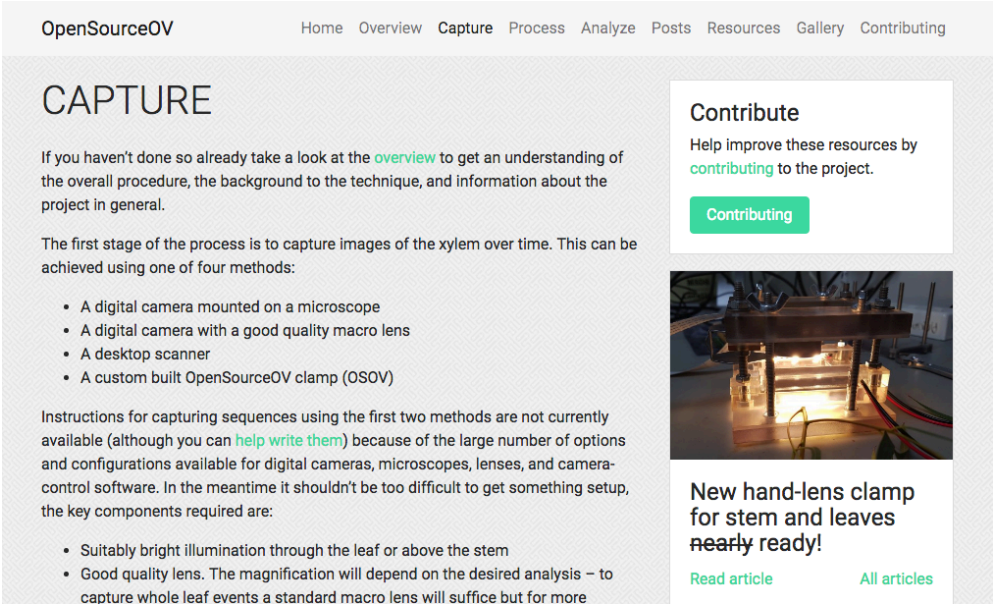

Fig. 3. The Capture section of the OpenSourceOV.org website.

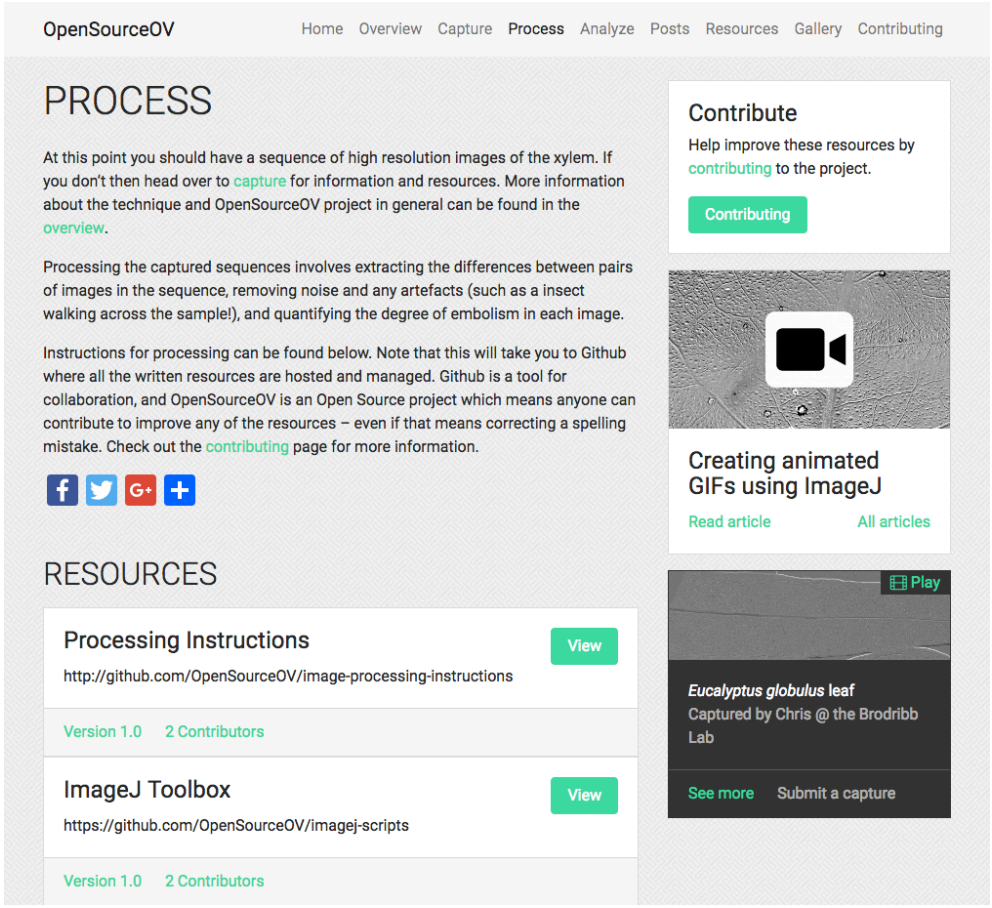

Fig. 4. The Process section of the OpenSourceOV.org website.

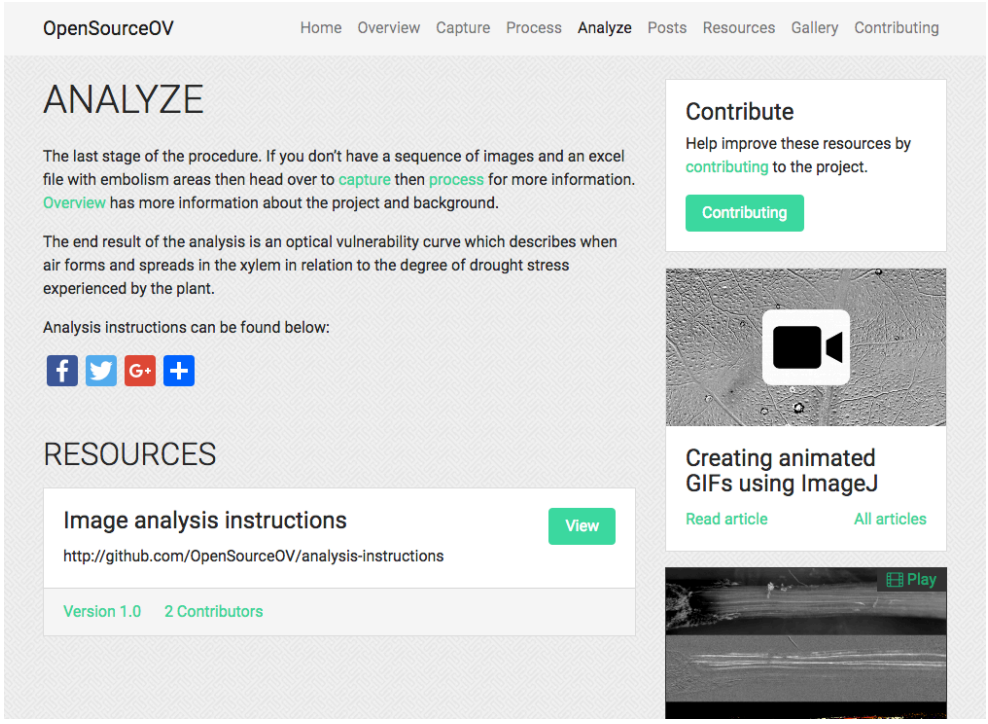

Fig. 5. The Process section of the OpenSourceOV.org website.

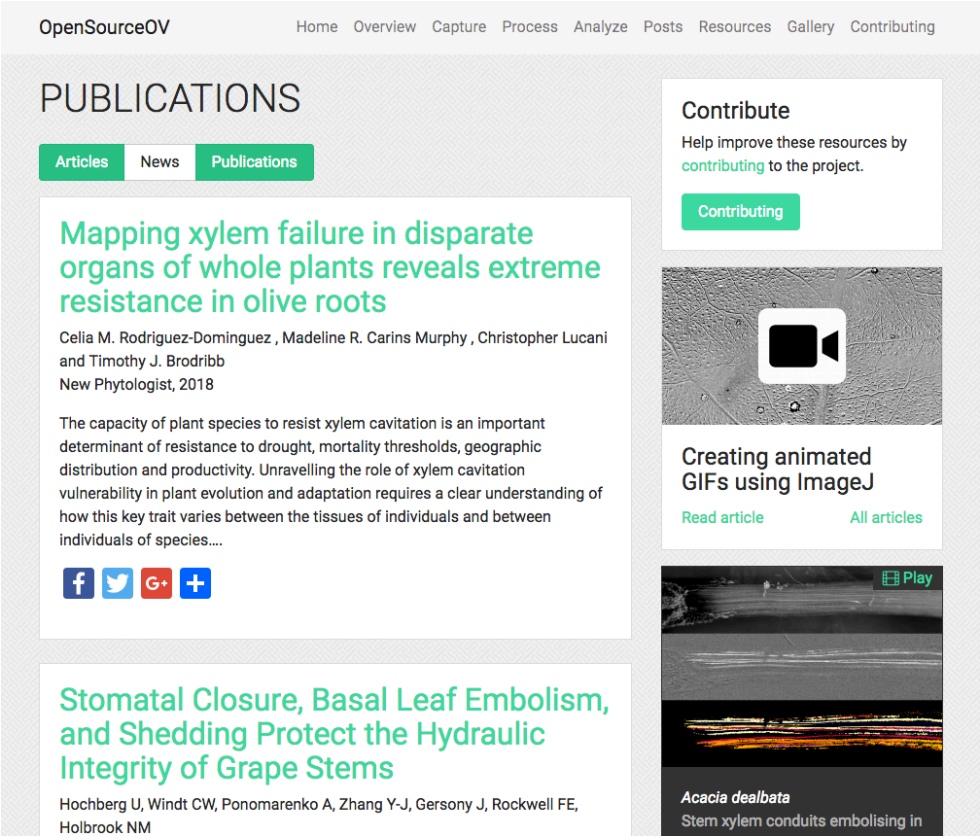

Fig. 6. The Posts section of the OpenSourceOV.org website.

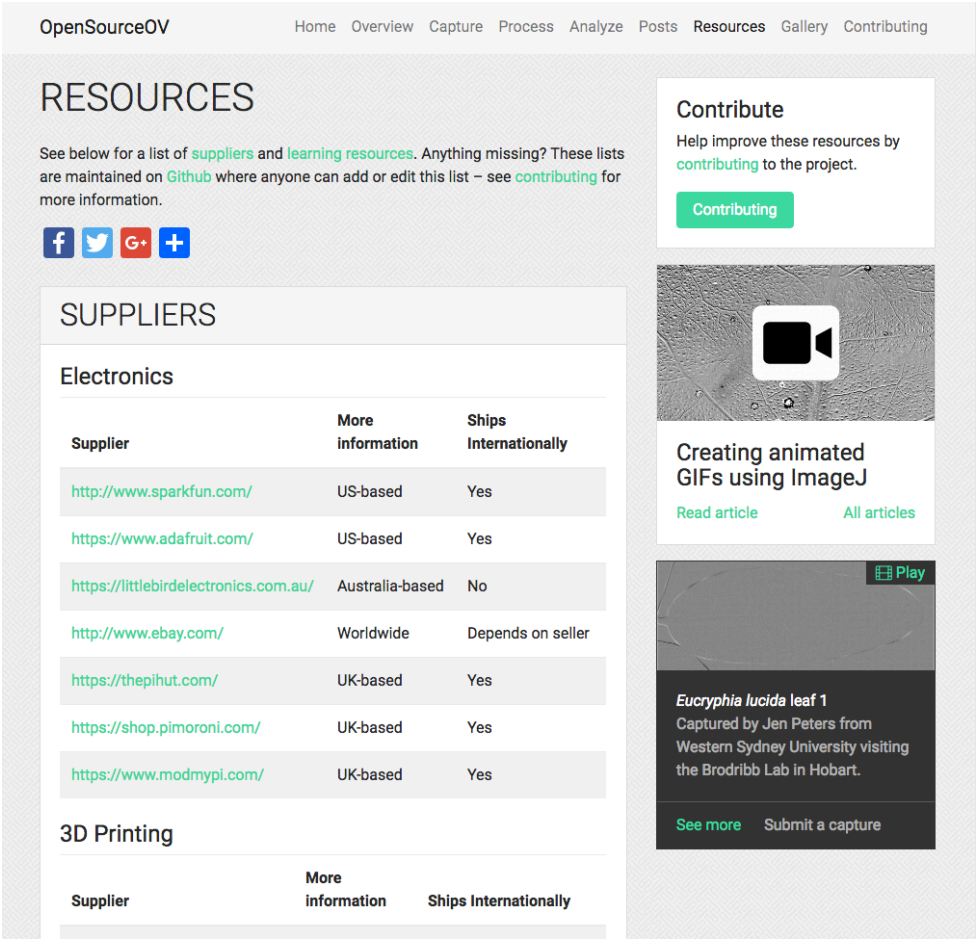

Fig. 7. The Resources section of the OpenSourceOV.org website.

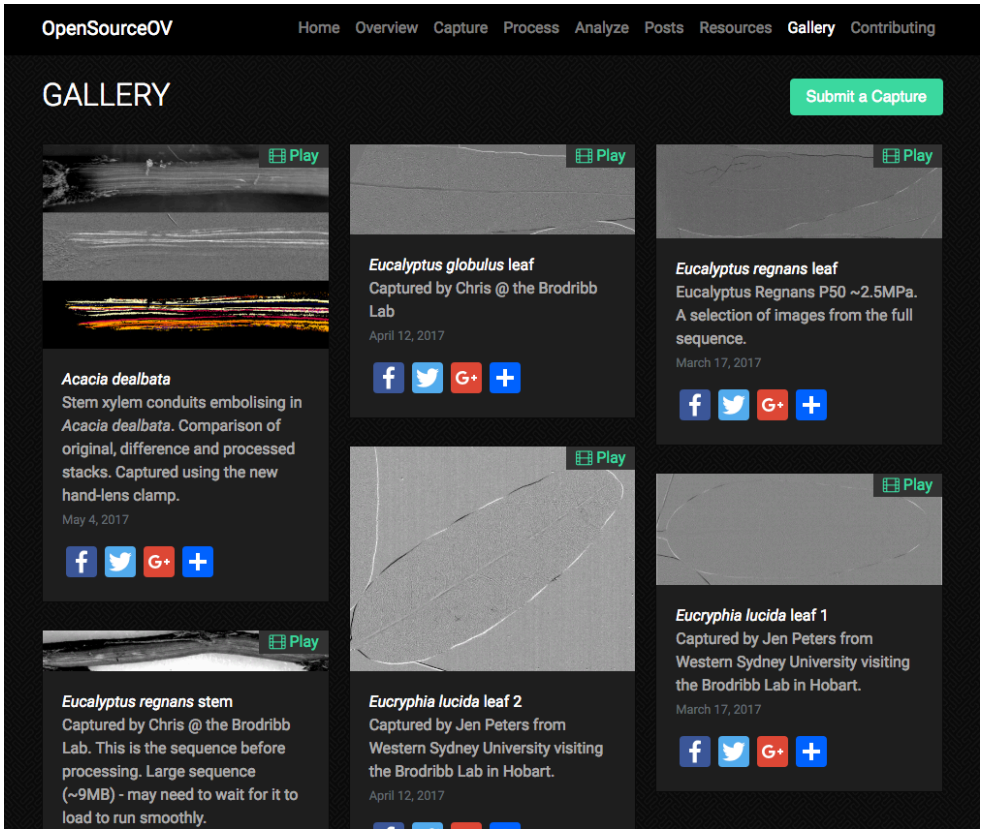

Fig. 8. The Gallery section of the OpenSourceOV.org website.

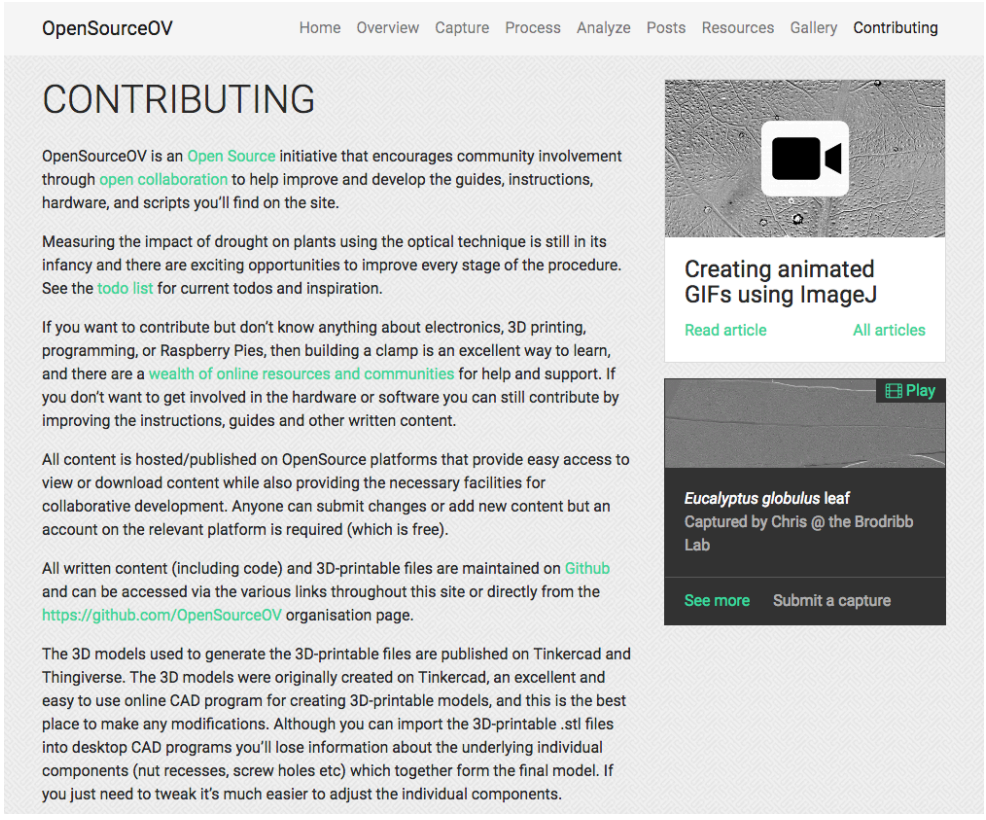

Fig. 9. The Contributing section of the OpenSourceOV.org website.

Appendix 2 - GitHub repositories

The OpenSourceOV GitHub repositories are given in Table 1.

Table 1. The sections of the OpenSourceOV.org website

Repository	Contents	Reference
clamp-build-instructions	CaviCam version 1 and version 2 build protocols. Transistor circuit version 1 and 2 build protocols. A guide for wiring connectors.	(Lucani, 2018d)
cavicapture	CaviCapture and CaviProcess programming code	(Lucani and Nolf, 2018a)
clamp-image-capture-instructions	CaviCam setup and image capture protocol	(Lucani, 2018e)
imagej-scripts	CaviTools ImageJ Plugin Toolbox scripts and plugins	(Lucani and Nolf, 2018b)
image-processing-instructions	Protocol for processing captured images and generating coloured images that illustrate the progression of embolism events using ImageJ and the CaviTools ImageJ Plugin Toolbox.	(Lucani, 2018g)
caviconsole	CaviConsole GUI	(Lucani 2018t)
raspberry-pi-setup	Protocol for setting up a new Raspberry Pi ready to use the CaviCam system	(Lucani, 2018h)
caviscan	AutoIT script – CaviScan - for controlling image capture using a desktop scanner	(Lucani, 2018b)
contributing	A guide for contributors	(Lucani, 2018f)
clamp-3d-printing-resources	CaviCam version 1 and version 2 .stl files for 3D printing	(Lucani, 2018c)
resources	List of suppliers and learning resources	(Lucani, 2018i)
scanner-image-capture-instructions	Protocol for capturing images using a desktop scanner and the CaviScan script.	(Lucani, 2018j)
analysis-instructions	Protocol for analysing sequence data	(Lucani, 2018a)